Structure and Function of Lysosomal Phospholipase A2 and Lecithin:Cholesterol Acyltransferase

by

Alisa Glukhova

A dissertation submitted in partial fulfillment
of the requirements for the degree of
Doctor of Philosophy
(Chemical Biology)
in the University of Michigan
2014

Doctoral Committee:

Professor John J. G. Tesmer, Chair
Professor Janet L. Smith
Professor James A. Shayman
Professor Roger K. Sunahara
Professor Richard R. Neubig, Michigan State University

Dedication

To my mother, who taught me passion and love for science.

Acknowledgements

Most of all I am grateful to my mentor John J. G. Tesmer for his advice and support during my graduate school training. I have learned a great deal during my PhD and I am confident that his suggestions and constructive criticism made me a better scientist.

I am thankful to my doctoral committee for all their input and suggestions on my research. I am also very grateful to GM/CA and LS-CAT staff members at Argonne Photon Source for their help with data collection, Dr. Cash for advice and support with mammalian cell culture, Michael Won for extensive LCAT crystallization screening and Kerry Johnson for her help with the GRK5 project. I am also thankful to my current and ex lab mates from the Tesmer lab for their scientific help, support and creation of a very stimulating and friendly working environment.

I would also like to thank our collaborators, James A. Shayman and the members of his laboratory for the great scientific input, advice and experimental assistance.

This work was supported by an American Heart Association Pre-Doctoral Fellowship 13PRE16880003 and Rackham Graduate Student Research Grant.

This work would not be possible without my friends and family. Their help and support over the years gave me the strength to accomplish this work and succeed in graduate school.

Table of Contents

List of Figures

List of Tables

List of Abbreviations

AF488 – AlexaFluor-488
AM – alveolar macrophages
ANS – 8-Anilino-1-naphthalenesulfonic acid
ApoA – apolipoprotein A
ATR-FTIR – attenuated total reflectance−Fourier transform infrared
BSA – bovine serum albumin
CAD – cationic amphiphilic drug
CaM – calmodulin
CFP – cyan fluorescent protein
CHO – Chinese hamster ovary
CoA – Coenzyme A
cPLA2 – cytosolic phospholipase A2
DODPC – 1,2-*O*-dioctadecenyl-*sn*-glycero-3-phosphocholine
DOPC – 1,2-dioleoyl-*sn*-glycero-3-phosphatidylcholine
DOPEt – 1,2- dioleoyl-*sn*-glycero-3-phosphoethanol
DOPG – 1,2-dioleoyl-*sn*-glycero-3-[phospho-rac-(1-glycerol)]
DOPS – 1,2-dioleoyl-*sn*-glycero-3-phosphoserine
DPPC - dipalmitoylphosphatidylcholine
DTT – dithiothreitol
endo F1 - endoglycosidase F1
endo H – Endoglycosidase H
endo Hf – Endoglycosidase Hf
FBS – fetal bovine serum
FED – fish eye disease
FLD – familial LCAT deficiency
FRET – Forster resonance energy transfer
GlcNAc – N-acetyl-glucosamines
GM-GSF – granulocyte-macrophage colony-stimulating factor
GnTI – N-acetylglucosaminyltransferase I
GPCR – G protein-coupled receptor
GRK – protein-coupled receptor kinase
HAG – 1-O-hexadecyl-2-acetyl-*sn*-glycerol
HDAC5 – histone deacetylase-5
HDL – high density lipoprotein
HEK – human embryonic kidney
IDFP – isopropyl dodec-11-enylfluorophosphonate
iPLA2 – Ca^{2+}-independent phospholipase A2
KIF – kifunensine
LCAT – lecithin:cholesterol acyltransferase
LDL – low density lipoprotein
LLPL – LCAT-like lysophospholipase

LPLA2 – lysosomal phospholipase A2
MAFP – methyl arachidonyl fluorophosphonate
MDCK – Madin-Darby canine kidney
β-ME – β-mercaptoethanol
MEF – myocyte enhancer factor two
MW – molecular weight
NAS – N-acetylsphingosine
NLS – nuclear localization sequence
Nu – nucleophile
β-OG – β-octylglucoside
OPPC – 1-oleoyl-2-palmitoyl-*sn*-glycero-3-phosphocholine
PAF – platelet activating factor
PAF-AH – platelet activating factor acetyl hydrolases
PAGE – polyacrylamide gel electrophoresis
PAP – pulmonary alveolar proteinosis
PAPC – 1-palmitoyl-2-arachidonoyl-*sn*-glycero-3-phosphocholine
PC – phosphatidylcholine
PDMP – D-*threo*-1-phenyl-2-decanoylamino-3-morpholino-1-propanol
PDPC – 1-palmitoyl-2-docosahexanoyl-*sn*-glycero-3-phosphocholine
PE – phosphatidylethanolamine
PEI – polyethylenimine
PH – pleckstrin homology
PIP2 – phosphatidylinositol 4,5-bisphosphate
PKA – protein kinase A
PKC – protein kinase C
PLA2 – phospholipases A2
PNGase F – peptide N-glycosidase F
pNPB – *p*-nitrophenylbutyrate
POPC – 1-palmitoyl-2-oleoyl-*sn*-glycero-3-phosphocholine
PPARγ – factor peroxisome proliferator-activated receptor gamma
RH – RGS-homology
ROS – rod outer segment
RXR – retinoid X receptor
SDS – sodium dodecyl sulfate
SeMet – selenomethionine
SFG – sum frequency generation
SWA – swainsonine
TEV – tobacco etch virus
TFE – tetrafluoroethylene
v/v – volume/volume
w/v – mass/volume

Abstract

Lysosomal phospholipase A2 (LPLA2) and lecithin:cholesterol acyltransferase (LCAT) belong to a structurally uncharacterized family of lipid metabolizing enzymes responsible for lung surfactant catabolism and reverse cholesterol transport, respectively. Whereas LPLA2 is predicted to underlie the development of drug-induced phospholipidosis, somatic mutations in LCAT cause familial LCAT deficiency (FLD). Herein are described multiple high resolution crystal structures of human LPLA2 and a low resolution structure of LCAT that confirms its close structural relationship to LPLA2. Insertions in the α/β hydrolase core of LPLA2 form domains with unique folds that are responsible for membrane interaction and binding the acyl chains and head groups of phospholipid substrates. The wide opening of the LPLA2 active site faces the membrane for an easy access to glycerophospholipids and lipophilic alcohols, its preferred substrates. Based on these structures, substrate modeling, and the position of disease-causing mutations in LCAT, we propose that orientation of the bound phospholipid in the active site underlies the specificity of LPLA2 for fatty acids in the *sn*-2 vs. *sn*-1 position, and that preference for length of the acyl chains is dictated by two hydrophobic grooves leading away from the catalytic triad of the enzyme. We proposed a 2-step mechanism for LPLA2 membrane binding, consisting of a transient LPLA2 interaction with the membrane via its surface hydrophobic residues. High-affinity membrane interaction occurs through the bound substrate and the catalytic intermediate. Based on LPLA2 structure we built an LCAT homology model and validated it by solving the 8.7 Å structure of LCAT. Then we used this model to map known genetic LCAT mutations leading to either fish eye disease (FED) or FLD. We determined that most FLD-causing mutations result in either structural defects or catalytic impairments. On the other hand, FED mutations mostly cluster on the surface of the hydrolase domain and might define a surface for LCAT interactions with apolipoprotein A (ApoA)-I, a key component of HDL. The LCAT structure thus paves the

way for rational development of new therapeutics to treat FLD, atherosclerosis, and acute coronary syndrome.

Chapter 1. Introduction

1.1 Lipases

Lipases are enzymes that hydrolyze lipids. Lipases function in eukaryotes and prokaryotes to maintain lipid homeostasis, hydrolyze ingested triglycerides and catabolize them when energy expenditure requires it. Depending on the substrate type, lipases can be further divided into phospholipases, triacylglycerol lipases, sphingomyelinases, etc. However, most commonly, the term “lipase” refers to triacylglycerol lipases (E.C.3.1.1.3), the enzymes that hydrolyze triacylglycerols to diacylglycerols and free fatty acids. Some lipases can also perform transesterification reactions when the leaving acyl group is conjugated to an acceptor molecule instead of water. Alcohols, thiols, and amines can be used as acceptor molecules (Sandoval, 2012). Bacterial lipases are the most extensively studied and many of their crystal structures have been determined (Arpigny & Jaeger, 1999; Jaeger *et al.*, 1994).

1.1.1 α/β hydrolase fold

Most triacylglycerol lipases have an α/β hydrolase fold (Ollis, Cheah, Cygler, & Dijkstra, 1992), characterized by a central β-sheet usually consisting of seven parallel and one antiparallel β-strand, surrounded by α-helixes on either side (Fig. 1). However, some lipase lack the β1 and β2 strands, for example, *Pseudomonas aeruginosa* lipase and *Bacillus subtilis* lipase (Nardini, Lang, Liebeton, Jaeger, & Dijkstra, 2000; van Pouderoyen, Eggert, Jaeger, & Dijkstra, 2001).

These enzymes contain a Ser/Asp/His catalytic triad with an active site serine nucleophile (Nu) located at the tip of a nucleophile elbow, an extremely sharp turn with strained backbone geometry between the β5 strand and the αC helix. Because of the tight geometry, glycines at position Nu-2 and Nu+2, are necessary to avoid steric

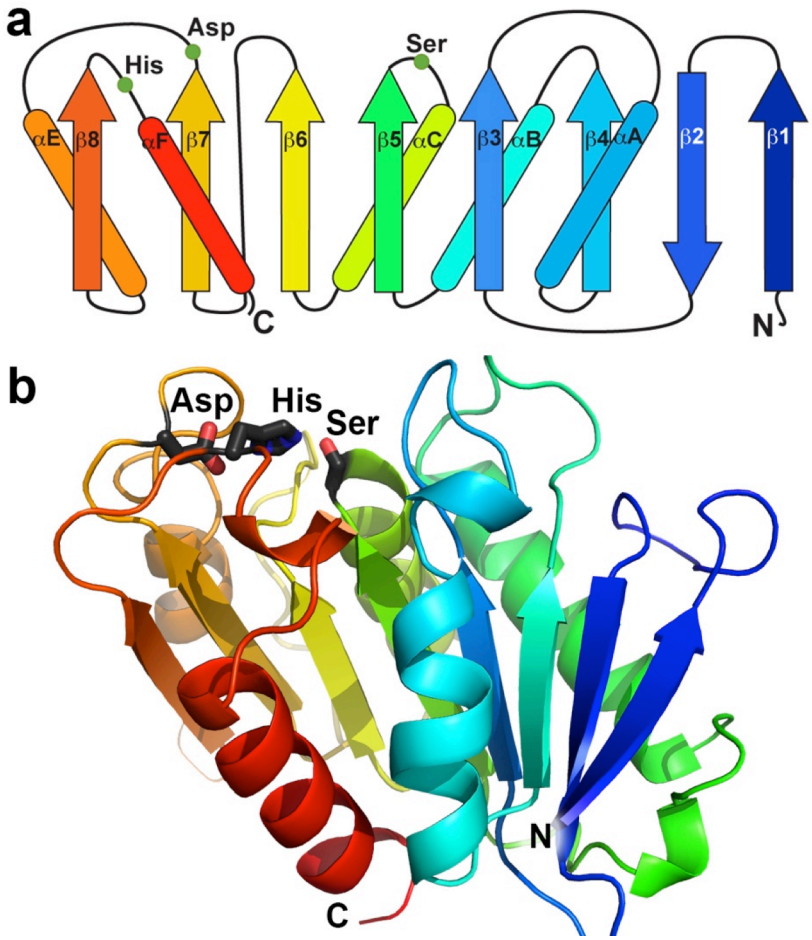

Figure 1. The canonical α/β hydrolase fold. **(a)** Topology diagram of a typical α/β fold. Green circles depict the catalytic triad residues. **(b)** The α/β hydrolase fold of a lipase from *S. exfoliates* (PDB 1JFR). Catalytic triad residues are shown as sticks. The backbone is colored in rainbow from blue (N-) to red (C-terminus).

clashes, generating the lipase motif GxSxG, where "x" can be any amino acid. The catalytic triad Asp is commonly found in a loop following β7, and the His in a loop after β8. Some of the helixes connecting β-strands can be absent. In addition, various insertions in the loops between the C-termini of β-strands and the N-termini of α-helixes often constitute additional domains and active site lid elements.

The oxyanion hole is formed by backbone amides of two amino acids: one in the position Nu+1 and the other from an adjacent loop region. In many lipases, the second oxyanion-forming residue adopts an optimal position only upon substrate binding when the lipase assumes an active conformation (Nardini & Dijkstra, 1999).

1.1.2 Catalytic cycle

The catalytic triad of lipases is functionally similar to that of trypsin, despite the lack of structural similarity (Arpigny & Jaeger, 1999), and the reaction mechanism is very similar between the two enzymes. First, when the substrate binds, the oxygen of the carbonyl group positions in the oxyanion hole (Fig. 2a). Then, the catalytic triad charge-relay system creates an activated oxygen atom on the nucleophile serine hydroxyl group, which attacks the carbonyl carbon on the substrate. This creates a transient tetrahedral intermediate, stabilized by interactions between the backbone amides of the oxyanion hole and the negatively charged oxygen atom on the carbonyl group of the scissile ester bond (Fig. 2b). The leaving group is then protonated by the His of the catalytic triad that had previously taken the H^+ from the Nu, leaving the catalytic intermediate attached to Nu (acyl enzyme, Fig. 2c). The His residue then activates an incoming water molecule, and the resulting OH^- group attacks the carbonyl group of the acyl enzyme, resulting in the formation of a second tetrahedral intermediate. The proton is returned from the His to Ser triggering the release of the

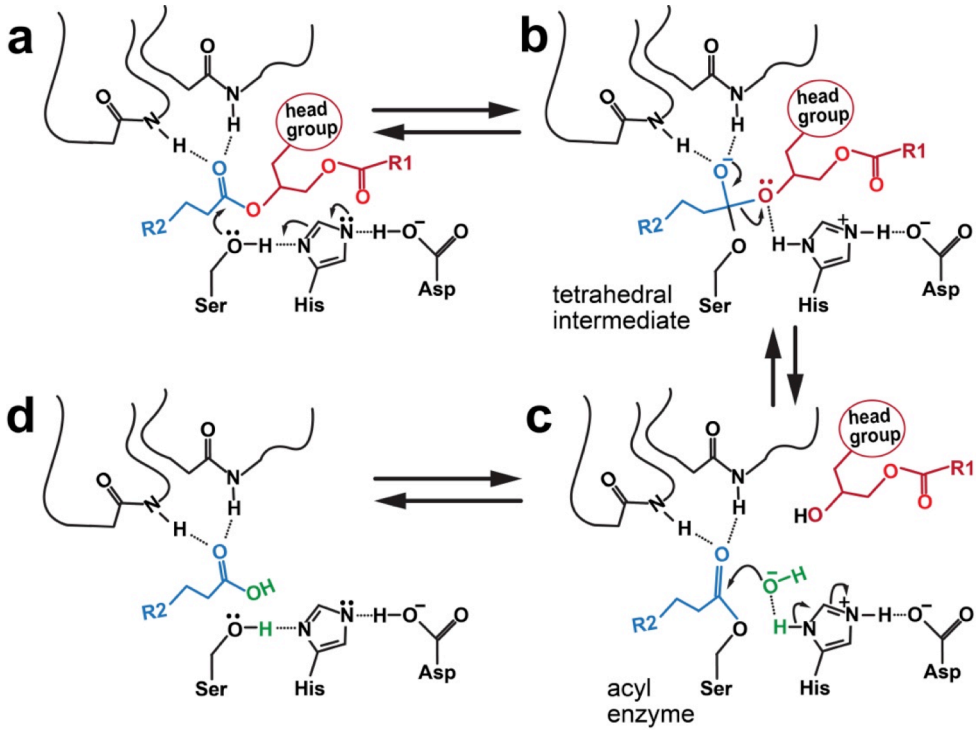

Figure 2. Reaction mechanism of the Ser/His/Asp catalytic triad.

product and the completion of the catalytic cycle (Fig. 2d).

Fluorophosphonate inhibitors covalently and nonspecifically inhibit many α/β hydrolase enzymes. The release of hydrofluoric acid traps the enzymes at the acyl enzyme step of their catalytic cycle. Such inhibitors were successfully used to solve lipase structures in their active conformation (Egloff, Marguet, Buono, & Verger, 1995; Roussel *et al.*, 2002).

1.1.3 Interfacial activation and lids

All lipases work at the water-lipid interface, and many of them are activated by lipid surfaces in a phenomenon known as “interfacial activation”. In the absence of such activation, the enzyme activity follows the typical Michaelis-Menten dependence on the substrate concentration. However, for many lipases a dramatic increase in activity occurs when the substrate is presented in the form of micelles or liposomes (Jaeger *et al.*, 1994).

Such behavior is usually attributed to the presence of a mobile “lid”, an element that closes off and blocks the active site in the absence of lipids. Upon interaction with a lipid interface, the lid is displaced, uncovering the active site, which ultimately leads to substrate binding and turnover. Dislocation of the lid also often leads to the exposure of large hydrophobic surfaces that increase the enzyme interaction with lipid substrates and the membrane itself.

Lids are formed by elements inserted into the loops of the α/β hydrolase domain and can be very different in their size and structure. As such, the mobile lid of *Pseudomonas aeruginosa* lipase is formed from three helixes (α4-α6) and that of *Candida rugosa* has a single mobile helix (Grochulski *et al.*, 1994; Nardini *et al.*, 2000). Non mobile elements, which cover the active site of *Pseudomonas aeruginosa* and human gastric lipase, were called the “cap” domain (Canaan, Roussel, Verger, & Cambillau, 1999; Nardini *et al.*, 2000). Mutations within the cap domain dramatically reduced the activity of human gastric lipase, indicating its importance in substrate binding (Miled *et al.*, 2003).

Interfacial activation of some lipases also includes a conformational change, which is required to bring the catalytic triad and the oxyanion hole into the proper alignment for catalysis (Schrag *et al.*, 1997; van Tilbeurgh *et al.*, 1993). Not all lipases have lids. Such enzymes also lack the interfacial activation and are constitutively active (Martinez *et al.*, 1994; van Pouderoyen *et al.*, 2001).

1.1.4 Phospholipase A2 enzymes

The phospholipases A2 (PLA2) are a group of enzymes, unrelated in their structures and catalytic mechanisms, grouped together on the basis of their common reaction of fatty acid hydrolysis from the *sn*-2 position of phospholipids (Schaloske & Dennis, 2006). This group includes small secreted PLA2s, cytosolic PLA2 (cPLA2), Ca^{2+}-independent PLA2 (iPLA2), platelet activating factor acetyl hydrolases (PAF-AH), lysosomal phospholipase A2 (LPLA2) and adipose specific phospholipase A2 (Dennis, Cao, Hsu, Magrioti, & Kokotos, 2011).

Only cPLA2, iPLA2, PAF-AH and LPLA2 have an α/β hydrolase fold. The catalytic mechanism between the groups is also different, with only PAF-AH and LPLA2 employing the Ser/His/Asp catalytic triad. Similar to bacterial lipases, cPLA2 has a cap domain with a lid, located at the top of the active site that blocks access to phospholipids. cPLA2 also has a C2 domain and its membrane binding is regulated by Ca^{2+} ions and phosphatidylinositol 4,5-bisphosphate (PIP_2). Once at the membrane, phospholipid binding triggers the opening of the lid (Dennis *et al.*, 2011). The model of a catalytic domain of iPLA2, built based on the crystal structure for cPLA2, suggests an absence of any cap domain or lid element. Membrane interaction for iPLA2 likely occurs via membrane penetration by a region of the catalytic domain. PAF-AH membrane binding occurs via surface-exposed hydrophobic α-helixes. LPLA2 is the only member of the group XV phospholipase and little is known about its membrane binding and its activation mechanism.

1.2 LPLA2, a unique group XV phospholipase A2

1.2.1 LPLA2 discovery

When incubating N-acetylsphingosine (NAS) with Madin-Darby canine kidney (MDCK) cells homogenate, an unknown polar product was found and later identified as 1-O-acyl-NAS. The homogenate enzymatic activity had a pH maximum of 4.2 and high affinity for NAS with K_m of 9.4 μM. In contrast to cPLA2 and Coenzyme A (CoA)-independent transacylases, the unknown enzyme did not utilize free fatty acids or CoA-fatty acids, but instead transferred fatty acids from glycerophospholipids, such as 1,2-dioleoyl-*sn*-glycero-3-phosphatidylcholine (DOPC) (Abe, Shayman, & Radin, 1996). The enzyme was later purified from bovine brain and characterized. It exhibited both acyltransferase and phospholipase A2 activity, was localized to the lysosomal fraction, and had an acidic pH optimum (pH 4.5). It was also Ca^{2+}, Mg^{2+} and ATP independent, and was insensitive to dithiothreitol (DTT) and bromoenol lactone (a cytosolic Ca^{2+}-independent phospholipase A2 inhibitor) (Abe & Shayman, 1998). Gene sequencing and cloning was performed by two independent groups and the enzyme was named LCAT-like lysophospholipase (LLPL) (Taniyama *et al.*, 1999) or LPLA2 (Hiraoka, Abe, & Shayman, 2002). However, it was discovered that lysophospholipase activity is negligible compare to the enzyme acyltransferase or phospholipase activities (Hiraoka *et al.*, 2002).

1.2.2 LPLA2 primary and secondary structure and N-glycosylation

LPLA2 shares 49% sequence identity with lecithin:cholesterol acyltransferase (LCAT). Both genes are located on chromosome16q22.1 and are spatially close. LPLA2 mRNA encodes a 1.3 kb product corresponding to protein 412 amino acids in length. Signal sequence predictions suggested a signal peptide cleavage site between amino acids 33 and 34 in human LPLA2, leaving a mature protein of 379 amino acids.

LPLA2 sequence similarity to LCAT suggests it has an α/β hydrolase fold, predicted for LCAT by threading algorithms (Peelman *et al.*, 1998). LPLA2 and LCAT

have no closely related homologs with a known structure. The LPLA2 primary sequence predicted a lipase motif AxSxG located in a sharp turn between a β-strand and an α-helix (Fig. 3), similar to that of *Bacillus subtilis* lipase but different from the GxSxG motif common to other lipases and LCAT (Ollis *et al.*, 1992). Mutation of the Ala163 in the lipase motif to the corresponding Gly found in LCAT results in LPLA2 that retains only 10% activity of the wild type enzyme. LCAT and LPLA2 sequence alignment identified Ser165, Asp327 and His359 as LPLA2 catalytic triad residues. Alanine substitutions at any of these positions completely eliminated LPLA2 activity (Hiraoka, Abe, & Shayman, 2005).

Human LPLA2 has four cysteines. Cys32 and Cys56 form a disulfide bridge that sets apart a so-called "lid" thought to be important in interfacial activation and

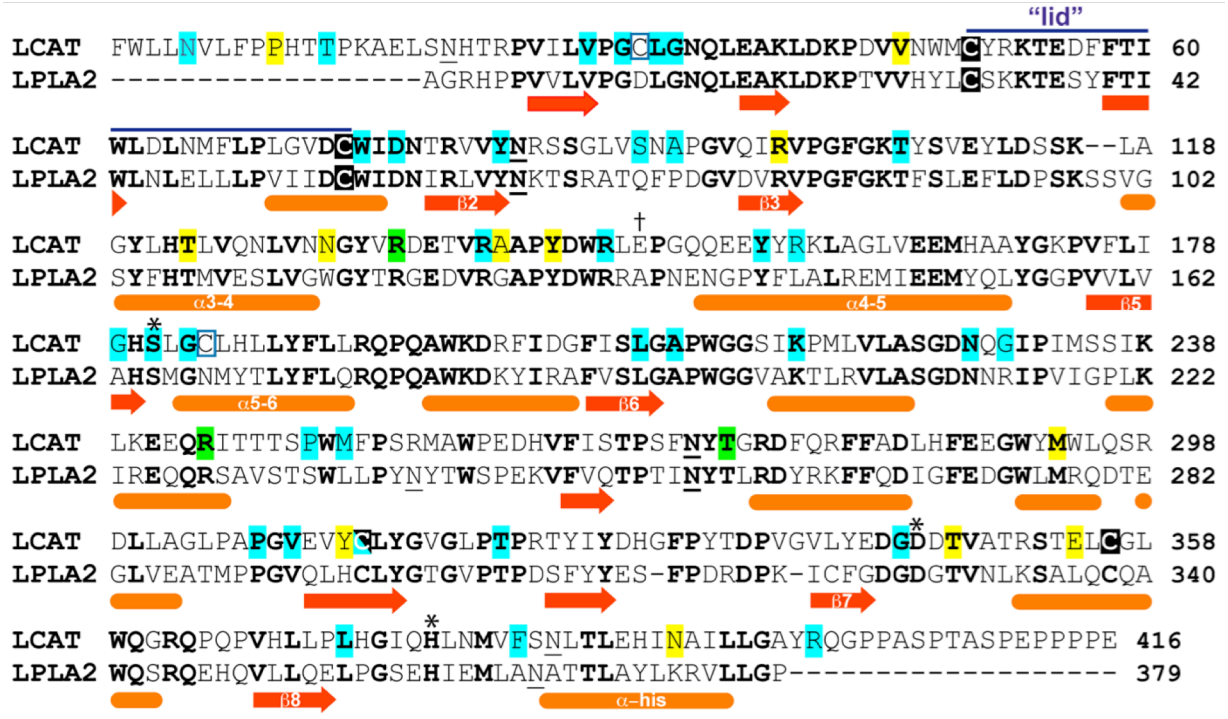

Figure 3. Sequence comparison of mature human LCAT and LPLA2. Missense mutations in LCAT resulting in disease are highlighted blue for FLD, yellow for FED, and green for both (substitution dependent). Catalytic triad residues are marked with an asterisk. Cysteine residues that participate in disulfide bonds are highlighted in black. Cyan boxes indicate the positions of free LCAT cysteins. The † indicates the position in LCAT that when mutated from an acidic residue allows the enzyme to accept acyl chains greater than 18 carbons in the *sn-2* position. The "lid" proposed to cover the active site is bracketed by a disulfide bond and is indicated by a purple line above the sequences. Red arrows and orange lines below the sequences indicate the predicted positions of secondary structure elements by PSIPRED. Strands and helixes are labeled according to Peelman et al. (Peelman et al., 1998).

membrane binding. Although DTT does not affect LPLA2 activity, mutations of Cys32 or Cys56 completely inactivate the enzyme. The remaining Cys297 and Cys338 remain free and are able to interact with organomercury agarose columns (Hiraoka *et al.*, 2005).

Asn66, Asn240, Asn256 and Asn365 were found in motifs that match that of the consensus for N-linked glycosylation (NxS/T) (F. Schwarz & Aebi, 2011). Polysaccharide addition was confirmed via binding to Concavalin A columns. Endoglycosidase F1 (endo F1) treatment of LPLA2 expressed in COS-7 cells removes N-linked glycosylation and shifts the enzymes apparent molecular weight from 50 kDa to 42 kDa as expected from the amino acid sequence (Hiraoka *et al.*, 2002). LPLA2 glycosylation is required for protein folding and full catalytic activity (Hiraoka, Okamoto, Ohguro, & Abe, 2013; O, Hill, Wang, McLeod, & Pritchard, 1993). Alanine substitutions at positions 240, 256 and 365 reduced LPLA2 catalytic activity to 37, 32, and 82%, respectively. The N66A substitution resulted in an insoluble and misfolded protein.

1.2.3 LPLA2 catalytic activity and substrate specificity

LPLA2 acts both as a phospholipase and an acyltransferase. In the phospholipase reaction, LPLA2 hydrolyses glycerophospholipids and then uses water as an acceptor for an acyl chain (Fig.4a). When certain lipophilic alcohols such as NAS are present, LPLA2 acts as an acyltransferase, generating O-linked acyl alcohols (Fig. 4b).

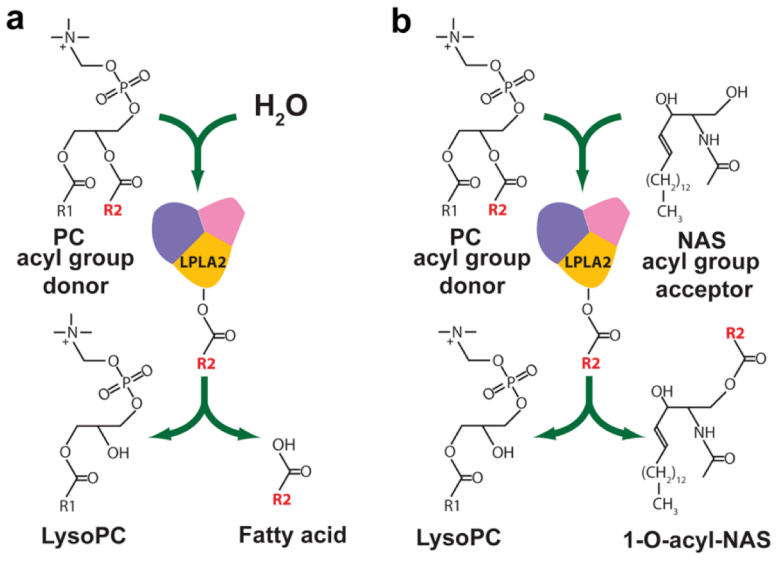

Figure 4. LPLA2 reaction schemes. **(a)** Phospholipase reaction. **(b)** Acyltransferase reaction

Presumably, the acidic pH optimum arises from LPLA2's reliance on electrostatic interactions for liposome binding (Abe & Shayman, 1998). Thus, hydrolysis of *p*-nitrophenylbutyrate (pNPB), a soluble LPLA2 substrate, can

occur over a wide range of pH (4-8). The LPLA2 pH optimum for liposome-based reactions is instead very narrow (4-5), and is the same as its pH dependence for liposome binding (Abe & Shayman, 2009).

Charge plays an important role in LPLA2 catalysis. LPLA2 has a strong preference for negatively charged glycerophospholipids as its substrates. Consequently, liposomes consisting of negatively charged 1,2-dioleoyl-*sn*-glycero-3-[phospho-rac-(1-glycerol)] (DOPG)/NAS, 1,2-dioleoyl-*sn*-glycero-3-phosphate/NAS or and 1,2-dioleoyl-*sn*-glycero-3-phosphoethanol (DOPEt))/NAS were turned over more efficiently then the zwitterionic DOPC/NAS. Incorporation of negatively charged inert sulfatide into DOPC/NAS liposomes increased the formation of 1-O-acyl-NAS proportionally to the ratio of DOPC/NAS to sulfatide. Sulfatide incorporation into negatively charged glycerophospholipid (1,2-dioleoyl-*sn*-glycero-3-phosphoserine, DOPG/NAS, and DOPEt/NAS) liposomes produces an additive effect and results in the most efficient LPLA2 substrate, sensitive enough to measure LPLA2 activity in blood plasma (Abe, Kelly, & Shayman, 2010). The sulfatide effect is counteracted by high salt concentrations, and when > 200 mM NaCl is present LPLA2 activity is reduced to 30%, presumably due to the loss of liposome association.

LPLA2 does not have strict specificity for *sn-1* or *sn-2* positions of glycerophospholipids. Rather, this choice is determined by the nature of the acyl groups themselves (Abe, Hiraoka, & Shayman, 2006). When given 1-palmitoyl-2-oleoyl-*sn*-glycero-3-phosphocholine (POPC)/NAS/sulfatide or 1-oleoyl-2-palmitoyl-*sn*-glycero-3-phosphocholine (OPPC)/NAS/sulfatide liposomes LPLA2 preferentially transfers the oleoyl (C18:1) group rather then palmitoyl (C16:0) group, no matter the position. The rate of formation for 1-O-oleoyl-NAS was 2.5 or 5 times higher then that of 1-O-palmitoyl-NAS in POPC or OPPC-containing liposomes, respectively. Comparison of 1-stearoyl-2-oleoyl-*sn*-glycero-3-phosphocholine or 1-oleoyl-2-steraroyl-*sn*-glycero-3-phosphocholine-containing liposomes confirmed that LPLA2 prefers to act on unsaturated fatty acids, and that 1-O-oleoyl-NAS formation always dominated over 1-O-stearyl-NAS (C18:0). The length of acyl groups also affects LPLA2 specificity. When given a choice between palmitic group in *sn-1* position and oleic or linoleic (C18:2) in *sn-2*, LPLA2 acts on the *sn-2* position two times more efficiently than on *sn-1*. However,

if the length of the acyl group in the *sn-2* position increases, for example, when using 1-palmitoyl-2-docosahexanoyl-*sn*-glycero-3-phosphocholine (PDPC)-containing liposomes, LPLA2 preference for *sn-2/sn-1* positions is only 1.5. Arachidonic acid in the *sn-2* position is particularly disfavored with a *sn-2/sn-1* ratio of 0.24 for 1-palmitoyl-2-arachidonoyl-*sn*-glycero-3-phosphocholine (PAPC).

When primary alcohols are present in the liposomes, LPLA2 acts as an acyltransferase (Abe, Hiraoka, & Shayman, 2007b). Investigation of preferred LPLA2 acceptors identified a common chemotype among them: ethanol derivatives with one long aliphatic chain and one short neutral residue, such as a methyl or acyl group in the C2 position. Thus, a short chain ceramide NAS, with an acetyl group in C2 position is favored over N-octanoylsphingosine or oleoylsphingosine (Abe *et al.*, 1996). Acylation always occurs at the primary alcohol group. Other acceptors include glycerol derivatives complying with the common acceptor structure described above. Glycerol itself is a very poor acceptor and works only at a concentration of 30%. However, glycerol derivatives, such as 1-O-hexadecyl-2-acetyl-*sn*-glycerol (HAG), are acylated on the remaining primary alcohol group at the C3 position with the formation of 1-O-hexadecyl-2-acetyl-3-oleoyl-*sn*-glycerol. This reaction is competitive with NAS acylation when both acceptors are present at the same time, and HAG inhibited NAS acylation with an IC_{50} of 25 μM.

Both NAS and HAG are biologically relevant molecules. NAS can be produced *in vivo* in HL-60 cells by transferring an acetyl group from PAF to sphingosine by CoA-independent transacetylase (T. Lee, Ou, Shinozaki, & Malone, 1996) and HAG can be converted to PAF by DTT-insensitive cholinephosphotransferase(T. C. Lee, Malone, Blank, Fitzgerald, & Snyder, 1990). In addition, LPLA2 can use biologically active oleoylethanolamide and anandamide as acceptors, changing their properties, such a lipophilicity, via acylation (Abe, Hiraoka, & Shayman, 2007b).

The acyltransferase reaction is reversible, and LPLA2 can deacylate 1-O-acyl-NAS when incubated for prolonged periods of time, releasing a fatty acid and NAS that can be utilized again in the acyltransferase reaction. LPLA2 deacylase activity might be important for regulation of the cellular phospholipid homeostasis by maintaining the levels of biosynthetically important lipophilic alcohols. Thus LPLA2 inhibition in MDCK

cells *in vitro* leads to accumulation of nonpolar lipids (Abe, Hiraoka, & Shayman, 2007b).

Although acyltransferase activity itself is not unique to LPLA2, its use of primary alcohols as acceptors is. Other known human enzymes possessing acyltransferases activity use sterols (LCAT (Szedlacsek *et al.*, 1995)) or lysophospholipids (cPLA2 (Reynolds, Hughes, Louis, Kramer, & Dennis, 1993)). This unique feature allows for a convenient assay for measuring LPLA2 activity in complex systems such as blood plasma. Only plasma from mice expressing LPLA2 was able to catalyze the formation of 1-O-acyl-NAS when incubated with DOPC/sulfatide/NAS (Abe *et al.*, 2010).

1.2.4 LPLA2 tissue distribution and physiological role

The tissue distribution of LPLA2 was investigated in rats using the highly sensitive and LPLA2-specific acyltransferase reaction, and the highest level of LPLA2 activity was found in rat alveolar macrophages (AM) (Abe *et al.*, 2004a). LPLA2 activity was 40-fold higher in AM than other tissues, including monocytes and peritoneal macrophages. It was, in fact, suggested that LPLA2 could serve as a marker for terminally differentiated AM. Consistent with increased LPLA2 activity, LPLA2 mRNA and protein levels were also significantly elevated in AM compared to other tissues. The major function of AM is degradation of pulmonary surfactant, the major component of which is dipalmitoylphosphatidylcholine (DPPC) (Agassandian & Mallampalli, 2013). *In vitro* analysis confirmed that LPLA2 hydrolyses DPPC in both the *sn-1* and *sn-2* positions (Abe *et al.*, 2004a).

Granulocyte-macrophage colony-stimulating factor (GM-CSF) deficient mice (GM-CSF$^{-/-}$) exhibit pathologic accumulation of lung surfactant due to a defect in saturated phospholipid catabolism (Dranoff, Crawford, Sadelain, & Ream, 1994; Ikegami *et al.*, 1996). This defect resembles pulmonary alveolar proteinosis (PAP), a rare human disease characterized by accumulation of lipid material in alveoli. GM-CSF$^{-/-}$ mice have reduced LPLA2 activity and protein levels (Abe *et al.*, 2008) that correlates with reduced LPLA2 mRNA levels in human PAP patients (Malur *et al.*, 2012).

PAP treatment with rituximab, an antibody to CD20, a B-lymphocyte specific antigen, increased levels of GM-CSF via reduction of its autoantibody and consequent

increase in lipid transporter ABCG1 and the transcription factor peroxisome proliferator-activated receptor gamma (PPARγ) (Malur *et al.*, 2012). Rituximab also restores LPLA2 to the levels of the control group.

Although there appears to be a link between GM-CSF, PPARγ and LPLA2, the exact mechanism of signaling is unknown. It was shown that LPLA2 expression could be induced by trans-retinoic acid via retinoid X receptor (RXR) (Abe, Poucher, Hiraoka, & Shayman, 2004b). RXR in turn can form heterotrimers with PPARγ, however, no involvement of PPARγ was found in LPLA2 gene activation by retinoic acid in THP-1 cells.

In response to phagocytic stimuli, AM can secrete LPLA2 into extracellular fluids where it can participate in extracellular lipid catabolism (Abe *et al.*, 2008). Catabolytes, such as lysophosphatidic acid or arachidonic acid, can serve as G protein-coupled receptor ligands or proinflammatory molecule precursors, respectively (Ricciotti & FitzGerald, 2011; van Meeteren & Moolenaar, 2007).

1.2.5 The LPLA2$^{-/-}$ mouse and phospholipidosis

To elucidate systemic LPLA2 role in lipid metabolism, Hiraoka *et al.* created a LPLA2$^{-/-}$ mouse (Hiraoka *et al.*, 2006). The absence of LPLA2 protein was confirmed by the Western blot and by lack of NAS-transacylase activity. Alveolar and peritoneal macrophages from LPLA2$^{-/-}$ mouse showed marked accumulation (2.5-fold and 40%, respectively) of phospholipids compared to mice expressing LPLA2, primarily resulting from increased levels of phosphatidylcholine and phosphatidylethanolamine. Further examination revealed that phospholipid accumulation was due to impaired phospholipase A2 activity in these tissues. Taken together these data indicate that LPLA2 is a major enzyme responsible for phospholipid catabolism in alveolar macrophages and, to a lesser extent, in peritoneal macrophages. Histological examination of lung tissues from LPLA2$^{-/-}$ mouse revealed an increase in number and size of AM and mononuclear cell infiltrate in airways and blood vessels, an inflammation hallmark. Analysis of alveolar and peritoneal macrophages by electron microscopy showed an accumulation of multilamellular inclusion bodies, a hallmark of cellular phospholipidosis.

As described above, LPLA2 relies on electrostatic charge for interaction with membranes and the presence of substances that weaken the interaction, such as high salt, or pH shifts, results in LPLA2 inhibition. Cationic amphiphilic drugs (CADs) are lipophilic molecules that insert into the membrane and become ionized at acidic pH. When entering the acidic lysosomal environment their head groups become positively charged, effectively trapping them in this compartment. CAD incorporation into lysosomal membranes thereby change its charge distribution and can potentially affect enzymes working at that interface (Reasor & Kacew, 2001). Administration of certain CADs, such as the antiarrhythmic amiodarone, can thus have serious side effects such as pulmonary toxicity due to phospholipid accumulation (Heath, Costa-Jussà, Jacobs, & Jacobson, 1985). Another CAD, D-*threo*-1-phenyl-2-decanoylamino-3-morpholino-1-propanol (PDMP), is known to cause phospholipidosis in Chinese hamster ovary (CHO) cells (Rosenwald & Pagano, 1994).

MDCK cells treated with amiodarone or PDMP resulted in ~2-fold increase of phospholipids, primarily PC and phosphatidylethanolamine (PE), similarly to the phenotype observed in AM of LPLA2$^{-/-}$ mouse (Abe, Hiraoka, & Shayman, 2007a). Electron micrographs of Madin-Darby canine kidney (MDCK) cells treated with these drugs showed accumulation of multilamellular bodies resembling inclusion bodies from LPLA2$^{-/-}$ AM and peritoneal macrophages. Direct evidence that amiodarone and PDMP inhibit LPLA2 comes from *in vitro* assays on DOPC/NAS/sulfatide liposomes, wherein they inhibit the NAS-acyltransferase reaction with IC_{50} of 15 and 40 μM, respectively. Such inhibition presumably results from impaired LPLA2 binding to lipid bilayers, because amiodarone was shown to inhibit LPLA2 co-sedimentation with DOPC/sulfatide liposomes (Abe & Shayman, 2009).

Phospholipid accumulation in AM of LPLA2$^{-/-}$ mouse can be reversed *in vitro* by introducing catalytically active recombinant LPLA2 to the cultured cells. LPLA2 reuptake occurs by carbohydrate recognition via mannose-6-phospate receptors. This results in cellular phospholipid profiles becoming similar to wild type. Such an approach can be potentially used in enzyme-replacement therapy for cationic drug induced phospholipidosis (Abe *et al.*, 2008).

1.2.6 LPLA2 in immune response

Mycobacterium tuberculosis is carried human to human through aerosol transmission. It takes residency in lungs and causes tuberculosis, a severe and often fatal infectious disease with more then eight million new cases reported annually. The first stage of tuberculosis infection is bacterial uptake by resident AM. They provide the initial platform for bacterial replication but also serve to initiate a local immune response in lung parenchyma (Korbel, Schneider, & Schaible, 2008).

Comparing lungs from mycobacterium infected wild type and LPLA2$^{-/-}$ mice revealed that bacterial growth and survival is favored in the knockout mice, presumably due to an impaired immune response (B. E. Schneider *et al.*, 2014). As such, histology of its lung tissues revealed a reduced number of immune cells. Bacteria count in spleens was diminished in the LPLA2$^{-/-}$ mice compared to the control group. Further analysis revealed that absence of LPLA2 diminishes recruitment and activation of cytotoxic CD8+ and antigen specific CD4^{+} T cells. This could be the result of either insufficient macrophage activation in lung tissues or impaired macrophage recruitment due to defective chemokine production during the infection. This data, together with excessive LPLA2 expression levels in alveolar macrophages, indicate that LPLA2 plays an important role in protective host immunity for aerosol transmitted agents, and tuberculosis, in particular.

A novel role for LPLA2 in autoimmunity was recently described (Paduraru *et al.*, 2013). LPLA2$^{-/-}$ mice have a reduced number of invariant natural killer T cells resulting not from their impaired development, but from deficient antigen presentation by CD1d molecules. Although the exact nature of CD1d lipid antigens is not clear, some reports indicated that lysophospholipids, products of a phospholipase A2 reaction, are associated with CD1d molecules. However, it is currently unknown if lysophospholipids are true antigens or if they have a regulatory role in loading actual antigens on CD1d. LPLA2 deletion seems to alter the lipids presented by CD1d molecules.

Older LPLA2 -/- mice are characterized by an excessive presence of auto antibodies, such as anti-nuclear and anti-dsDNA antibodies. In addition they develop lymphoid hypertrophy and have high immunoglobulin levels. Such condition resembles

systemic lupus erythrematosis, an autoimmune decease characterized by antibody development to the organisms own antigens (Murphy, Lisnevskaia, & Isenberg, 2013). Thus, LPLA2 importance in immunity is supported by multiple studies, although the exact mechanism remains unknown.

1.2.7 LPLA2 role in atherosclerosis

LPLA2 was found to be protective in atherosclerosis. When $ApoE^{-/-}$ mice, a laboratory model for atherosclerosis, were crossed with $LPLA2^{-/-}$ mice, Taniyama *et al.* observed an increased number of atherogenic lesions, suggesting that LPLA2 presence might mitigate the development of atherosclerosis by reducing apoptosis in macrophages and consequently reducing thrombogenicity of the atherogenic plaque (Mallat & Tedgui, 2001). As such, LPLA2 was proposed to a have dual role in apoptosis prevention. First, it might be responsible for oxidized LDL degradation in lysosomes. In $LPLA2^{-/-}$ mice accumulation of oxidized LDL leads to their encapsulation by macrophages, followed by foam cell formation during the first stages of plaque development (Maiolino *et al.*, 2013). Second, LPLA2 reduces ceramide levels by converting it into inert 1-O- acylceramides. Ceramide levels are known to increase in lipoproteins found in atherogenic lesions and may in itself enhance the atherogenicity of lipoprotein particles (Auge, Nègre-Salvayre, Salvayre, & Levade, 2000).

1.3 LCAT, a cholesterol esterifying enzyme

1.3.1 Primary sequence and structure predictions

As mentioned above, mature LCAT is 49% identical in sequence to LPLA2. Sequence similarity is equal throughout the sequence with notable exceptions at the N- and C- termini and the signal sequence which contains 24 amino acids and is unrelated to that of LPLA2 (C. Y. Yang, Manoogian, Pao, & Lee, 1987).

Yang *et al.* first recognized the resemblance of the LCAT active site to those of serine esterases, such as trypsin, carboxylesterase and pancreatic lipase, and identified S181 as a part of GxSxG consensus (C. Y. Yang *et al.*, 1987). S181 was later confirmed as an active site serine via site-directed mutagenesis (Francone & Fielding, 1991b; Qu, Fan, Blanco-Vaca, & Pownall, 1994).

Using threading algorithms, Peelman *et al.* predicted that LCAT has an α/β hydrolase fold consisting of a central parallel 7–stranded β-sheet (Peelman *et al.*, 1998). To be consistent with the nomenclature for other α/β hydrolases (Ollis *et al.*, 1992), the first LCAT β-strand was designated as β2. Such arrangement places S181 in the position of the nucleophile elbow at a sharp turn between β-strand 5 and helix 5-6 (Fig. 3). The same authors also identified and confirmed by mutagenesis residues composing the catalytic triad, H377 and D345, and what they believed was the oxyanion hole, composed of L182 and F103.

Peelman *et al.* also proposed an existence of a “lid”, a domain similar to the one found in many lipases where it serves to close off the hydrophobic active site when the enzyme is not engaged in catalysis. Many such lids are set apart by a disulfide bridge. LCAT has six cysteine residues with positions 50-74 and 313-356 forming disulfide linkages (C. Y. Yang *et al.*, 1987). LCAT C50-C74 region was proposed to be homologous to the C60-C97 lid domain of *Candida rugosa* lipase. Consistent with this, its deletion completely abolished LCAT activity (Peelman *et al.*, 1998).

Recently, another LCAT model was created using the Robetta web server (Sensi *et al.*, 2014). Authors of this manuscript came to similar conclusions as Peelman *et al.*, regarding the overall α/β fold, catalytic triad, oxyanion hole and lid positions. In addition

they presented the first model of LCAT elements outside of the hydrolase domain including the whole LCAT sequence into prediction. The extreme N-terminus of LCAT was built *ab initio*. Overall, this model predicts a very open cholesterol-binding site crowned by the lid, with all additional elements composing a single domain with a β-sheet at its center. As will be shown later (Chapter 4.6), this model is incorrect, reflecting difficulties in modeling structures of proteins with low homology to unknown structures.

Both of these models place C31 and C184 in the vicinity of the active site. Their role in LCAT activity was probed through modification and mutagenesis. Jauhiainen *et al.* used monofunctional (dithionitrobenzoic acid and *p*-aminophenylarsendichloride) and bifunctional reagents (*p*-bromoacetylaminophenylarsenonide) to probe these cysteines (Jauhiainen & Dolphin, 1986; Jauhiainen, Stevenson, & Dolphin, 1988). The bifunctional reagent completely inhibited LCAT phospholipase and acyltransferace activity and suggested a vicinal position of the two cysteines at a distance of 3.5 – 3.6 Å between their sulfur atoms. Interestingly, both dithionitrobenzoic acid and *p*-aminophenylarsendichloride modifications inhibited acyltransferase, but not phospholipase activity, suggesting that either C31 or C184 or both are located at the acceptor-binding site. Cysteine substitution with a small amino acid glycine, C31G or C184G, had no effect on LCAT activity, confirming that cysteine residues themselves do not participate in catalysis but are rather located in the close proximity to the active site (Francone & Fielding, 1991a). C31 substitution to hydrophobic amino acids (C31Y, C31F and C31I) enhanced LCAT transacylase activity at least 50% compared to the wild type enzyme, indicating that hydrophobic interaction might participate in acceptor binding. Recombinant LCAT protein, mutated to enhance its catalytic activity, was patented as a therapeutic for the treatment of atherosclerosis, thrombosis, coronary heart disease and for the decrease or prevention of cholesterol accumulation (Boone, Meininger, Schwarz, & Shan, 2012).

1.3.2 LCAT N- and O-linked glycosylation

Plasma LCAT is heavily modified with N- and O-linked glycosylation that can constitute up to 25% of its mass. Glycosylation directly or indirectly (through effects on protein secretion and/or stability) affects LCAT activity. As a result, under glycosylated LCAT expressed in baculovirus-infected Sf21 cells had reduced activity compared to plasma LCAT or recombinant protein expressed in CHO cells (Miller, Wang, Sorci-Thomas, Anderson, & Parks, 1996). The majority of polysaccharide modifications of plasma LCAT are N-linked, and LCAT treatment with peptide N-glycosidase F (PNGaseF), which removes all N-linked sugars under denaturing conditions, reduces the apparent LCAT molecular weight (MW) to the expected 46kDa (Collet & Fielding, 1991). However, mass spectrometry also identified O-linked glycosylation at T407 and S409 consisting of sialylated galactose β1→3N-acetylgalactosamine structures. LCAT O-linked glycosylation was not extensively studied and its role is unknown (Schindler, Settineri, Collet, Fielding, & Burlingame, 1995). However, C-terminally truncated LCAT ($LCAT_{1-401}$) retains full acyltransferase activity, suggesting that O-glycosylation does not play an important role in an enzyme function (Francone, Evangelista, & Fielding, 1996; Y. P. Lee *et al.*, 1997).

N-linked glycosylation occurs at N20, N84, N272 and N384 (Fig. 3). Electrospray ionization mass spectrometry identified polysaccharide composition at positions N20, N84 and N272 to consist of triantennary and at N384 of biantennary complex structures (Schindler *et al.*, 1995). LCAT is a secreted protein and N-glycosylation is important for its expression. Thus, tunicamycin, an inhibitor of the first step of N-glycosylation in the endoplasmic reticulum (Elbein, 1987), completely abolishes active LCAT expression in CHO cells. Similarly, inhibition of the first stages of N-glycan processing in the endoplasmic reticulum, such as with castanospermine, deoxynojirimycin or methyldeoxynojirimycin, also resulted in the secretion of inactive LCAT. However, inhibitors of the later stages in N-glycan processing, such as by swainsonine or deoxymannojirimycin, had no effect on LCAT secretion and activity (Collet & Fielding, 1991).

Multiple groups have tried to distinguish the roles of individual N-glycosylation sites via site-directed mutagenesis (Francone, Evangelista, & Fielding, 1993; Kosman &

Jonas, 2001; O *et al.*, 1993; Qu, Fan, Blanco-Vaca, & Pownall, 1993). The greatest impact on LCAT expression and acyltransferase activity is caused by substitutions at N84 and N272. The effect of mutation at N272 varied from a lack of expression for N272T (Qu *et al.*, 1993) to reduced acyltransferase activity for N272Q (1% and 14% of wild type for acyltransferase and phospholipase activities, respectively (Francone *et al.*, 1993)). A mutation of N84 also coincided with significant loss of LCAT transacylase activity from 8% relative to wild type for N84Q and to 26% for N84T (Francone *et al.*, 1993; Qu *et al.*, 1993). Disruption of N-linked glycosylation at positions N20 or N384 had very little effect on LCAT activity or protein expression levels.

The potential function of N-glycosylation in maintenance of LCAT stability was investigated using the N84Q and N384Q mutants (Kosman & Jonas, 2001). In agreement with previous data, the N384Q mutant had activity similar to the wild type LCAT, but it gradually declined over the course of a 7-month incubation at 4 °C whereas wild type activity remained essentially the same. Circular dichroism (CD) and 8-Anilino-1-naphthalenesulfonic acid (ANS) fluorescence studies confirmed that N384Q denatures at a faster rate then wild type LCAT. N84Q CD spectra and ANS fluorescence curves closely resemble those of N384Q after denaturation and suggest that substitution at position N84 increases the rate of LCAT denaturation even further. Thus, LCAT glycosylation probably prevents denaturation and aggregation of this enzyme in plasma.

1.3.3 HDL composition

Like LPLA2, LCAT can either hydrolyze phospholipids or perform a transesterification reaction, transferring a fatty acid from the *sn-2* position of glycerophospholipids to cholesterol (Fig.5). *In vivo* this reaction primarily takes place on high density lipoprotein (HDL) particles and low density lipoprotein (LDL) particles. Based on their electrophoretic mobility on agarose gels, HDL and LDL particles are also called α- and β- lipoproteins, respectively. LDL particles are metabolic products of very low-density lipoproteins and mainly serve to remove excess triglycerides from peripheral tissues. In contrast, HDL particles remove excess cholesterol in the form of cholesterol esters and deliver it to either sterogenic tissues for utilization in metabolic processes or to the liver for degradation.

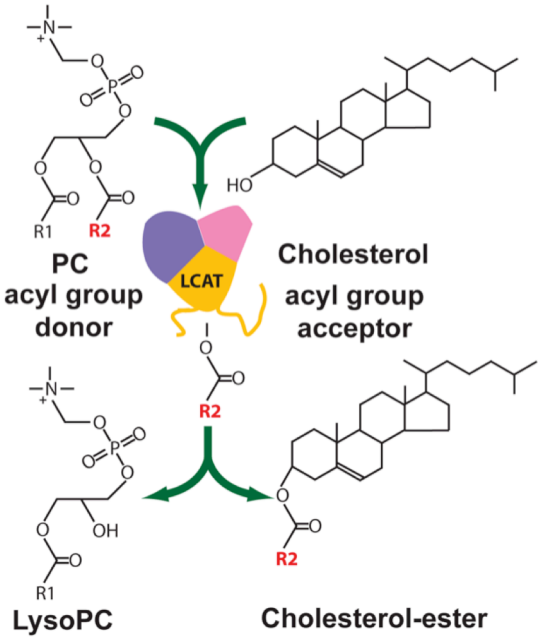

Figure 5. LCAT acyltransferase reaction

HDLs and LDLs have very different lipid and protein content (Table 1). The most abundant protein in HDL particles is ApoA-I, followed by ApoA-II and minor apo-proteins (ApoE and ApoCs) (Jonas & Phillips, 2008). The only protein component of LDL particles is ApoB100 (Segrest, Jones, De Loof, & Dashti, 2001).The majority of lipids on HDL and LDL particles are cholesterol, cholesterol esters, glycerol- and phospholipids. Phospholipids are primarily represented by phosphatidylcholine (PC), sphingomyelin, and minor amounts of lysoPC. Lipid acyl group composition is represented by palmitic (16:0), stearic (18:0), oleic (18:1), linoleic (18:2) and arachidonic (20:4) fatty acids (Jonas & Phillips, 2008).

1.3.4 LCAT association with lipoprotein particles

The rates of LCAT hydrolase and acyltransferase reactions on lipoprotein interfaces strongly depend on the kinetics of LCAT binding to HDLs and LDLs, which in turn depends on interaction with lipids and apo-proteins. Based on the discrepancies between LCAT enzymatic activity HDL-binding constants, it is generally accepted that LCAT catalytic reaction on lipoprotein particles can be divided in two steps. The first step is lipid binding, which is independent of apoproteins (Bolin & Jonas, 1994). The second step is LCAT activation by lipoproteins.

LCAT catalysis on the lipoprotein interface is affected by pH and salt concentrations. Highest LCAT activity is observed at 0.15M NaCl, the physiological salt concentration in human plasma. At that salt concentration, the pH optimum of the enzyme is 8.5 (Jonas, Daehler, & Wilson, 1986). Salt concentration has no effect on LCAT hydrolysis of the soluble substrates

Lipid composition can also affect LCAT binding. As such, sphingomyelin inhibits LCAT activity in a concentration-dependent manner by impairing its binding to the lipid interface (Bolin & Jonas, 1996). On the other hand, the presence of 14% cholesterol in 1-palmitoyl-2-oleoyl PC (POPC) vesicles increases LCAT binding affinity 4-fold (from 2.2 μM Kd to 530 nM), as measured using radiolabeled LCAT and ApoA-I (Miller & Parks, 1997).

Overall, LCAT is only transiently associated with lipoprotein particles and falls off after each catalytic cycle. As such, the dissociation rate constant for HDLs and LCAT is identical to the LCAT catalytic rate constant (0.05 s^{-1}), suggesting that LCAT falls

Table 1. Composition of HDL and LDL particles.

	LDL	HDL
size, Å	250	120-70
total protein, (% weight)	20-25	52-60
ApoA-I, (% protein weight)	-	70
ApoA-II, (% protein weight)	-	20
ApoB-I, (% protein weight)	100	-
ApoCs and ApoE, (% protein weight)	-	10
total lipid, (% weight)	75-80	40-48
phospholipids, (% lipid weight)	28-30	42-51
cholesterol, (% lipid weight)	10-12	6-8
cholesterol ester, (% lipid weight)	47-51	24-45
glycerolipids, (% lipid weight)	7-11	6-7

Adapted from (Jonas & Phillips, 2008) and (Segrest et al., 2001).

off HDL particles after each catalytic cycle (Adimoolam, Jin, Grabbe, Shieh, & Jonas, 1998).

1.3.5 Substrate selectivity. Donor preference

As in LPLA2, LCAT glycerophospholipids selectivity is influenced by their head groups and length and saturation of the acyl groups. LCAT prefers neutral phospholipid head groups, such as ethanolamine and choline. Intermediate LCAT activity can also be observed with phosphatidylglycerol. Phosphatidylserine and phosphatidic acid are the poorest LCAT substrates (Pownall, Pao, & Massey, 1985).

Human LCAT can hydrolyze a wide range of diacyl-phospholipids as a part of reconstituted HDL particles, from C12:0 to C22:6, with arachidonic acid being a notable exception. The highest rate of cholesterol transesterification was observed with linoleic (18:2), erucic (22:1) and docosohexaenoic (22:6) fatty acids (Grove & Pownall, 1991). Comparing more physiological phospholipids, containing palmitic acid in the *sn-1* position and various unsaturated fatty acids in *sn-2*, human LCAT had the highest rate of cholesterol transesterification with 1-palmitoyl-2-oleoyl PC (POPC) followed by 1-palmitoyl-2-linoleoyl PC (PLPC) with the lowest rate corresponding to the longest and most unsaturated phospholipids PAPC, 1-palmitoyl-2-eicosa-pentaenoyl PC and PDPC (Parks, Thuren, & Schmitt, 1992). The nature of the double bonds in unsaturated glycerophospholipids, and, hence, membrane fluidity, also has an effect on LCAT activity. Thus, LCAT transacylase activity on trans 18:1 or 18:2 fatty acid in *sn-2* position is at least five times lower then for equivalent cis- acyl groups (Parks, Huggins, Gebre, & Burleson, 2000).

Interestingly, LCAT from other mammalian species have different preferences for fatty acid content. Notably, rat, dog and sheep LCATs can readily utilize diarachidonyl PC (Grove & Pownall, 1991). Parallel comparison of human and rat LCAT specificity for POPC or PAPC incorporated in recombinant HDL particles revealed that rat LCAT could utilize both phospholipids equally (PAPC/POPC ratio is 0.97) whereas human LCAT prefers POPC (PAPC/POPC ratio is 0.33). Alteration of human LCAT specificity can be achieved by a single substitution, E149A, (Fig. 3) converting it into the rat enzyme (J.

Wang, Gebre, Anderson, & Parks, 1997; Zhao, Gebre, & Parks, 2004; Zhao, Wang, Gebre, Chisholm, & Parks, 2003). It was proposed that Glu149 is located in the vicinity of the active site and the charge of Glu149 of the human enzyme hinders the binding of long-chain fatty acids.

LCAT has a clear positional specificity for acyl groups in *sn-2* position. Thus, in the presence of symmetric phospholipids, LCAT transfers acyl groups from *sn-2* positions with almost 100% selectivity, independent of the chain length or saturation state (from palmityc to arachidonic acids) (Liu, Subramanian, & Subbaiah, 1998). However, human LCAT has considerable *sn-1* activity if the *sn-2* position is occupied by an extra long polyunsaturated fatty acid, such as arachidonic or docosohexaenoic acids. In such cases the nature of fatty acid in *sn-1* position is the primary determinant of LCAT positional specificity. For example, if arachidonic acid is present in the *sn-2* position and palmitic in *sn-1*, almost half of synthesized cholesterol ester will be palmitoyl-cholesterol. This *sn-1*/*sn-*2 ratio decreases with increased length of fatty acid in the *sn-1* position (Liu *et al.*, 1998; Subbaiah, Liu, & Paltauf, 1994). In agreement with disparate specificity of rat LCAT, its positional specificity is not altered dramatically by the presence of long unsaturated fatty acids in the *sn-2* position (Liu *et al.*, 1998).

In addition to glycerophospholipids, LCAT can use platelet activation factor (PAF) as a substrate. This reaction does not require lipoprotein cofactors and results in the formation of lysoPAF and acetate in the hydrolase reaction or, if lysoPC is present, of lysoPAF and the 1-acyl derivative of PAF. These reactions lead to PAF inactivation and, as such, LCAT might play a role in PAF metabolism. However, this reaction is about ten times slower than the rate of the forward reaction of cholesterol esterification and about 200 times slower than PAF hydrolysis by PAF-acetylhydrolase (Liu & Subbaiah, 1994). In addition to PAF, LCAT is able to hydrolyze and inactivate other oxidized polar phospholipids (Goyal, Wang, Liu, & Subbaiah, 1997). Because LDL oxidation is an early event during atherosclerosis, LCAT might be involved in preventing an accumulation of oxidized lipids in LDL particles in plasma, thereby maintaining healthy lipid metabolism in humans (Itabe *et al.*, 1999).

1.3.6 Substrate and acceptor selectivity

In the presence of suitable acceptors, LCAT transfers an acyl group from a phospholipid donor to an alcohol, forming an ester bond. The most efficient LCAT acceptors are sterols, however it can also esterify primary aliphatic alcohols. Esterification of aliphatic alcohols strongly depends on their chain length. The best aliphatic alcohol acceptor is 1-O-hexadecanol and increasing or decreasing its acyl chain progressively reduces its esterification by LCAT (Kitabatake, Piran, Kamio, Doi, & Nishida, 1979).

Cholesterol is the most abundant sterol in plasma of healthy humans and is a good acceptor for the acyl group in transesterification reaction. However, other sterols can also serve as acceptors in transacylase LCAT reaction. The general rules for sterols to be efficient acceptors are: 1) β-configuration of hydroxyl group at C3 and 2) the A and B rings have to be in either planar or trans configuration. Sterols that do not satisfy these requirements, such as coprostanol, epicholesterol, epicholestanol, or epiandrosterol have at least a 100-fold lower esterification rate then cholesterol. Modifications of the aliphatic tail of the cholesterol do not have a profound effect on LCAT activity. The addition of a double bond at C22 and extra acetyl group at C24 reduces the sitosterol esterification rate by about 50%. Complete removal of the aliphatic side chain leads to a slight increase in androsterol esterification rate (Piran & Nishida, 1979). The same rules for LCAT acceptors were shown to apply *in vivo* when LCAT was assayed on sterols derived from plasma of Smith–Lemli–Opitz syndrome and sitosterolemia patients, which have increased amounts of plant sterols in their plasma (Lin, Steiner, Merkens, Pappu, & Connor, 2010). Oxisterols are also good LCAT acceptors. 27-hydroxycholesterol, for example, has the same esterification rate as cholesterol (Szedlacsek *et al.*, 1995).

LCAT is able to at least partially reverse the cholesterol esterification reaction. When LCAT was incubated with proteoliposomes containing doubly labeled [^{3}H]cholesterol-[^{14}C]oleate, the formation of cholesterol-[^{14}C]oleate and [^{3}H]cholesterol-linoleate was observed but not [^{14}C]PC, indicating that the reversal is limited to the acyl transfer step of the enzymatic reaction (Sorci-Thomas, Babiak, & Rudel, 1990).

LCAT also possesses lysolecithin acyltransferase activity. In this transesterification reaction, LCAT uses an extra lysoPC molecule as an acceptor for the acyl group. Such reactions can occur on LDL particles which have significant lysoPC content (Jonas & Phillips, 2008; Liu & Subbaiah, 1993; Subbaiah & Bagdade, 1978; Subbaiah, Albers, Chen, & Bagdade, 1980).

1.3.7 LCAT activation by apoproteins

Very early in LCAT studies it was found that LCAT activity on lipoproteins is significantly enhanced in the presence of protein cofactor derived from HDL particles (C. J. Fielding, Shore, & Fielding, 1972). It was shown that ApoA-I, ApoA-II ApoE and ApoCs increase the V_{max} of LCAT esterification reactions on HDLs or LDLs when using either cholesterol or lysoPC as acceptors, with ApoA-I having the greatest effect (Jonas, Sweeny, & Herbert, 1984; Liu & Subbaiah, 1993; Zorich, Jonas, & Pownall, 1985). Activation happens at or before the acyl-intermediate formation step and, as such, can affect both esterase or transacylase reactions of LCAT (Yokoyama, Fukushima, Kupferberg, Kézdy, & Kaiser, 1980). However, apolipoproteins do not affect the rate of hydrolysis for soluble substrates of LCAT (Bonelli & Jonas, 1989) suggesting that activation is only important for LCAT action on lipid surfaces.

Multiple laboratories investigated the region of ApoA-I responsible for LCAT activation. Deletion of helixes 6 and 7 (amino acids 143-164, 165-186 or the whole region 148-186) from ApoA-I almost completely abolished LCAT activation (Minnich *et al.*, 1992; Sorci-Thomas, Kearns, & Lee, 1993). However, deletion of other regions in the ApoA-I N- and C-terminal region (amino acids 66-87, 99-120, 187-208, 209-219 and 212-233) also significantly reduced LCAT activation (Minnich *et al.*, 1992; Sorci-Thomas *et al.*, 1993). In addition, there are known mutations in humans in the central ApoA-I region that are characterized by reduced ability to activate LCAT (E110K, V156E and H162Q) (Hoang, Huang, Sasaki, & Sviridov, 2003).

LCAT regions responsible for enzyme activation by apoproteins is not well defined. However, natural LCAT mutations causing fish eye disease (described later), such as T123I, N131D and N391S are thought to interfere with either HDL binding or the ApoA-I activation mechanism (Vanloo *et al.*, 2000). Inaccessibility of amino acids

121-136 to antibody binding upon LCAT interaction with lipoproteins further suggests that the α3-4 helix, defined by Peelman *et al.* (Peelman *et al.*, 1998), is in close proximity to the potential LCAT-ApoA-I binding interface (Murray *et al.*, 2001).

Interestingly, an amphiphilic docosapetide unrelated to apoproteins in its sequence is also able to activate LCAT, albeit to a lesser extent then the ApoA-I protein (18% cholesterol esterification rate and 50% fatty acid release) (Yokoyama *et al.*, 1980), suggesting that amphipathic helixes have the ability to activate LCAT.

1.3.8 LCAT and reverse cholesterol transport

LCAT binds to nascent discoidal pre-β HDL particles, generated from lipid-free or lipid-poor ApoA-I lipidation via ABCA1 transporter (Fig.6). Only one LCAT molecule can bind per HDL particle (Bolin & Jonas, 1994). LCAT activation by ApoA-I results in cholesterol esterification and formation of very hydrophobic cholesterol esters that migrate into the core of HDL particles. This results in the formation of mature spherical α-HDLs which are distinguished by increased amount of cholesterol esters compared to discoidal pre-β HDL (Kunnen & Van Eck, 2012).

Very early after LCAT discovery, Glomset *et al.* recognized its role in reverse cholesterol transport (RCT) (Glomset, Janssen, Kennedy, & Dobbins, 1966). Conversion of cholesterol to cholesterol-esters on HDL particles creates a gradient of cholesterol between lipoproteins and cell membranes and allows for cholesterol efflux from peripheral tissues and macrophages, preventing cholesterol transport back to extrahepatic tissues. Cholesterol transport itself could proceed either by passive diffusion or via active export through the ABCG1 transporter. α-HDLs then deliver the excess cholesterol to hepatocytes in the liver to be ultimately secreted in the form of bile salts (Kunnen & Van Eck, 2012).

Currently, however, the role of LCAT in reverse cholesterol transport is being questioned. The controversy arose due to new insights into the mechanism of cholesterol efflux from the cells, which, as opposed to previous data, is an ATP-dependent process happening through multiple transporters and thus should not depend significantly on the gradient of

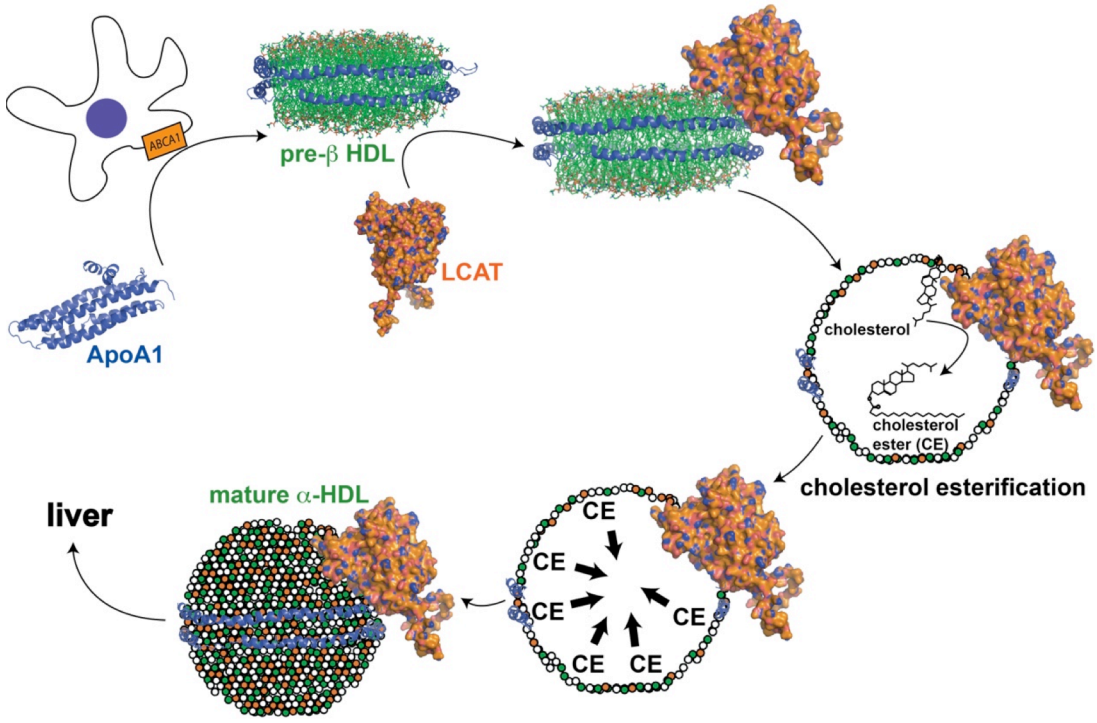

Figure 6. LCAT role in HDL maturation.

cholesterol. In addition, patients with LCAT deficiency accumulate cholesterol only in certain tissues, such as corneas, kidneys, and erythrocytes.

Many studies using transgenic animals have been done to determine the effect of LCAT gene deletion or overexpression on the cholesterol levels in an attempt to find a link between LCAT activity and atherosclerosis and cardiovascular disease. Unfortunately, the results of these studies are inconsistent with each other partially due to the use of different model systems (reviewed in (Kunnen & Van Eck, 2012)). Thus, the role of LCAT in atherosclerosis remains to be determined. However, even now, LCAT biotherapeutics are being patented for the treatment of “atherosclerosis, thrombosis, coronary heart disease and for decreasing or prevention of accumulation of cholesterol” in humans (Boone, Meininger, Schwarz, & Shan, 2012).

1.3.9 LCAT familial diseases

There are more then 90 different LCAT mutations described in humans that cause rare familial autosomal recessive diseases - familial LCAT deficiency (FLD) and fish eye disease (FED) (www.lcat.it). Usually, only homozygous mutations result in clinical phenotypes with heterozygotes retaining half-maximal HDL-associated cholesterol levels (Calabresi, Simonelli, Gomaraschi, & Franceschini, 2012). FLD patients completely lack LCAT activity in plasma on HDL and LDL lipoproteins (defined as α- and β- activity) (Fig. 7). Biochemical manifestation results in very low HDL- and LDL- associated cholesterol, low plasma cholesterol-ester levels, and highly variable levels of triglycerides. The FLD phenotype includes corneal opacification, proteinuria, and anemia. Morbidity is typically due to renal failure.

The FED phenotype is less severe compared to FLD and manifests only in corneal opacification due to cholesterol accumulation in corneas. In FED, LCAT activity on LDL particles is preserved (β-activity) while HDL-associated LCAT activity (α-activity) is significantly reduced. Consistent with the uncertain role of LCAT in atherosclerosis, FED and FLD patients do not seem to have an increased risk of cardiovascular disease (Calabresi *et al.*, 2012).

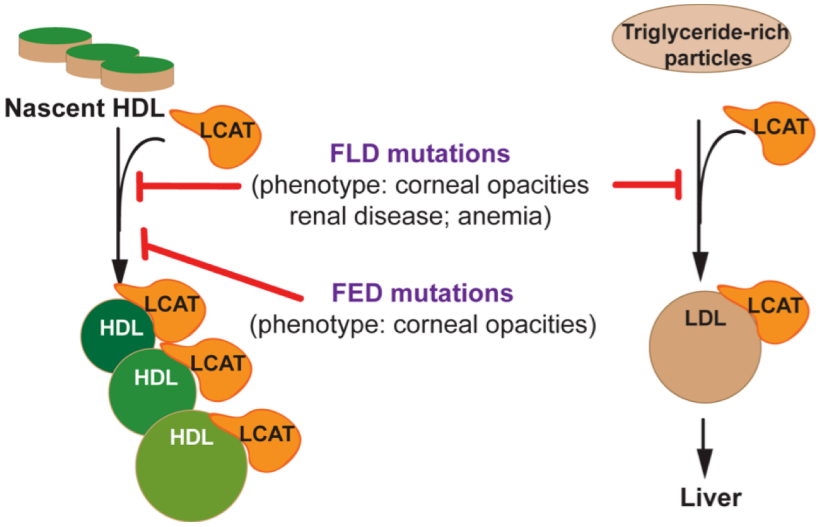

Figure 7. LCAT mutations causing FLD or FED phenotype differently affect LCAT association with different lipoproteins.

Chapter 2. LPLA2 and LCAT expression and deglycosylation.

2.1 Attempts to deglycosylate LPLA2 produced in HEK293T cells

The primary goal of this project was to crystallize and determine the structure of LPLA2 using the x-ray diffraction method. The Shayman laboratory had already purchased significant quantities of recombinant human LPLA2 containing a His_6 tag on its C-terminus from Proteos, Inc. The protein was expressed in HEK 293T cells and was purified in a glycosylated form. Although we were able to obtain crystals of LPLA2 (Chapter 3), they exhibited poor diffraction with severe anisotropy. We hypothesized that the poor diffraction quality was due to the presence of N-linked glycosylation, which occurs at four Asn residues (N66, N240, N256 andN365) and is very heterogeneous, constituting up to a quarter of LPLA2 apparent molecular weight (Hiraoka *et al.*, 2002). Thus, given large amount of available material, we attempted to remove sugar moieties posttranslationally using endo- and exoglycosidases.

2.1.1 LPLA2 deglycosylation with endoglycosidases

Endoglycosidases cleave the inner part of carbohydrates releasing intact sugar moieties. Several types of endoglycosidases exist, exhibiting different specificities for the polysaccharide moieties they cleave and, also, for their cleavage site within the polysaccharide chain.

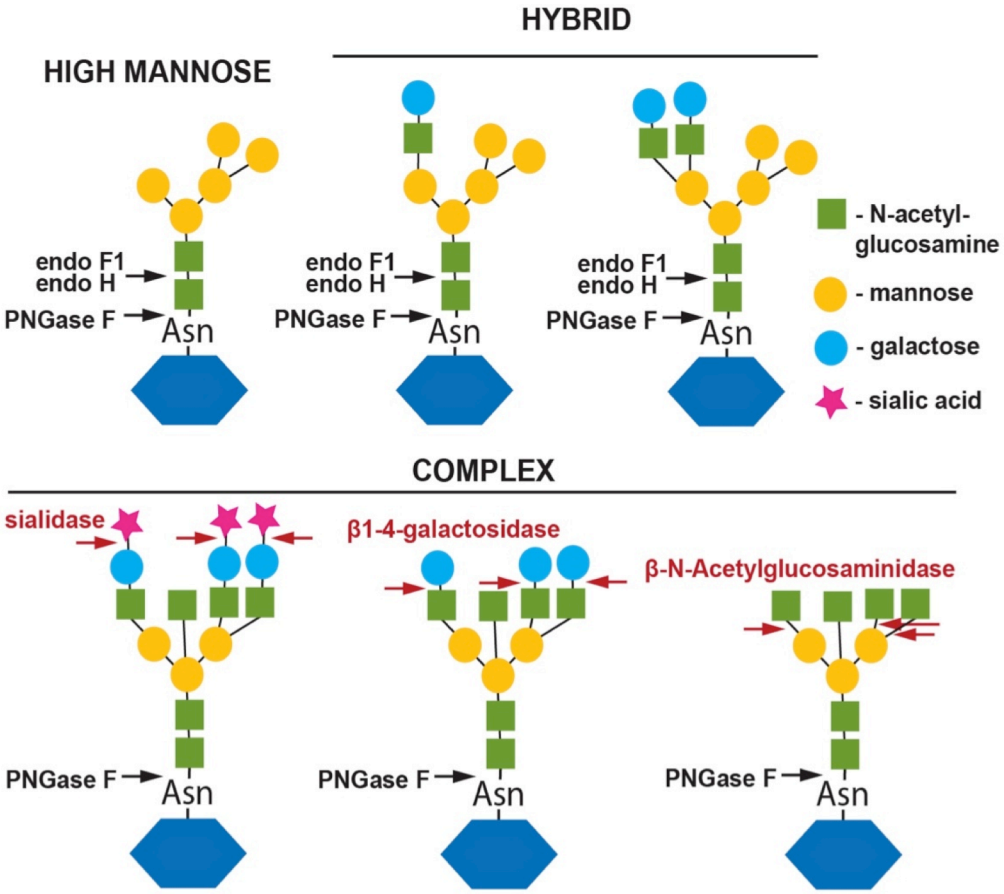

Figure 8. Types of carbohydrates and their susceptibility to endo- and exoglycosidases used in this study.

2.1.1.1 Cleavage with peptide-N-glycosidase F (PNGase F)

PNGase F cleaves between the innermost N-acetylglucosamine residue and Asn of the protein releasing the intact glycan chain and reducing the Asn to Asp. PNGase F has a very broad specificity for the polysaccharide chain and thus can cleave complex, hybrid, high- and low mannose chains (Maley, Trimble, Tarentino, & Plummer, 1989) (Fig. 8). PNGase F is more effective after sodium dodecyl sulfate (SDS)-denaturation of target proteins, presumably, due to increased accessibility of its cleavage site.

We digested LPLA2 with PNGase F (5:1) molar ratio in 20 mM HEPES pH 7.5, 150 mM NaCl at 20 °C and took samples at the indicated time points (Fig. 9). The assay was performed using both native and SDS-denatured LPLA2 (5 min incubation at 80 °C

with 0.5% SDS and 40 mM DTT). SDS-denatured LPLA2 is completely digested by PNGase F after 15 min of incubation judged by complete disappearance of the fuzzy LPLA2 band at 50 kDa (Fig, 9, 0') and an appearance of a well-defined band at 40 kDa (estimated molecular weight of glycan-free LPLA2 is 43 kDa). However, in the absence of SDS, only a small band of deglycosylated LPLA2 appears after 15' incubation. This band most likely represents the PNGase digest of the small fraction of denatured LPLA2 present in the sample, as it does not appear to increase after 1 h. Thus, it appears that PNGase F is able to deglycosylate only denatured LPLA2.

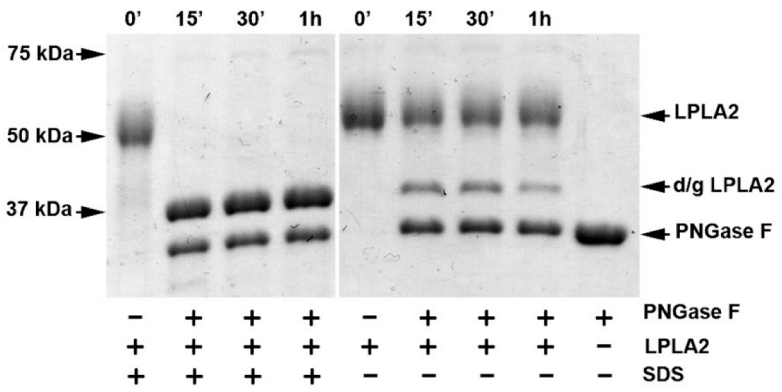

Figure 9. PNGase F deglycosylates LPLA2 efficiently only after SDS-denaturation. d/g LPLA2, deglycosylated LPLA2.

Next, we tried to determine if partial unfolding with detergents could promote PNGase digestion of LPLA2 (Fig. 10a). LPLA2 was incubated with PNGase F (3:1 molar ratio) in 50 mM HEPES pH 7.5 for 3 or 24 h in the presence of either 1% β-OG or 10 mM CHAPS (concentration of both detergents is just below their critical micelle concentration). Similar to the PNGase F digest of native protein, only a small fraction of LPLA2 is shifted to lower MW on the gel. The percentage of digested LPLA2 seemed to be independent of the detergent presence of and did not seem to increase after 24 h of incubation, in particular, in the samples incubated at 20 °C. Such behavior is, again, consistent with PNGase F acting on spontaneously denatured LPLA2.

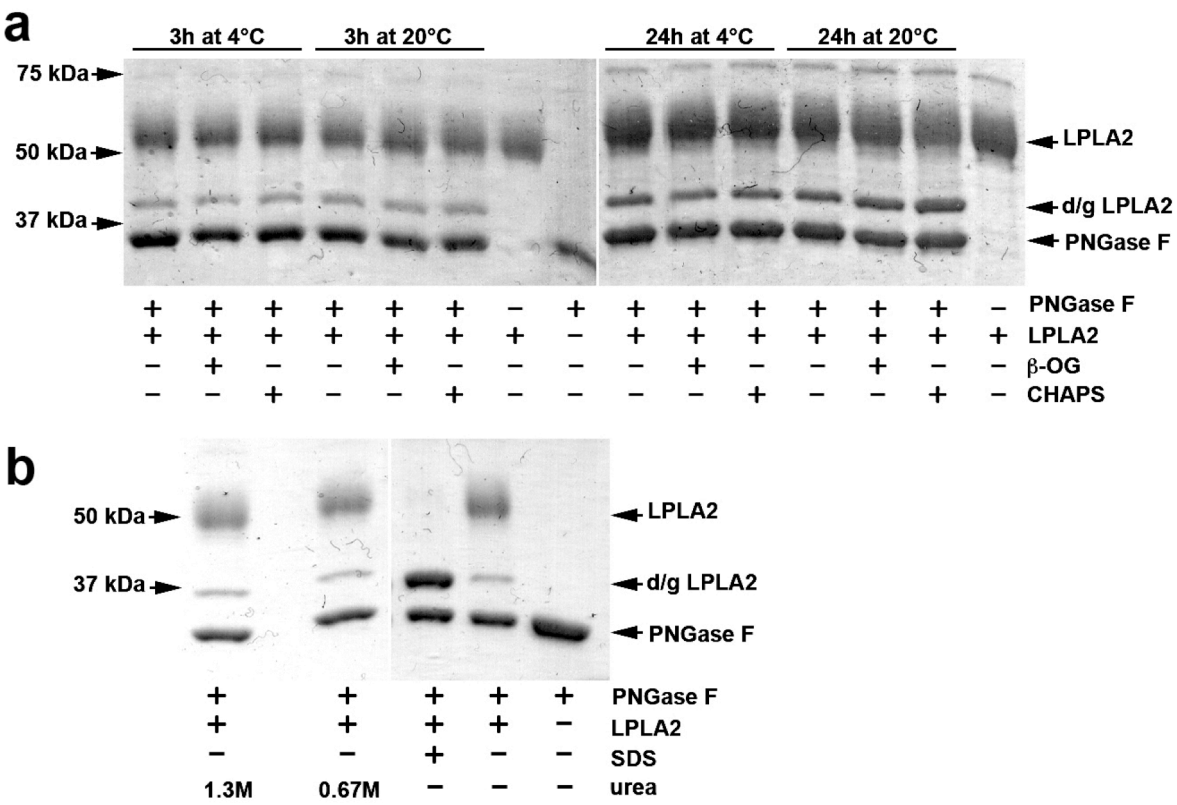

Figure 10. LPLA2 deglycosylation by PNGase F in the presence of mild detergents. **(a)** PNGase F digest in the presence of β-OG and CHAPS. **(b)** PNGase digest in the presence of urea.

As PNGase F is stable in up to 5 M urea (Maley *et al.*, 1989) we also tried various urea concentrations for partial LPLA2 unfolding (Fig. 10b). LPLA2, PNGase F and 0.67 or 1.3 M urea were incubated for 30' in conditions indicated for Fig. 10. Similarly to PNGase deglycosylation in the presence of other mild detergents, β-octylglucoside (β-OG) and CHAPS, no polysaccharide removal occurred. An increase of urea concentration to 4M also did not have any effect (data not shown).

In summary, any attempts to remove polysaccharide moieties from LPLA2 with PNGase F prove to be unsuccessful without complete SDS-denaturation the protein.

2.1.1.2 Cleavage with endoglycosidases Hf and F1

Endoglycosidases H (endo H) and F1 (endo F1) both hydrolyze polypeptide-attached carbohydrates between two inner-core N-acetyl-glucosamines (GlcNAc) leaving one GlcNAc attached to the asparagine residue of the protein. The enzymes have similar specificities for the carbohydrate moieties: both endo F1 and endo H cleave high-mannose or hybrid structures. Endo F1 could also cleave sulfated high mannose structures and endo H is very efficient in releasing polysaccharides with fucose attached to the core GlcNAc (Sigma-Aldrich Co. LLC, 2008; Trimble & Tarentino, 1991). Both enzymes have been successfully used for deglycosylation of native proteins for subsequent crystallization (V. T. Chang *et al.*, 2007; Grueninger-Leitch, D'Arcy, D'Arcy, & Chène, 1996). Endo Hf is an MBP-fusion of endo H and maintains the same properties and specificity.

First, we attempted to remove LPLA2 carbohydrates using endo Hf. We mixed 10 μg of native or SDS-denatured LPLA2 with 1000 U of endo Hf (NEB) in two different buffers – pH 7.5 (20 mM HEPES, 150 mM NaCl) or pH 5.25 (100 mM Na citrate; pH optimum for endo Hf (Sigma-Aldrich Co. LLC, 2008)) and incubated at 20 °C for 1 h (Fig. 11a) and for 24 h (data not shown). We observed no polysaccharide removal in any of the endo Hf containing samples, including the ones containing denatured LPLA2. To confirm that the enzyme was catalytically active in our reaction we have tested its activity using RNase B (Sigma) as a substrate (Fig. 11b). We tested both pH 6.0 and 4.5 (buffered by 100 mM Na citrate), and after 1 h at 37 °C, we observed complete deglycosylation indicated by a shift in apparent molecular weight of RNAse B, proving that endo Hf is capable of releasing carbohydrates at conditions tested. Its inability to deglycosylate LPLA2 is, therefore, most likely due to the complex structure of LPLA2 glycans, which are apparently unrecognizable by endo Hf.

Previously, LPLA2 partially purified from COS-7 cells overexpressing LPLA2 was shown to be sensitive to endo F1 digest (Hiraoka *et al.*, 2002). Thus, we tested our available LPLA2 preparation from HEK 293T cells for its susceptibility to endo F1. We expressed and purified endo F1 (plasmid was a kind gift from Dr. Warren, University of British Columbia) according to the previously described protocol (Kwan, Boraston,

McLean, Kilburn, & Warren, 2005). The enzyme was enzymatically active under the same conditions used for endo Hf treatment, judged by its ability to remove polysaccharides from RNase B (Fig. 11b). We next tested its ability to deglycosylate LPLA2 under the same conditions. We used 1:3 molar ratio of endo F1 to LPLA2 and the same buffers described for the RNase B digest. However, we observed no shift in the apparent molecular weight of LPLA2 at all temperatures tested (4, 20 and 37 °C), both pH (4.5 and 6.0) or after prolong incubation for 15 h. Increasing the enzyme concentration 5-fold (Fig. 11c, lane "5x endo F1") or SDS denaturation (Fig. 11c, lane 1) also did not promote LPLA2 deglycosylation.

Discrepancy with previously published data regarding LPLA2 sensitivity to endo F1 is probably due to the source of the protein. Hiraoka *et al.* used cell lysates for deglycosylation experiments, which likely did not contain mature LPLA2 since it was not yet fully processed for protein secretion (Hiraoka *et al.*, 2002). On the other hand, LPLA2 produced by Proteos, Inc. was purified in a secreted form from the cell media and thus most likely contained complex polysaccharide moieties resistant to endo Hf and endo F1.

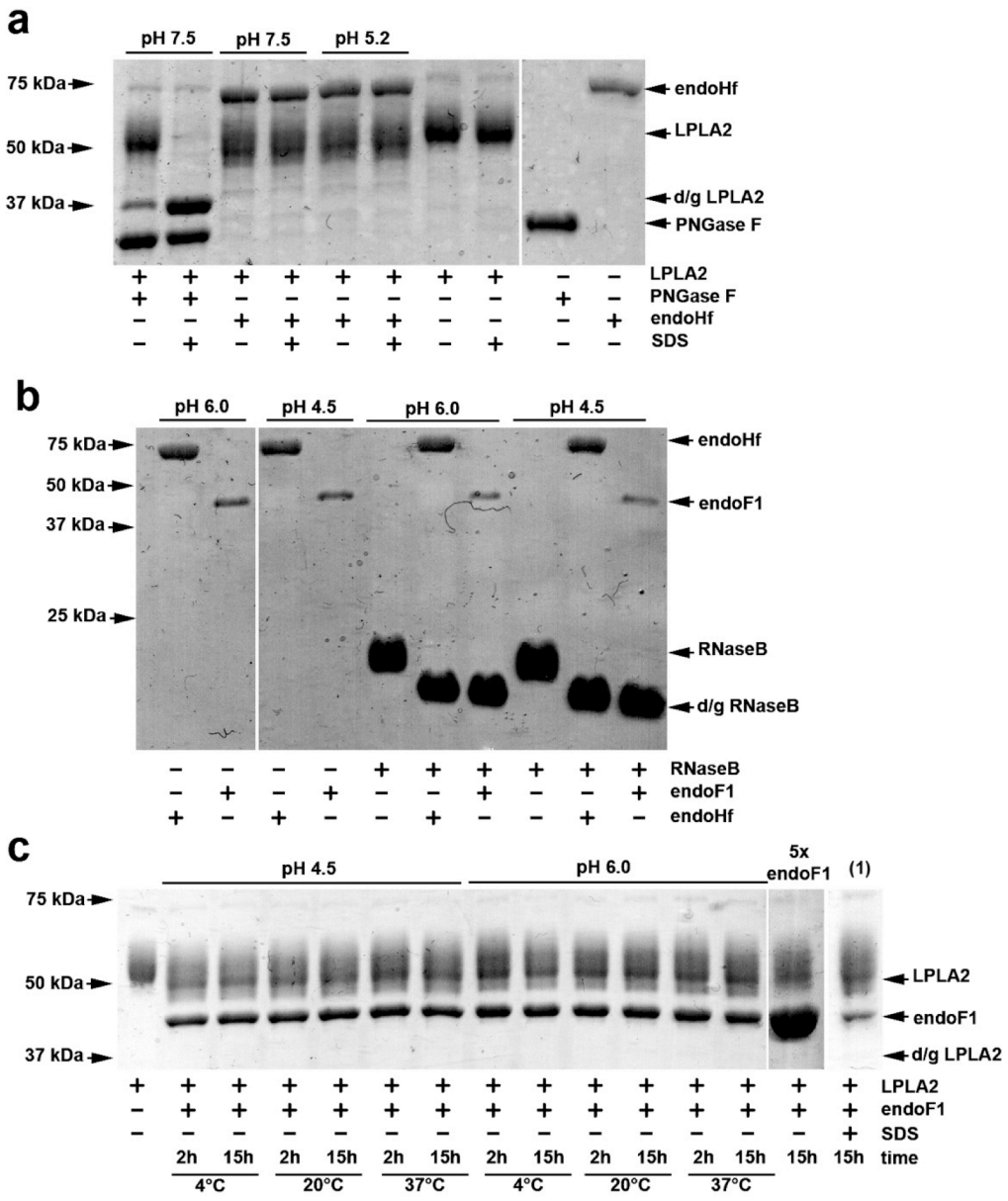

Figure 11. LPLA2 deglycosylation with endo Hf and endo F1 glycosidases. **(a)** LPLA2 deglycosylation with endo Hf. **(b)** RNase B deglycosylation with endo Hf and endo F1. **(c)** LPLA2 deglycosylation with endo F1.

2.1.2 LPLA2 deglycosylation with exoglycosidases

Next we attempted to use exoglycosidases in hopes to reduce glycosylation heterogeneity in native conditions. Exoglycosidases release terminal monosaccharides from the non-reducing end of polysaccharides. The specificity of exoglycosidases is usually determined by the type of monosaccharide they release and the type of the carbohydrate link.

First, we attempted to remove terminal sialic acid residues using sialidase (NEB). Sialidase removes sialic acid linked through α2-3, α2-6, and α2-8 bonds (www.neb.com). For this we incubated 13 μg of LPLA2 with 50 U of sialidase in 100 mM Na citrate pH 6.0 for 3 and 15 h at 4, 20 and 37 °C and looked for the shift in LPLA2 apparent molecular weight on Coomassie stained SDS-polyacrylamide gel electrophoresis (PAGE) gel (Fig. 12a). After 3 h at 4 °C we observed a small shift and compression of the LPLA2 band that was most likely due to reduced heterogeneity of the sample upon the sialidase treatment. Comparing results after 3 or 15 h we concluded that reaction was finished after 3 h. As only one sialic acid caps each branch of carbohydrates, it is conceivable that the modest shift we observed reflected the removal of all LPLA2-bound sialic acid residues. And, though the sample was still highly heterogeneous, as judged by the remaining broadness of the LPLA2

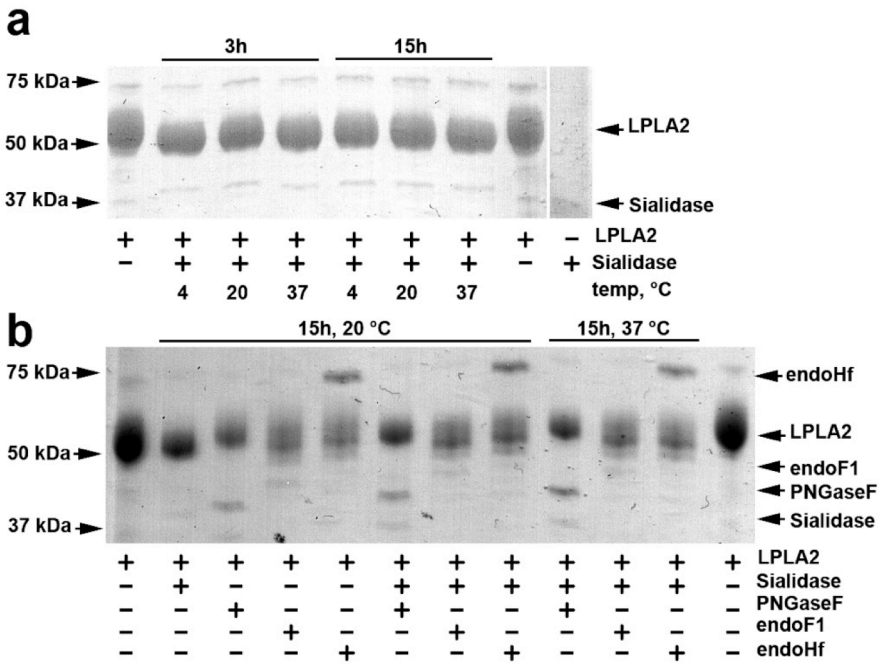

Figure 12. LPLA2 deglycosylation with endo- and exo-glycosidases. **(a)** LPLA2 digest with sialidase. **(b)** LPLA2 digest with a combination of sialidase and endo Hf or endo F1.

band after sialidase treatment, we proceeded with crystallization trials (Chapter 3). We have also attempted to combine sialidase with endo F1 in hopes that after the release of sialic acid from the reducing end of carbohydrates, the high mannose or hybrid glycosylation moieties suitable for endo F1 digest will be exposed. We performed the reaction in the same conditions as the sialidase digest for either 3 h (data not shown) or 15 h at 20 and 37 °C (Fig. 12b). We did not observe any additional glycan removal when combining sialidase with either endo F1 or endo Hf that could not be attributed to the action of sialidase alone.

Next, we attempted to include more exoglycosidases for sequential saccharide removal. We chose to use β1-4-galactosidase and β-N-acetylglucosaminidase (NEB), because these enzymes were readily available and because β1-4-galactose and β-N-acetyl-glucose are common components of complex carbohydrate moieties. For 7 μg of LPLA2 we used 36 pmol of endo F1, 25 U of sialidase, 4 U of β1-4-galactosidase and 2U of β-N-acetylglucosaminidase. All reactions were performed in 100 mM Na citrate buffer pH 6.0 at 20 °C for 5 h (data not shown) or 15 h (Fig. 13). Again, no additional shift in LPLA2 mobility was observed compared to the sample containing only LPLA2 and sialidase.

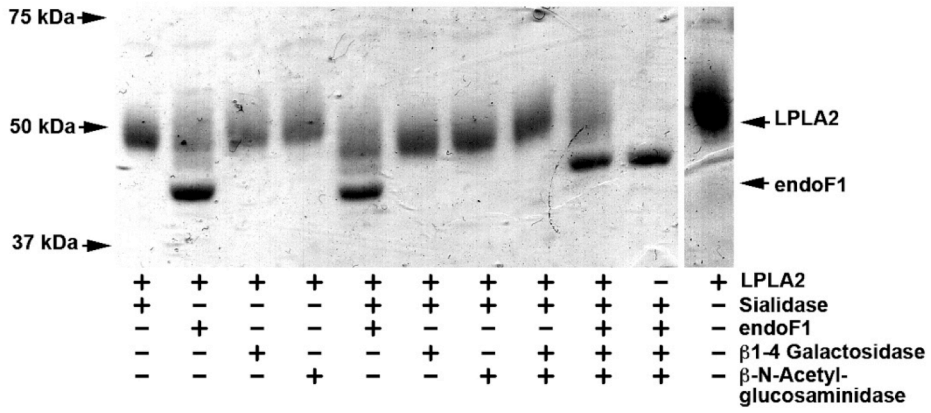

Figure 13. LPLA2 digest with various exoglycosidases.

Thus, the complex glycosylation moieties of LPLA2 either do not contain β1-4-galactose and β-N-acetyl-glucose, or, more likely, these residues are blocked by other monosaccharides at their reducing end and, thus, are not susceptible for digest with their respective exoglycosidases. And, though, there are many more exoglycosidases

available we have decided that without knowing the exact structure of LPLA2 carbohydrates it would be unwise to try them at random. Thus, we switched to new strategies with the goal of expressing LPLA2 with predefined glycan moieties.

2.2 LPLA2 expression in HEK 293S GnTi$^-$ cell line

To limit the complexity of glycosylation in mammalian expression systems several cell lines have been created with various mutations of the enzymes in the glycosylation pathways, such as a series of mutant CHO Lec cell lines bearing mutations conferring resistance to various lectins (Stanley, 1989). Similarly, Reeves *et al.* isolated a mutant HEK 293S cell line that was resistant to ricin (Reeves, Callewaert, Contreras, & Khorana, 2002), which lacked N-acetylglucosaminyltransferase I (GnTI) activity and was designated GnTI$^-$. Loss of GnTI activity resulted in N-linked glycans that have a common mannose$_5$GlcNAc$_2$ structure (Fig. 8, “high mannose”) that is very sensitive to endo H (V. T. Chang *et al.*, 2007).

First we attempted to establish a protocol for transient LPLA2 expression in adherent monolayers of HEK 293S GnTi$^-$ cells grown in DMEM high-glucose media, supplemented with 10% fetal bovine serum (FBS), 1 mM pyruvate, 2 mM L-glutamine, 100 U/ml penicillin, and 100 µg/ml streptomycin. The original plasmid, containing LPLA2, was provided by Proteos, Inc. and the encoded codon-optimized full-length LPLA2 gene, including its signal sequence, followed by a 6xHis tag and tobacco etch virus (TEV) protease cleavage site, followed by sequence corresponding to mature LPLA2 in PCEP4 plasmid. For convenience (PCEP4 plasmid is very large – 11 kb) the construct was subcloned into the smaller pcDNA4 vector (pcDNA4-LPLA2). When optimizing the expression protocol we varied cell confluence at the time of transfection, type and ratio of DNA transfection reagent and expression time. Aliquots of conditioned media were pulled from the Petri dishes at indicated time intervals (Fig. 14). At the end of the experiment (72 h) cells were trypsinized and cell lysates were also analyzed.

Fig. 14 shows a representative Western blot stained with anti-His antibodies (Sigma) from the best expression experiment. The gel mobility of LPLA2 expressed in HEK 293S GnTI$^-$ cells is intermediate between that of LPLA2 from HEK 293T cells containing complex carbohydrates and LPLA2 after PNGase deglycosylation under

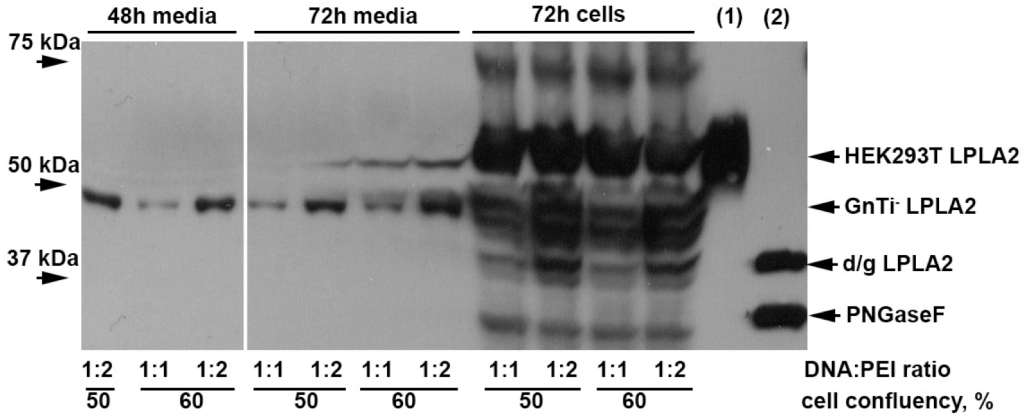

Figure 14. LPLA2 test expression in adherent HEK293S GnTi$^-$ cells. Conditioned cell media was collected at indicated time points and analyzed by the Western blot under denaturing conditions using anti-His_6 antibodies. At the end of the experiment, cells were harvested and analyzed. Lane (1), LPLA2 from HEK 293T cells, lane (2), LPLA2 from HEK293T cells after PNGase F digest.

denaturing conditions. This, together with the relative compactness of LPLA2 band, is consistent with a homogenous high-mannose type of LPLA2 glycosylation.

DNA:polyethylenimine (PEI) ratio has the most effect on the level of LPLA2 expression. In addition to the 1:1 and 1:2 ratios shown on Fig. 14, we have also tested 1:3 and 1:4 ratios (data not shown), however the 1:2 ratio produced the highest LPLA2 expression levels. We also tested the commercially available lipophilic transfection reagent TransIT (Myrus), however, the results were indistinguishable from PEI (data not shown). Cell confluency at the time of transfection did not significantly affect the levels of expression and could be raised up to 80% without drastic effects (Fig. 14 and data not shown). Protein expression can be detected as early as 48 h and LPLA2 levels continued to rise up to 96 h post transfection (data not shown). We also compared the levels of LPLA2 secreted into the media to LPLA2 retained inside the cells (Fig. 14 “72 h cells” vs. “72 h media”). Although the lysed cells had many contaminants that cross-reacted with anti-His antibodies, taking into account the relative volumes of conditioned media and cell lysates, we concluded that most of LPLA2 is being secreted. The small LPLA2 fraction observed from the “cells” sample most probably reflected the protein going through the maturation process inside the endoplasmic reticulum and Golgi apparatus.

Next, we performed a test expression and purification of the LPLA2 expressed in the HEK 293S GnTI$^-$ (GnTI$^-$ LPLA2) using the protocol yielding the highest LPLA2 levels. Cells were transfected using 1:2 DNA:PEI ratio at 80% confluency and the conditioned media was harvested 4 d later. Media from cells expressing LPLA2 was supplemented with HEPES pH 7.5 to a final concentration of 50 mM and then loaded on a 0.3 ml Ni-NTA-column. After washing with 10 ml buffer containing 20mM HEPES pH 7.5, 300 mM NaCl, and 10 mM imidazole pH 8, LPLA2 was eluted using the same buffer containing 200 mM imidazole pH 8.

The resulting sample was visualized on a silver-stained SDS-PAGE gel and Western blots with anti-His or anti-LPLA2 antibodies (Fig. 15). As can be seen from Fig. 15a, the sample of LPLA2 after Ni-column purification still contained many impurities, presumably due to the high serum content of the media (10%). GnTI$^-$LPLA2 treatment with endo F1 in native conditions or PNGase F treatment in the presence of SDS resulted in decrease of its apparent molecular weight and gel mobility becoming identical to that of PNGase F-treated denatured LPLA2 expressed in HEK 293T cells (Fig. 15c). Band corresponding

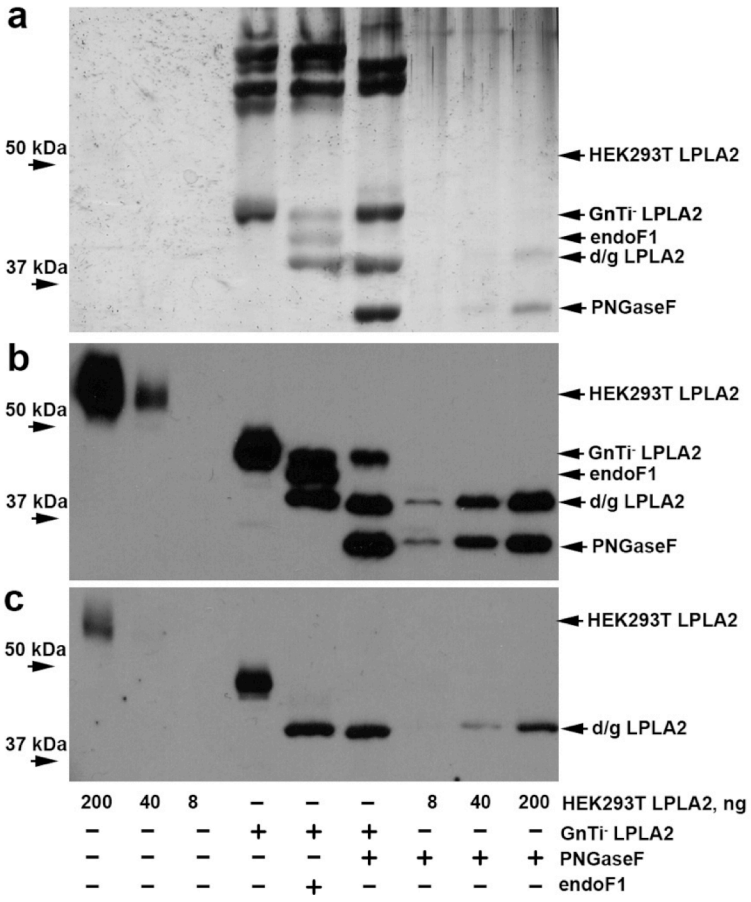

Figure 15. Deglycosylation of Ni-NTA purified LPLA2 produced in HEK293S GnTi$^-$ cells. (a) Silver stained SDS-PAGE gel. (b) The Western blot with anti-His antibodies. (c) The Western blot with anti-LPLA2 antibodies.

to endo F1-treated LPLA2 migrated slightly slower than PNGase F-treated LPLA2 due to the presence of four remaining GlcNAc (one at each of the four glycosylation sites) resulting in about 1 kDa difference between these LPLA2 species. Thus, LPLA2 expressed in HEK 293S GnTI$^-$ cells and secreted into the media is sensitive endo F1 treatment.

HEK 293S GnTI$^-$ cells can also be grown in suspension cultures to higher cell densities relative to adherent cells and could potentially produce the higher amounts of protein needed for crystallographic studies. Therefore, we began optimization of LPLA2 expression in suspension culture of HEK 293S GnTI$^-$ cells. We started by switching cells to shaking cultures in FreeStyle media containing 10% FBS. Although the cell growth and viability were unaffected, the protein expression levels were significantly lower then in corresponding adherent cultures (Fig. 16).

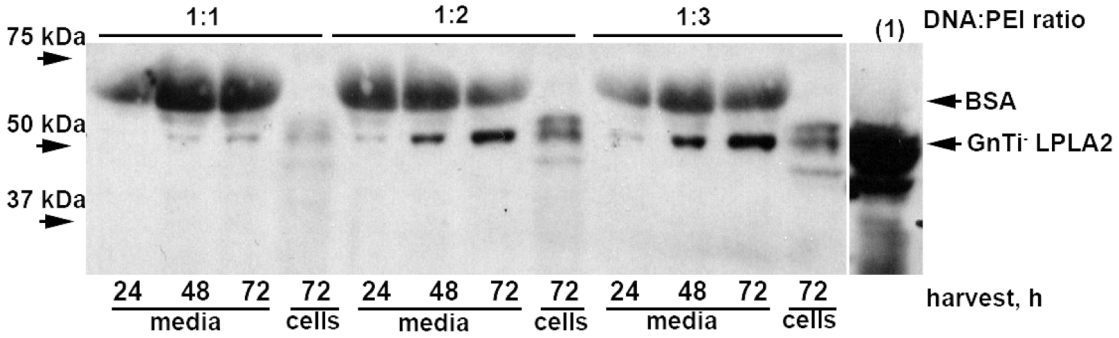

Figure 16. LPLA2 expression in suspension culture of HEK293S GnTi- cells. lane (1) shows LPLA2 expressed in adherent culture. Shown here is a Western blot with anti-LPLA2 antibodies.

Concurrently, Proteos, Inc. established a protocol for high-scale expression of LPLA2 from suspension HEK 293S GnTI$^-$ cells that was successful for purification for up to 2 mg of LPLA2 per l of media, which we adopted for all our subsequent LPLA2 expression and purification experiments. The protocol included gradual cell adaptation to the FreeStyle media with lower FBS content (0.5%), lowering DNA:transfection reagent ratio to 1:1.5 (this later proved to be not significant) and transfection at higher cell densities ($1.5x10^6$/ml instead of $0.7 x10^6$/ml we used before).

Thus our routine protocol for LPLA2 expression and purification from HEK 293S GnTI$^-$ cells for subsequent crystallization was as follows. HEK293S GnTi$^-$ cells were grown in suspension in FreeStyle media supplemented with 0.5% FBS. At a cell density

of $1.5x10^6$/ml cells were transiently transfected using a 1:2 molar ratio of pcDNA4-LPLA2:PEI and conditioned media was harvested 5 d later. Then, media was supplemented with HEPES pH 7.5 to a final concentration of 50 mM and then loaded on a 3 ml Ni-NTA-column. After washing with 100 ml buffer containing 20 mM HEPES pH 7.5, 300 mM NaCl, and 10 mM imidazole pH 8, LPLA2 was eluted using the same buffer containing 200 mM imidazole pH 8 (Fig. 17, lane 1). TEV (5% of total protein) and a 1:10 molar ratio of endoF1:LPLA2 were added to the eluate and the protein was dialyzed overnight at 4 °C against 20 mM HEPES pH 7.5, 100 mM NaCl, and 1 mM DTT (Fig. 17, lane 2). The protein was then passed through a second Ni-column to remove the cleaved His tag and undigested protein. The flow-through was further dialyzed against 20 mM HEPES pH 7.5 and 150 mM NaCl and then concentrated to 13 mg/ml (Fig. 17, lane 3). Yields were about 2 mg/l of media of pure and homogeneous sample that was suitable for crystallographic experiments (Chapter 3).

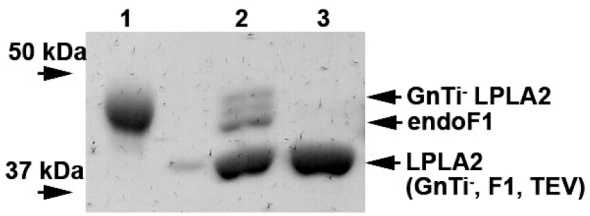

Figure 17. Purification of LPLA2 expressed in culture of HEK293F GnTi- cells. lane 1 – elution after the first Ni column, lane 2 – sample after TEV and endo F1 digest, lane 3 – final sample after the second Ni column. Coomassie stained gel from the SDS-PAGE under denaturing conditions.

The summary of different LPLA2 glycosylation species with corresponding glycan structures is shown on Fig. 18a. All shown LPLA2 glycoforms, with the exception of PNGase F-treated denatured LPLA2 have been crystallized (Chapter 3). As mentioned in the introduction (Chapter 1) LPLA2 glycosylation is important for its enzymatic activity and mutations abolishing N-linked glycosylation led to partial loss of LPLA2 activity (Hiraoka *et al.*, 2013). To validate that LPLA2 expressed in HEK293S GnTi$^-$ cells and deglycosylated with endo F1 ($LPLA2_{GnTI;F1}$) is functionally indistinguishable from LPLA2 expressed in HEK 293T cells, we performed comparative biochemical assays.

First, we compared the enzymatic activities of $LPLA2_{GnTI;F1}$ and LPLA2 expressed in HEK 293T cells using both soluble and liposome based substrate (Fig. 18b and c). LPLA2 can hydrolyze pNPB to *p*-nitrophenoxide and butyric acid. pNPB

(Sigma) was diluted to 10 mM using the reaction buffer (20 mM HEPES pH 7.5, 150 mM NaCl) containing 10% DMSO, and the reaction was started by addition of 40 µl 0.1 µM LPLA2 to 10 µl of pNPB. Release of the *p*-nitrophenoxide was monitored by increased absorbance at 400 nm on a Spectramax plate reader. Activity of LPLA2 expressed in HEK293S GnTi$^-$ cells after endo F1 treatment was at least as high as LPLA2 from HEK 293T cells.

Next, we compared the acyltransferase activity of the two LPLA2 species. This

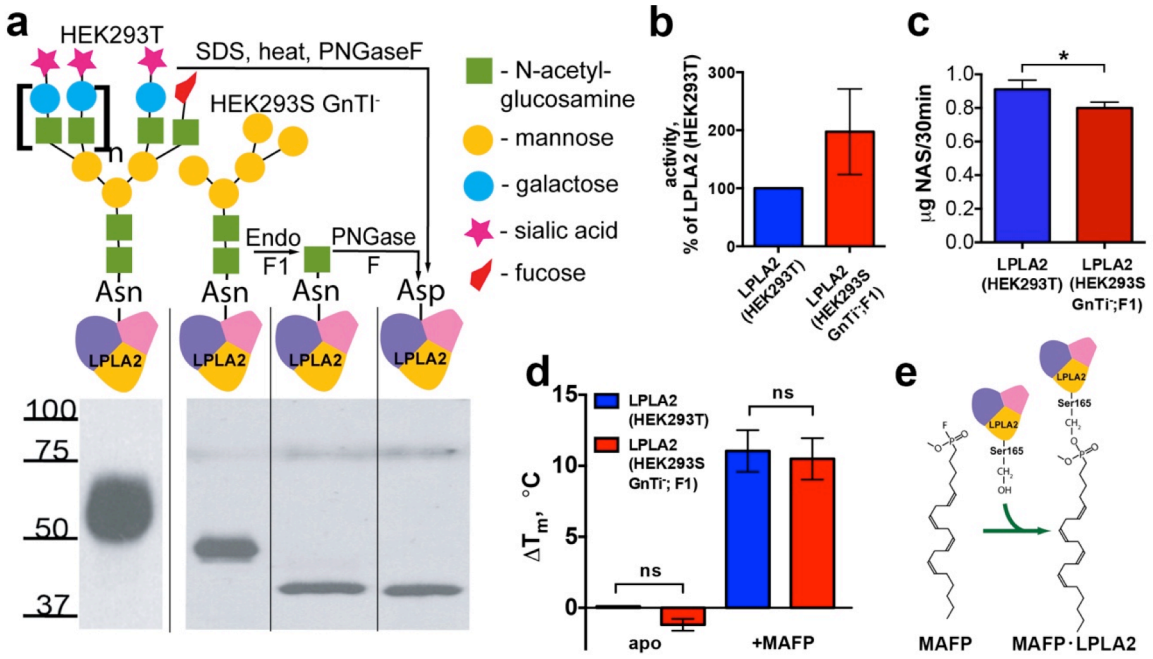

Figure 18. Expression, deglycosylation, and covalent modification of LPLA2. **(a)** Coomassie stained gel of various glycosylated forms of LPLA2. The enzyme has four N-linked glycosylation sites that proved resistant to deglycosylation when expressed in HEK293T cells. Crystal structures were obtained for all but the peptide-*N*-glycosidase F (PNGaseF) treated form. **(b)** LPLA2 expressed in HEK293S GnTi$^-$ cells after endoF1 treatment is just as if not more active than wild-type when evaluated using pNPB as a substrate, indicating that deglycosylation of all but the terminal sugar does not greatly affect the structure of the enzyme. **(c)** Acyltransferase activity of endoF1-treated LPLA2 is similar to that of wild-type. Error bars in panels B and C represent the standard deviation of three independent experiments. Assays were performed by V. Hinkovska-Galcheva. **(d)** T_m of LPLA2 expressed in various cell lines before and after reaction with MAFP. In panel d, the error bar represents the standard deviation of three independent experiments performed in triplicate. * $p<0.05$; ns, not significant. **(e)** Scheme of LPLA2 reaction with MAFP

activity relies on the ability of LPLA2 to bind liposomes and lipid substrates. The transacylase activity assay of LPLA2 was performed using a reaction mixture containing 48 mM Na citrate pH 4.5, 10 µg/ml bovine serum albumin, and liposomes (127 µM phospholipid) and LPLA2 in 500 µl of total volume. Liposomes consisting of DOPC-sulfatide-NAS (3:0.3:1, molar ratio) were prepared as previously described (Abe *et al.*, 1996). The reaction was initiated by the addition of the enzyme. The reaction mixture was incubated for 30 min at 37 ˚C and terminated by adding 3 ml of chloroform-methanol (2:1) plus 0.3 ml of 0.9% (w/v) NaCl. The mixture was centrifuged for 5 min at room temperature. The resulting lower organic layer was transferred into another glass tube and dried under a stream of N_2 gas. The dried lipid was dissolved in 40 µl of chloroform-methanol (2:1) and applied on an HPTLC plate and developed in a solvent system consisting of chloroform-acetic acid (90:10, v/v). The plate was than dried and soaked in 8% (w/v) $CuSO_4 \cdot 5H_2O$, 6.8% (v/v) H_3PO_4, 32% (v/v) methanol. The uniformly wet plate was briefly dried by a hair dryer and charred for 15 min in a 150 ˚C oven. The plate was scanned and the content of the product (1-O-acyl-NAS) was estimated by NIH-ImageJ 1.37v. The activity of LPLA2 from HEK293S GnTi$^-$ cells after endo F1 treatment was slightly lower (about 10%).

Next, we compared melting temperatures of LPLA2 glycoforms using differential scanning fluorimetry method (Fig. 18d). 0.1 mg/ml LPLA2 variant was mixed with 0.1 mM 1-anilinonaphthalene- 8-sulfonic acid (ANS) in the absence or presence of 100 µM methyl arachidonyl fluorophosphonate (MAFP), a covalent LPLA2 inhibitor that upon reaction with LPLA2 forms a complex resembling an acyl enzyme step in LPLA2 catalytic cycle (Fig. 18e), in 20 mM HEPES pH 7.5 and 150 mM NaCl. Samples were then heated from 25 to 90 °C at 1 ˚C/min in a ThermoFluor Analyzer (Johnson & Johnson). Plate fluorescence was measured in 1 °C intervals after cooling to 25 °C using a 475-525 nm emission filter. T_m values were calculated as the inflection point of the melting curve using the instrument software. As can be seen from Fig. 18d, the difference between apo- and MAFP-bound $LPLA2_{GnTI;F1}$ and LPLA2 from HEK 293T cells was not statistically significant. Thus, we concluded that $LPLA2_{GnTI;F1}$ biochemically is very similar to fully glycosylated LPLA2 from HEK 293T cells.

2.3 LCAT expression for crystallographic studies

2.3.1 LCAT expression in HEK 293T cells

LCAT is a close homolog of LPLA2 and we speculated that it could be expressed using the protocols for LPLA2 expression for HEK 293T and HEK 293S GnTI$^-$ cells. First, we expressed LCAT in HEK 293F cells using transient transfection. The DNA construct contained LCAT sequence optimized for expression in mammalian systems (Invitrogen) encoding full-length human LCAT gene with its signal sequence followed by a C-terminal His tag subcloned into the pcDNA4 vector. All cell culture protocols were the same as for the suspension-grown HEK 293S GnTI$^-$ cells for the exception of the cell media: HEK 293F cells did not require FBS supplementation of the FreeStyle media. LCAT was purified similarly to LPLA2, but the endoF1 and TEV digests were omitted as well as the second Ni-column purification step. Yields were about 1.5 mg/l of media.

LCAT expressed in HEK 293F cells had an apparent molecular weight of about 65 kDa, judged by its mobility on the Coomassie stained SDS-PAGE, and, presumably was glycosylated with complex carbohydrates similarly to LPLA2 expressed in HEK 293T cells (Fig. 19). Furthermore, like LPLA2, LCAT was resistant to the treatment by both endo Hf and endo F1 endoglycosidases. PNGase F treatment of SDS-denatured LCAT for 1 h at 20 °C resulted in a shift of the LCAT band to about 45 kDa, an expected molecular weight of this protein based on its protein

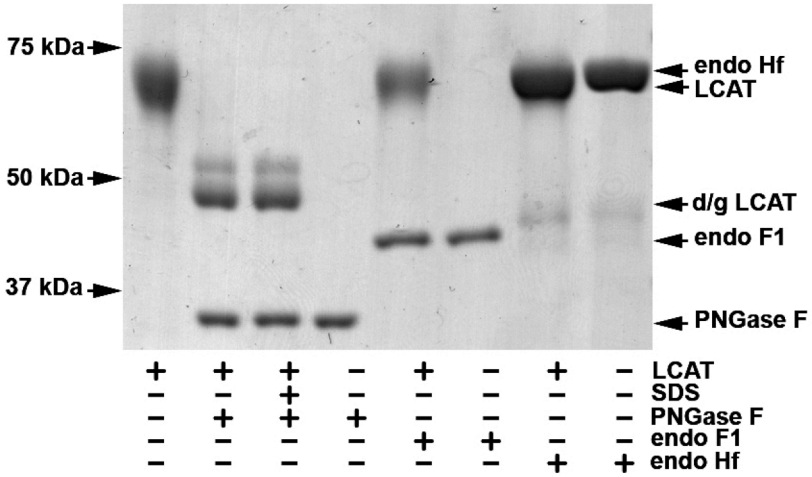

Figure 19. Deglycosylation of LCAT expressed in HEK 293F cells. Coomassie stained gel of purified LCAT from HEK 293F cells before and after treatment with various endoglycosidases.

sequence. Small residual band might correspond to the O-glycosylated LCAT (Schindler *et al.*, 1995). Surprising, however, was the ability of PNGase F to act on native protein. It has been reported previously that LCAT expressed in CHO was amenable to PNGase deglycosylation under native conditions (Chisholm, Gebre, & Parks, 1999), however, its similarity to LPLA2 made this observation unanticipated. In addition to being 50% identical to LPLA2, three out of four N-linked LCAT glycosylation sites are conserved between two proteins, suggesting a similar chemical environment for the protein-carbohydrate bonds and, thus, similar sensitivity to PNGase F.

To further investigate this phenomenon we used gel-filtration to separate deglycosylated LCAT from PNGase F. Fig. 20 demonstrates the Coomassie-stained SDS-PAGE gel of LCAT expressed in HEK 293F cells before (Fig. 20 lane 1) and after PNGase F treatment in native conditions (Fig. 20 lane 2). Digested LCAT was applied onto a Superdex 200 column equilibrated in the 20 mM HEPES pH 7.5 150 mM NaCl. The chromatogram showed two peaks – one corresponding to PNGase F (apparent molecular weight 16 kDa) and one corresponding to LCAT (apparent molecular weight 65 kDa) (data not shown). One representative fraction of the LCAT peak is shown in Fig. 20 lane 3. As can be seen, its gel mobility is identical to that of glycosylated LCAT before PNGase treatment.

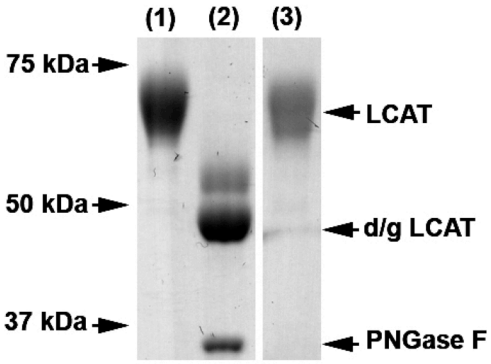

Figure 20. LCAT deglycosylation with PNGase F. (Coomassie-stained SDS-PAGE)

The most likely explanation for the observed phenomenon is that PNGase F digest of “native” LCAT samples actually occurred during boiling samples in SDS-containing loading buffer in preparation for the SDS-PAGE when LCAT denaturation was happening before PNGase F inactivation. The melting temperature of LPLA2 is about 10 ° higher then that of LCAT in ThermoFluor experiments, therefore, heat inactivated PNGase F faster then it could denature LPLA2. Thus, unfortunately, similarly to LPLA2, we were unable to deglycosylate LCAT produced in HEK 293F cells without

prior denaturation of the protein. Nevertheless, we attempted to crystallize this form of LCAT, but our crystallization trials thus far yielded no hits.

Compared to LPLA2, LCAT has additional N- and C-terminal extensions that are not predicted to have secondary structures (Fig. 3). The C-terminal extension is enriched in prolines and O-linked glycosylation sites (Schindler *et al.*, 1995). The C-terminus of LCAT is not expected to be important for its catalytic activity (Francone *et al.*, 1996; Y. P. Lee *et al.*, 1997). On the other hand, N-terminus has been proposed to be involved with LCAT association with HDL and LDL particles (Vickaryous, Teh, Stewart, & Dolphin, 2003).

We have expressed and purified C-terminally ($LCAT_{1-397}$) and both N- and C-terminally ($LCAT_{21-397}$) truncated LCAT. $LCAT_{21-397}$ lacks the N- and C-terminal extensions absent in LPLA2 (Fig. 3). In addition, it also lacks the first N- glycosylation site (N20), however, elimination of the first glycosylation site should not result in significant reduction of the LCAT enzymatic activity (O *et al.*, 1993; Qu *et al.*, 1993). Both constructs have C-terminal 6xHis tags and were purified according the same protocol as $LCAT_{FL}$. Expression levels were comparable to those of the full-length protein ($LCAT_{FL}$). A representative Coomassie stained gel from the small scale LCAT purification is shown on Fig. 21a. LCAT truncation mutants migrate faster on the gel

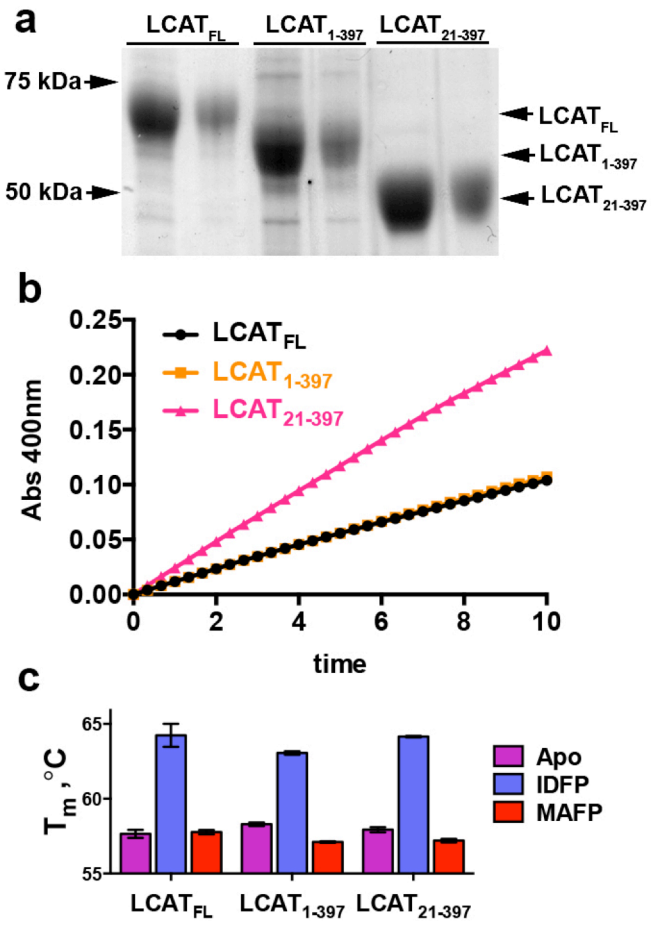

Figure 21. Activity and melting temperatures of different LCAT truncation mutants expressed in HEK 293T cells. **(a)** Coomassie-stained denaturing SDS-PAGE of $LCAT_{FL}$, $LCAT_{1-397}$ and $LCAT_{21-397}$ **(b)** $LCAT_{FL}$, $LCAT_{1-397}$ and $LCAT_{21-397}$ exhibit no significant difference in activity using pNPB as a substrate, **(c)** T_m values of LCAT variants before and after reaction with MAFP and IDFP.

according to their reduced molecular weight.

Next we compared the activity of all three LCAT variants using the soluble substrate pNPB. A representative experiment is shown on Fig. 21b and 22a. It appears that C-terminal deletion had no effect on LCAT ability to hydrolyze pNPB. Deletion of the LCAT N-terminus, on the other hand, resulted in increased rate of hydrolysis.

We have also compared the melting temperatures of all three LCAT truncations with and without inhibitors using ThermoFluor assay (Fig. 21c and 22b). Here we used two different fluorphosphonate inhibitors that differ in the length of their acyl chains, isopropyl dodec-11-enylfluorophosphonate (IDFP) and MAFP (Fig. 22c). It has been reported that human LCAT disfavors phospholipids containing arachidonic acid as its substrate due to the presence of a charged amino acid at position 149 (E149) (J. Wang *et al.*, 1997; Zhao *et al.*, 2003; 2004). Consistently, LCAT variants do not bind and are not stabilized by MAFP in the ThermoFluor assay. On the other hand, the shorter IDFP inhibitor stabilized all variants equally by about 6 °C.

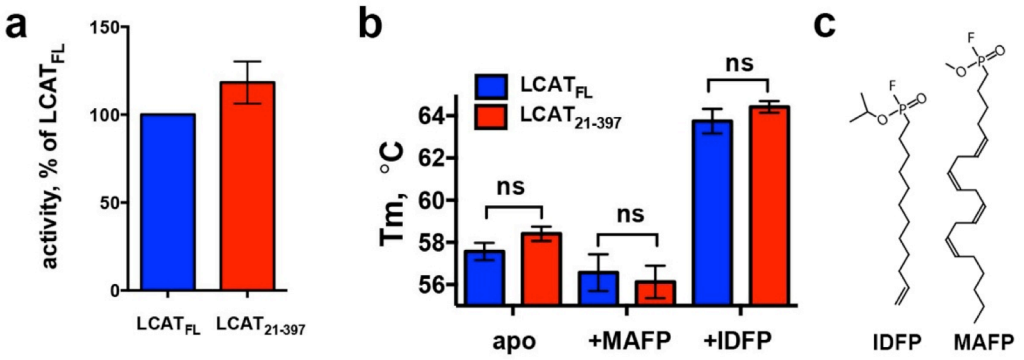

Figure 22. Biochemical properties of LCAT variants. **(a)** $LCAT_{FL}$ and $LCAT_{21-397}$ exhibit no significant difference in activity using pNPB as a substrate, indicating that the N and C terminal extensions do not contribute to catalytic activity. **(b)** T_m values of LCAT variants before and after reaction with MAFP and IDFP (all experiment were performed in triplicates, error bars represent a stand deviation). **(c)** IDFP and MAFP

2.3.2 Creation of stably transfected HEK 293S GnTI$^-$ cell lines overexpressing LCAT or LPLA2

Following the same strategy we used for LPLA2, we attempted to transiently express LCAT in HEK 293S GnTI$^-$ cells in order to get underglycosylated high-mannose carbohydrates amenable to endo F1 treatment. We used the same constructs described in Section 2.3.1, $LCAT_{FL}$, $LCAT_{1-397}$ and $LCAT_{21-397}$. In addition, we tested a longer $LCAT_{1-401}$ truncation that contained the R399A substitution caused FLD (H. Miettinen, Gylling, Ulmanen, Miettinen, & Kontula, 1995). All cell culture protocols were the same as described for LPLA2 in Section 2.2, and purification identical to that of the fully glycosylated LCAT species described in Section 2.3.1.

Representative Coomassie-stained gel of purified LCAT truncations before and after endo F1 treatment is shown on Fig. 23. All LCAT variants appear to be heterogeneous, judged by the multiple bands before and after endo F1 digest. Endo F1 treatment caused the shift in the apparent molecular weight of LCAT constructs due to removal of N-linked carbohydrates. However, the heterogeneity of the sample remained unaffected. Such heterogeneity might be a result of additional O-glycosylation or modifications of N-linked polysaccharides, such as fucosylation, rendering the carbohydrates resistant to endo F1. In addition, the yields of all four variants were very low, estimated at less than 100 μg/L of media, about 20-fold lower then LPLA2 yields from this cell line.

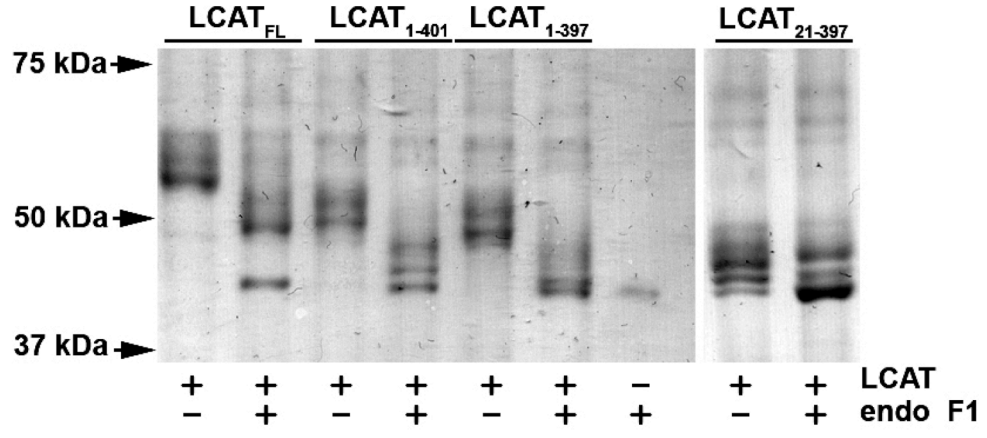

Figure 23. Purified LCAT truncation mutants $LCAT_{FL}$, $LCAT_{1-401}$, $LCAT_{1-397}$ and $LCAT_{21-397}$ before and after endo F1 treatment. Coomassie-stained SDS-PAGE.

The possible cause of low protein yields could be cellular toxicity of the expressed protein, misfolding, protein aggregation, poor secretion, or poor ribosomal synthesis. Visual observation did not reveal any loss in cell viability upon LCAT expression. However, we also tested the expression of the catalytically inactive S181A $LCAT_{FL}$, where the serine of the catalytic triad was substituted to alanine. The expression level of this mutant was similar to that of $LCAT_{FL}$.

To test for potential protein aggregation and misfolding we examined HEK 293S GnTI$^-$ cells for LCAT accumulation using the Western blot and did not detect significant cross reactivity with anti-His antibodies (data not shown). This data argued against protein aggregation, however, it did not exclude the possibility that misfolded protein was rapidly degraded in cells.

The signal sequence of secreted proteins could dramatically affect their expression level (Stern, Olsen, & Trölße, 2007). To investigate such a possibility, we substituted LCAT signal sequence with that of LPLA2. However, no improvement in protein expression levels was observed. Thus we concluded that reduced glycosylation state of LCAT somehow affected its folding and secretion, possibly, through directing it to rapid degradation within the cell.

Because we were still detecting only small amounts of expressed LCAT, we attempted to improve the yields by creating stably transfected HEK 293S GnTI$^-$ cell lines. In addition to a $LCAT_{FL}$-expressing cell line we also created a LPLA2 expressing cell line which later proved to be very useful for the expression of the selenomethionine (SeMet)-labeled LPLA2 (Chapter 3).

We used LPLA2 and $LCAT_{FL}$ constructs cloned into PCEP4 and pcDNA4 plasmids, harboring the resistance to hydromycin and zeocin antibiotics, respectively. Plasmids were linearized using SspI restriction endonuclease for pcDNA4 and NruI for PCEP4 plasmid. HEK 293S GnTI$^-$ cells were grown as adherent monolayers and transfected using the previously described protocol for transient expression of LPLA2 (Section 2.2). On the next day after transfection we began the selection by adding 50 μg/ml of zeocin (Invitrogen) to cultures transfected with pcDNA4 plasmid and 75 μg/ml of hydromycin (Invitrogen) to cultures transfected with PCEP4. Most cells died over the next 5 d, with only a few surviving cells transfected cultured that later gave rise to cell

colonies. The Western blot detected protein expression only in pcDNA4-transfected cultures and not in the PCEP4 cultures, thus, they were dropped from future trials. After cells were recovered (about three weeks after the addition of antibiotic), selection pressure was increased to 200 µg/ml zeocin in 50 µg/ml steps. Media was exchanged every 5 d and cells were viable for at least four collections for protein purification purposes. Estimated yield were about 9 mg/L for LPLA2 and 6 mg/L for $LCAT_{FL}$.

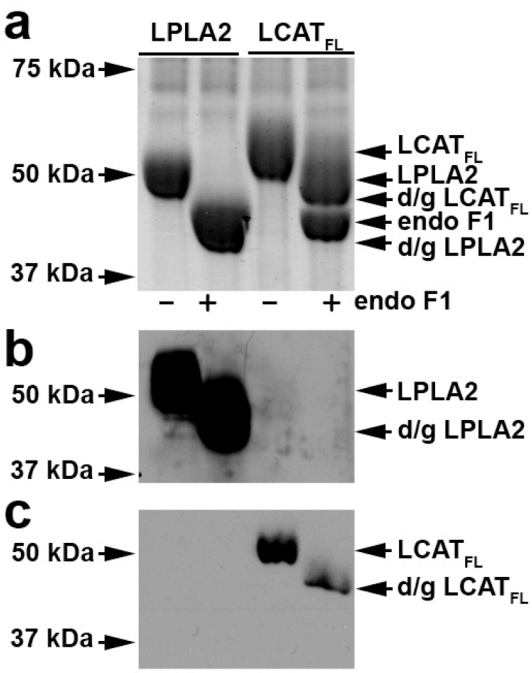

Figure 24. LCAT and LPLA2 expressed in stably transfected HEK 293S GnTi- cells before and after endo F1 treatment. **(a)** Coomassie stained gel. **(b)** The Western blot stained with anti-LPLA2 antibodies. **(c)** The Western blot stained with anti-LCAT antibodies.

The Coomassie stained gel of representative protein samples purified using the Ni-resin before or after the endo F1 digest are shown in Fig. 24. Both LPLA2 and LCAT expressed in their corresponding stable cell lines are amenable to endo F1 digestion resulting in single band for LPLA2 and LCAT. LCAT also exhibited some heterogeneity. The Western blot stained with anti-LPLA2 antibodies (Fig. 24b) or anti LCAT antibodies (Fig. 24c) confirmed the identity of the expressed protein.

Next we performed large-scale LCAT expression and purification for crystallographic experiments (Fig. 25). As both endo F1 and $LCAT_{FL}$ constructs had non-cleavable His_6 tags, we performed the endo F1 digest with a very small amount of glycosidase (1:50 molar ratio of endo F1 to $LCAT_{FL}$) that we believed would not affect our downstream assays or crystallization experiments. As can be seen from Fig. 25, endo F1 completely digests $LCAT_{FL}$ after 15 h incubation at 4 °C. The remaining heterogeneity of LCAT is probably due to some additional modification, such as O-glycosylation. We attempted to separate different glycosylation species of LCAT using

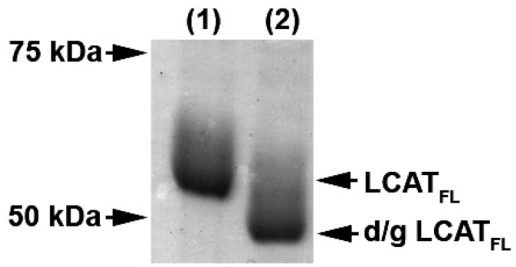

Figure 25 Large-scale LCATFL prep before and after endo F1 treatment. Coomassie-stained denaturing SDS-PAGE.

chromatography on Phenyl Sepharose, however, $LCAT_{FL}$ eluted as a single peak (data not shown). We also tried to use gel filtration in an attempt to separate different species by their size, but LCAT appeared to interact with the Superdex resin. Thus, we proceeded with crystallization experiments without further purification.

Melting temperatures of apo- and IDFP-bound $LCAT_{FL}$ expressed in HEK 293F cells and HEK 293S GnTI$^-$ cells after endo F1 digest were nearly identical (data not shown) indicating that the enzyme is functional, thus, and if crystallized, would most likely represent a biologically relevant state.

2.3.3 Expression of under glycosylated LCAT species using glycosylation inhibitors

In an attempt to produce underglycosylated LCAT species that would be amenable to endoglycosidase action we also tried using the inhibitors of the N-linked glycan maturation pathway. First, we chose to use kifunensine (KIF), an inhibitor of α-mannosidase I. Proteins expressed in HEK 293T cells in the presence of this inhibitor exhibit oligomannose carbohydrate types, similar to those of the HEK 293S GnTI$^-$ cell line (V. T. Chang *et al.*, 2007). We added KIF to the suspension cultures at the time of their transfection with pcDNA4-LCAT$_{FL}$ plasmid. Cell media was harvested 4 d later and the protein was purified using methods described above for LCAT$_{FL}$. The Coomassie – stained gel of purified LCAT$_{FL}$ from cultures grown in the presence of 100 and 250 ng/ml of KIF is shown on Fig. 26. Compared to LCAT$_{FL}$ expressed in HEK 293F cells without the inhibitor, the glycosylation of KIF-LCAT$_{FL}$ appears to be different, however no less diffuse or heterogeneous. Low yields of this protein (less then 100 μg/L) and resistance to endo F1 led us to pursue other strategies.

Next, we tried the α-mannosidase II inhibitor, swainsonine (SWA). SWA inhibits the step of glycan processing, after the one blocked by kifunensine, and the carbohydrate, produced in the presence of SWA are hybrid-types (V. T. Chang *et al.*, 2007). Fig. 27 shows a representative gel of purified LCAT$_{21-397}$ expressed in the presence of different amounts of SWA and treated with endo F1 or endo Hf glycosidases. Test expression was also done with LCAT$_{FL}$ and LCAT$_{1-397}$ and the results completely mimic those of LCAT$_{21-397}$ (data not shown). The most striking difference between LCAT

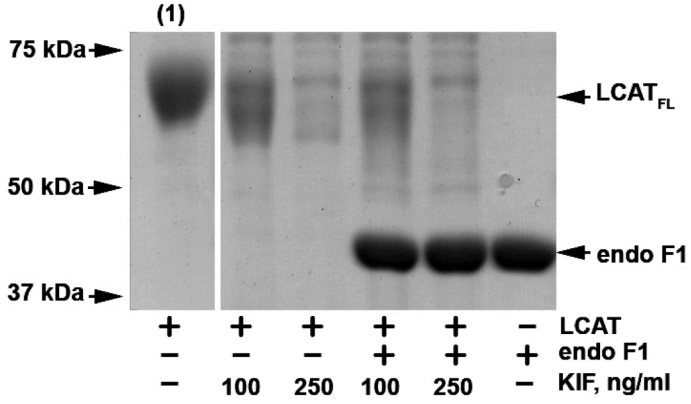

Figure 26. LCAT$_{FL}$ expressed in the presence if kifunensine (KIF) is resistant to endo F1. Lane1-glycosylated LCAT expressed in the absence of KIF.

produced in HEK 293F cells in the presence of KIF and SWA was the amount of expressed protein. While KIF treatment resulted in hardly any protein, glycosylation-processing inhibition by SWA led to almost the same amount of protein as the "no inhibitor" sample. Treatment with 14 μM SWA resulted in more homogenous $LCAT_{21-397}$ band compare to the "no SWA" sample (Fig. 27). Furthermore, SWA-$LCAT_{21-397}$ could be almost completely deglycosylated with endo Hf, resulting in a single band at 43 kDa. Increasing SWA concentration in the cell culture media had no additional effect on the band homogeneity or its digestion by endo Hf. Interestingly, SWA-$LCAT_{21-397}$ was resistant to endo F1. One significant difference between endo F1 and endo Hf is their ability to hydrolyze core-fucosylated glycans: endo Hf is about 50-fold faster than endo F1 (Sigma-Aldrich Co. LLC, 2008). Thus, LCAT expressed in the presence of SWA, likely, contains significant amount of fucosylated carbohydrates. $LCAT_{21-397}$ could be further separated from endo Hf by gel filtration, as it no longer interacted with the resin and eluted as a single tight peak (data not shown).

Thus, LCAT expression in HEK 293F cells in the presence of SWA seems very promising for producing pure homogenous protein in sufficient quantities for future crystallization trials. However, this protein is yet to be tested in activity and stability assays.

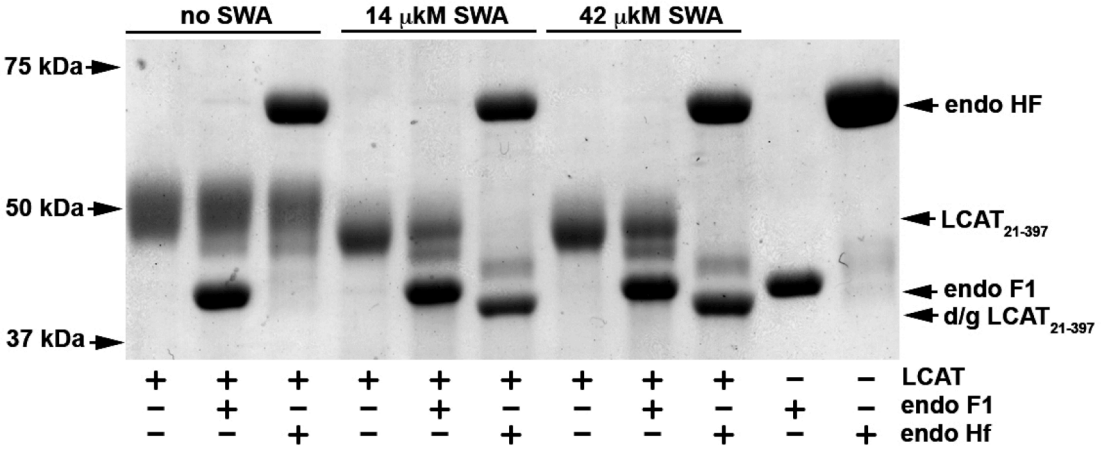

Figure 27. $LCAT_{21-397}$ expressed in HEK 293F cells in the absence and presence of swainsonine (SWA) before and after deglycosylation with endo F1 or endo Hf.

Chapter 3. Crystallization and structure determination of LPLA2 and LCAT

3.1 Crystallization of LPLA2 expressed in HEK 293T cells

First, we crystallized the highly glycosylated LPLA2 purified from HEK 293T cells produced by Proteos, Inc. Rhombohedral crystals grew in 100 mM Na citrate pH 3.5-4, 20% PEG 3350, and 100 mM NaCl to 300x300x30 μm (Fig. 28a). To confirm that crystals indeed contained LPLA2, we transferred ten crystals into the harvesting solution (20 mM HEPES pH7.5, 250 mM NaCl, 100 mM Na citrate pH 4 and 20% PEG 3350), washed them three additional times with the same buffer to remove non-crystalline LPLA2, and then resuspended the crystals in SDS-PAGE loading buffer and separated on the gel. After transfer to nitrocellulose e membrane the Western blot was stained with anti-LPLA2 antibodies (Fig. 28b). In addition to testing the identity of the crystallized protein, we also wanted to identify whether or not we crystallized a small homogeneous fraction of the heterogeneously glycosylated LPLA2. However, the mobility and heterogeneity of crystallized LPLA2 was identical to that of the sample purified from HEK 293T cells (Fig. 28b).

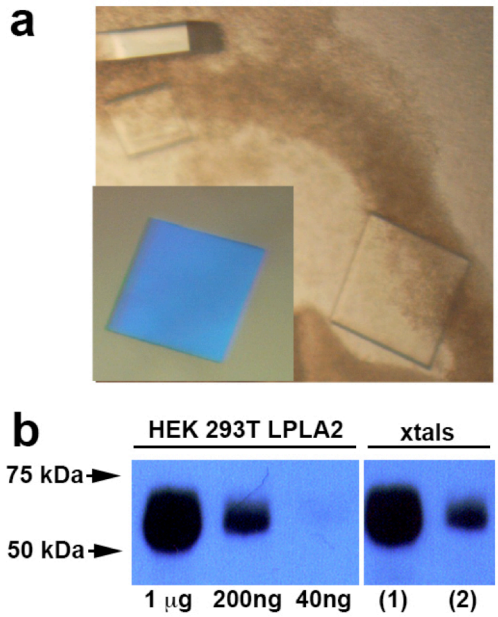

Figure 28. Crystals of glycosylated LPLA2 expressed in HEK 293T cells. (a) LPLA2 crystals. Inset shows the crystal in polarized light. (b) The Western blot of purified LPLA2 and crystals harvested from the cryo loops after data collection. Lane 2 contains the same sample as in lane 1 diluted 5 times.

Table 2. Data collection and refinement statistics for glycosylated LPLA2

	apo LPLA2 (HEK293T)
Data collection	
Beamline	GM/CA 23 ID-D
Space group	$P\,2\,2_1\,2_1$
Cell dimensions	
a, *b*, *c* (Å)	72.4 125.3 140.2
α, β, γ (°)	90 90 90
Resolution (Å)	30 – 3.4 (3.46 – 3.40)
R_{merge}	0.140 (0.590)
$I/\sigma I$	8.6 (1.5)
Completeness (%)	89.0 (89.6)
Redundancy	3.2 (3.1)
Refinement	
Resolution (Å)	93.42 – 3.4 (3.49 – 3.40)
No. reflections	15210 (1039)
R_{work}/ R_{free}	0.306/0.322
No. atoms	
Protein	6270
Ligand/ion	0
Water	0
B-factors	
Protein	123.3
Ligand/ion	
Water	
R.m.s deviations	
Bond lengths (Å)	0.023
Bond angles (°)	1.71
Ramachandran favored (%)	89
Ramachandran outliers (%)	2.4

Each structure was solved using a single crystal.
*Highest resolution shell is shown in parentheses

For cryoprotection we soaked the crystals in harvesting solution containing 20% glycerol for 5-10 min. Data was collected at LS-CAT and GM/CA at Argonne Photon Source (statistics shown in a Table 2 is for GM/CA data collection) from crystals frozen in nylon cryoloops (Hampton). Representative diffraction images at 0° and 90° φ we show in Fig. 29. The crystals diffracted to 3.4 Å spacings. However, as can be seen directly from the images, the diffraction was very anisotropic and maxima did not extended past 8 Å in one of the dimensions, which resulted in lower completeness overall and in highest resolution shell (89% and 90%, respectively). In addition, the crystals exhibited very high mosaicity (3°) reflecting overall disorder in the crystal

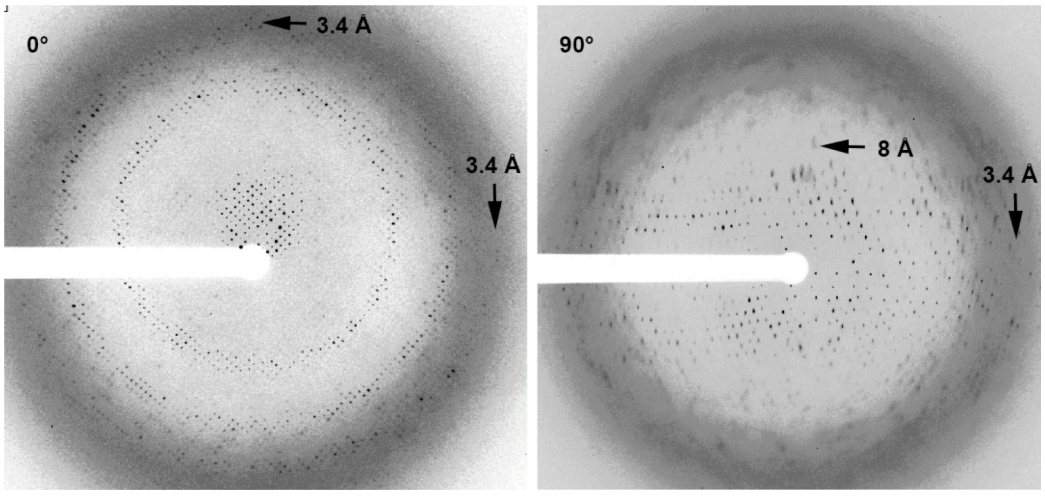

Figure 29. Diffraction images of HEK 293T LPLA2 crystals at 0° and 90° φ angle. Arrows indicate the highest resolution shell.

packing, which we attributed to either the highly complex heterogeneous glycosylation state of LPLA2 expressed in HEK 293T cells and/or overall flexibility of the protein.

To reduce flexibility we stabilized LPLA2 with the covalent inhibitor MAFP, which increases LPLA2 melting temperature by 12 °C (Section 2.2). We tested LPLA2 stabilization by MAFP at different pH and salt concentrations. MAFP stabilized LPLA2 at a wide range of pH from 4.5 to 9.5 and at both 130 mM NaCl (Fig. 30) and 500 mM NaCl (data not shown). Interestingly, whereas the LPLA2 melting temperature changes by only by 3.5 ° from pH 4.5 to pH 9.5, the LPLA2·MAFP complex melting temperature was bell-shaped, likely corresponding to the pH optimum of the catalytic triad, which depends on the protonation state of the catalytic histidine. This pH optimum is, however, different from the pH optimum of LPLA2 transacylase activity when using liposome-based substrate (pH 4.5) (Abe & Shayman, 1998). Most likely, LPLA2 activity on liposomes requires low pH for electrostatic interactions between LPLA2 and the lipid surface. Crystals of LPLA2·MAFP were grown under the same conditions as Apo LPLA2, but they diffracted to the same resolution limits and their space group was identical. No improvement in diffraction quality was observed.

We also crystallized LPLA2 expressed in HEK 293T cells after sialidase treatment (Section 2.1.2). However, these crystals were identical to crystals of fully glycosylated LPLA2 (data not shown).

Due to low resolution and high mosaicity of this LPLA2 crystal form we did not attempt experimental phasing and instead focused on getting new LPLA2 crystal forms using protein purified from the HEK 293S GnTI$^-$ cell line.

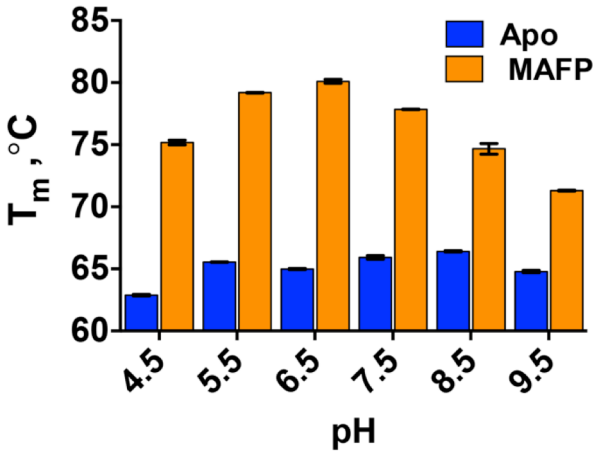

Figure 30. Melting temperatures of Apo and MAFP-bound HEK 293T LPLA2 at different pH values.

3.2 Crystallization and structure determination of LPLA2 purified from HEK 293S GnTI$^-$ cells

As described in Section 2.2, the activity and melting temperature of LPLA2 expressed and purified from HEK 293S GnTI$^-$ cells and digested with endoglycosidase F1 (LPLA2$_{F1}$) is similar to that of heavily glycosylated LPLA2 from HEK 293T cells. LPLA2$_{F1}$ was crystallized by vapor diffusion in hanging drops over reservoirs containing 100 mM HEPES pH 7.5, 3.5% PEG 8000, 28% MPD, and 300 mM ammonium phosphate. If crystals did not appear after 5 d, they were streak seeded using smaller LPLA2 crystals obtained at higher MPD and PEG concentrations. Due to the high MPD concentration, additional cryoprotection was unnecessary. LPLA2$_{F1}$ crystals had P1 symmetry and diffracted to 1.83 Å spacings (Tables 3 and 4). To collect a high quality dataset with a low symmetry space group we employed the 5 μm mini-beam and vector data collection at GM/CA at APS. For this, the elongated plate-like crystal was oriented in the beam in such a way that φ angle rotation would be aligned along its longest axis. Then the best diffracting region was found using the rastering technique at GM/CA at APS. The 160 μM vector within the best diffracting zone, running in parallel to the rotation axis, was "split" into 16

Table 3. Data collection and refinement statistics for LPLA2 expressed in HEK 293S GnTi$^-$ cells

	apo LPLA2	SeMet LPLA2
Data collection		
Beamline	GM/CA 23 ID-D	GM/CA 23 ID-D
Space group	*P* 1	*P* 2_1
Cell dimensions		
a, *b*, *c* (Å)	62.8 91.2 100.3	91.2 114.3 100.4
α, β, γ (°)	78.1 88.5 88.5	90 102 90
Wavelength (Å)	0.97937	0.97937
Resolution (Å)	30 –1.83 (1.86 – 1.83)*	29.7 – 2.79 (2.94 – 2.79)*
R_{merge}	0.095 (0.631)	0.161 (0.529)
I/σ_I	17.9 (2.2)	13.0 (5.2)
Completeness (%)	97.8 (96.4)	99.2 (95.4)
Redundancy	4.0 (3.9)	15.2 (14.5)
Refinement		
Resolution (Å)	30 – 1.84 (1.89 - 1.84)	
No. reflections	174208 (11119)	
R_{work}/ R_{free}	0.157/0.175	
No. atoms		
Protein	12493	
Ligand/ion	492	
Water	1023	
B-factors		
Protein	18.9	
Ligand/ion	37.8	
Water	36.6	
R.m.s deviations		
Bond lengths(Å)	0.016	
Bond angles (°)	1.39	
Ramachandran favored (%)	98	
Ramachandran outliers (%)	0	

Each structure was solved using a single crystal.
*Highest resolution shell is shown in parentheses.

spots, 10 μM apart. Each spot was used to collect 23 degrees of data (1° oscillation) for the full 360 ° total dataset. Data was processed using HKL2000 software package (Otwinowski & Minor, 1997).

Table 4. Scaling statistics for $LPLA2_{F1}$ crystals.

Shell limit (Å)		Average I	Average error	Normalized Chi^2	Linear R-factor
Lower	Upper				
30	4.96	4975.8	124.7	2.536	0.058
4.96	3.94	7135	176.6	2.313	0.053
3.94	3.44	4710.3	138.2	1.906	0.058
3.44	3.13	2953.4	107.7	1.617	0.067
3.13	2.9	1745.2	83.2	1.38	0.082
2.9	2.73	1182.5	71.4	1.237	0.1
2.73	2.6	993.8	69.2	1.187	0.113
2.6	2.48	778.3	65.3	1.091	0.132
2.48	2.39	674.2	64.2	1.057	0.148
2.39	2.31	599.2	64.2	1.012	0.165
2.31	2.23	522.4	64.1	0.999	0.189
2.23	2.17	456.7	64	0.96	0.212
2.17	2.11	395.7	64	0.903	0.238
2.11	2.06	363.9	65.3	0.902	0.266
2.06	2.01	315	65.5	0.873	0.305
2.01	1.97	265	65.5	0.79	0.347
1.97	1.93	226.5	66	0.777	0.41
1.93	1.9	199.9	66.5	0.772	0.472
1.9	1.86	163.8	67.1	0.726	0.564
1.86	1.83	146	67.6	0.686	0.631
All reflections		1454.9	81.2	1.191	0.095

First we attempted to solve the structure by molecular replacement using PHASER (McCoy *et al.*, 2007) and LPLA2 models built by the Robetta (Kim, Chivian, & Baker, 2004), I-Tasser (Y. Zhang, 2008) or RaptorX (Peng & Xu, 2011) servers. However, PHASER yielded no solution, most probably due to the low sequence identity of the proteins used to create initial LPLA2 models (16-19%). Next we turned to experimental phasing and attempted to soak heavy atoms into existing LPLA2 crystals.

We tried soaks with 5 mM K_2PtCl_2, $HgCl_2$, K_2OsO_4, $KAu(CN)_2$; 2 mM Ethylmercuril thiosalicylate Na-salt (EMTS); 10 mM $HoCl_3$ and UO_2Cl_2 for up to 3 d at 4 °C and rapid soaks which incubated $LPLA2_{F1}$ crystals with 400 mM of CsCl or NaBr for 5 min. In most cases, incubation with heavy atoms resulted in a significant decrease of diffraction resolution (less then 5 Å) and overall quality (increased spot streakiness and mosaicity). However, crystals soaked with the uranium-containing compound diffracted to 2.2 Å. We collected data at 0.99987 Å (U f''= 6.87), processed it the same way as for the $LPLA2_{F1}$ data. However, no peaks were observed in the anomalous difference Patterson maps. Due to nonisomorphism (different unit cell) within the $LPLA2_{F1}$ crystals without soaking, we were unable to search for the difference Patterson map peaks.

Proteins, labeled with selenomethionine (SeMet) can often be crystallized under conditions identical to nonlabeled protein. Selenium has 18 more electrons compare to sulfur, which makes it suitable for isomorphous diffraction experiments. In addition Se has a weak anomalous signal, which, if measured accurately, could be useful for single-wavelength anomalous diffraction (SAD) experiments. Labeling with SeMet is commonly used for proteins expressed in bacterial systems. In such cases bacteria are simply grown in minimal media supplemented with all essential amino acids and SeMet instead of methionine. In these prokaryotic systems, SeMet could be toxic for bacteria and yields of labeled protein are often significantly lower than for unlabeled protein. There are even fewer examples for SeMet labeling in more complex eukaryotic systems, such as in insect or mammalian cell cultures, because the toxic effects of SeMet are, usually, even more detrimental there.

We first attempted to label LPLA2 expressed in transiently transfected HEK 293S GnTI$^-$ cells, using a protocol modified from Barton *et al.* (Barton, Tzvetkova-Robev, Erdjument-Bromage, Tempst, & Nikolov, 2006). For this we grew HEK 293S GnTI$^-$ cells in 35x150 mm dishes in DMEM high-glucose media, supplemented with 10% FBS, 1 mM pyruvate, 2 mM L-

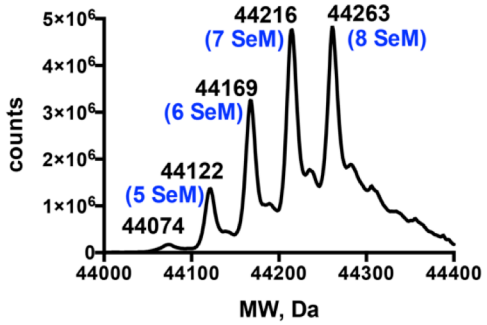

Figure 31. Deconvoluted electrospray spectra of SeMet-$LPLA2_{F1}$. Molecular weight of LPLA2 with all LPLA2 with all Met substituted to SeMet is 44265 Da. SeM - selenomethionine

glutamine, 100 U/ml penicillin, and 100 µg/ml streptomycin to 90% confluence. Then the media was exchanged for complete media, deficient in cystine and methionine (Gibco), supplemented with 30 mg/l of cystine and 63 mg/l of SeMet, and followed by a transfection with PCEP4-LPLA2 plasmid (1:2 DNA:PEI ratio). Media was harvested after 3 d and processed as described above for $LPLA2_{F1}$.The yield was 200 µg total from 35x150 mm plates.

To increase the yield of SeMet labeled LPLA2, we used our stably transfected HEK 293S GnTi$^-$ cell line (Section 2.3.2). Grown in seven plates in the presence of 200 µg/ml zeocin in DMEM high-glucose media, supplemented with 10% FBS, 1 mM pyruvate, 2 mM L-glutamine, 100 U/ml penicillin, and 100 µg/ml streptomycin to 90-95% confluence. Then cultures were split into 38 plates without antibiotic and grown for additional 3 d to 100% confluence. Subsequently, the media was changed to complete medium, deficient in cystine and methionine (Gibco), supplemented with with 30 mg/l of cystine and 63 mg/l of SeMet, harvested after 3 d and purified according to the protocol for $LPLA2_{F1}$. The yield was 1 mg of SeMet-$LPLA2_{F1}$ from 1l of media.

SeMet incorporation was confirmed using electrospray mass spectrometry with positive ion detection of the intact protein, wherein four separate peaks corresponding to 8, 7, 6, and 5 methionines of LPLA2

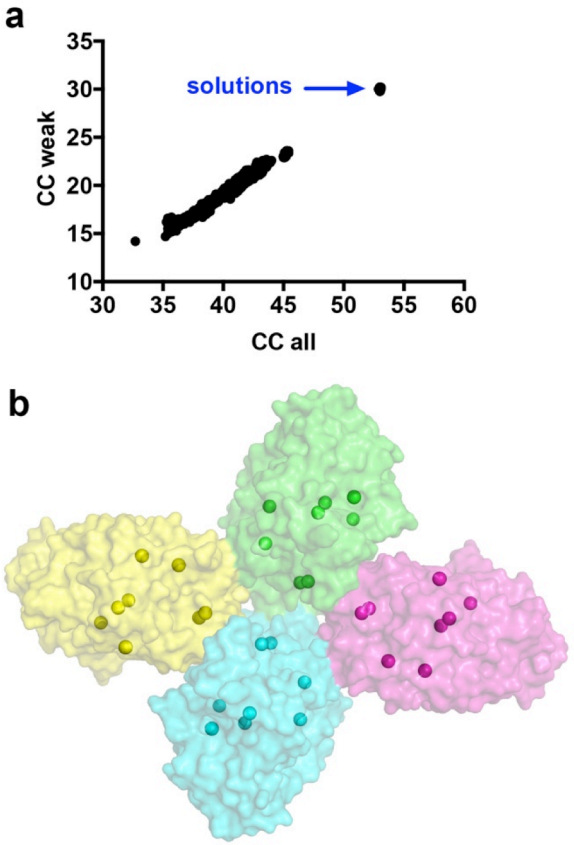

Figure 32. SeMet substructure of SeMet-$LPLA2_{F1}$ crystals. (a) Cross-correlation (CC) between observed and calculated Bijvoet differences for all (CC all) and weak (CC weak) reflections. (b) Se substructure (spheres) within the LPLA2 asymmetric unit (surface representation). Each LPLA2 monomer is colored separately.

being substituted with SeMet were observed (mature LPLA2 has eight methionines) (Fig. 31). From the relative peak heights, the total incorporation was estimated to be 70-80%. SeMet-LPLA2$_{F1}$ crystals grew under the same experimental conditions as LPLA2$_{F1}$.

For experimental phase determination, the SeMet-LPLA2$_{F1}$ dataset was collected using a 5 µm mini-beam and vector data collection at GM/CA at APS. Each site was used for collecting 20 ° wedges (10 ° direct and 10 ° inverse beam) for a total of 36 spots that were 8 µM apart. As selenium has a weak anomalous signal, we used XDS for more accurate diffraction spot integration. In contrast to HKL2000, XDS uses a 3D profile fitting radius (Kabsch, 2010) and is superior for non perfect streaky images of SeMet-LPLA2$_{F1}$. The data was merged with SCALA in the CCP4 suite (Evans, 2006; Winn *et al.*, 2011).The selenium substructure, consisting of 32 Se sites (4 LPLA2 molecules per asymmetric unit with eight methionines in each), was identified using 10000 trials in ShelxD (T. R. Schneider & Sheldrick, 2002) (Fig. 32a) and initial phases (figure of merit = 0.35) were determined by single anomalous diffraction in AutoSol as implemented in the Phenix software package (P. D. Adams *et al.*, 2010; Terwilliger *et al.*, 2009) (Fig. 32b). The initial atomic model was created with Phenix AutoBuild (Terwilliger *et al.*, 2008). This preliminary SeMet-LPLA2 structure was used as a search model in molecular replacement using PHASER (McCoy *et al.*, 2007) to solve the native LPLA2$_{F1}$ structure (Table 3 and Fig. 33) as these crystals were nonisomorphous with those of SeMet-LPLA2$_{F1}$. Refinement was performed with alternating rounds of TLS and restrained refinement in REFMAC5 (Murshudov *et al.*, 2011) and model building in Coot (Emsley, Lohkamp, Scott, & Cowtan, 2010). During refinement, local NCS restraints were applied when appropriate. Structure validation was performed using the Molprobity server.

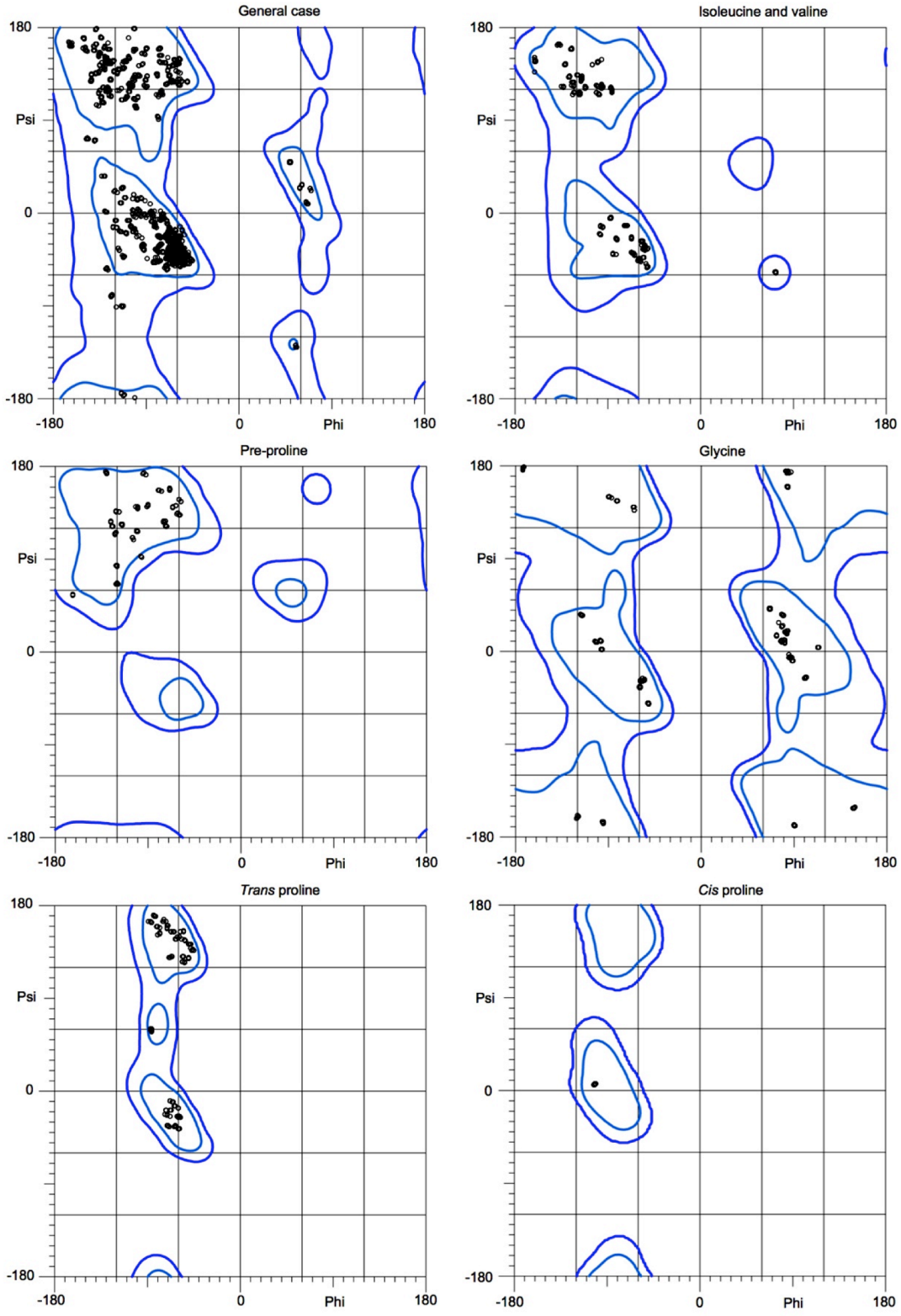

Figure 33. Ramachandran plot for $LPLA2_{F1}$. 97.9% (1567/1600) of all residues were in favored (98%) regions. 100.0% (1600/1600) of all residues were in allowed (>99.8%) regions.

3.3 Structure determination of different LPLA2 crystal forms by molecular replacement

To get more information about the LPLA2 catalytic mechanism, we attempted to obtain the structure of LPLA2 bound to its substrates. We have tried soaking NAS, N-acetyl-serine (resembles NAS head group), glycerol (acyl group acceptor at concentrations higher then 30% (Abe, Hiraoka, & Shayman, 2007b)), 1,2-dioctanoyl-PC (short chain PC analog), 1,2 heptanoyl-thio-PC (nonhydrolysable short chain PC analog), POPC and lysoPC by themselves and with detergents (2% n-dodecyl-beta-D-maltoside or β-OG). However, no ligand electron density could be observed after structure solution and refinement.

In addition, we have also explored co-crystallization of $LPLA2_{F1}$ and its catalytically dead mutant, S165A, with DOPC-sulfatide liposomes (1.25 mM DOPC: 0.13 mM sulfatide), as co-crystallization with micelles has been used previously to obtain a phospholipid-bound structure of pancreatic lipase (van Tilbeurgh *et al.*, 1993). After mixing LPLA2 with liposomes we set up the sparse matrix JCSG+ and Classics Lite Suite screens (Qiagen). Crystals of $LPLA2_{F1}$-S165A were grown using a condition from the Classics Lite Suite (Qiagen): 100 mM Na cacodylate pH 6.5, 10% PEG 8000, 200 mM $MgAc_2$ and cryoprotected in solution containing 100 mM Na cacodylate pH 6.5, 50mM Na citrate pH 4.5, 20 mM HEPES pH 7.5, 10% PEG 8000, 200 mM $MgAc_2$, and 30% ethylene glycol. The crystal structure of S165A-$LPLA2_{F1}$ was solved using molecular replacement method with $LPLA2_{F1}$ as a search model. Although we were able to obtain a novel LPLA2 crystal form (Table 5), the lipase active site remained empty.

Thus, we turned to nonspecific covalent phospholipase inhibitors, IDFP and MAFP. These inhibitors have been used previously to obtain the crystal structures of the human pancreatic lipase and dog gastric lipase in their active conformation (Egloff *et al.*, 1995; Roussel *et al.*, 2002).

Both IDFP and MAFP increase LPLA2 melting temperature when tested in the ThermoFluor assay (Fig. 34). The longer MAFP inhibitor changes LPLA2 melting temperature by 12 °C, while IDFP, whose acyl chain is eight carbon atoms shorter then that of MAFP, changes LPLA2 melting temperature only by 10 °C. This trend is

consistent with the low efficiency of LPLA2 hydrolysis for short acyl chain phospholipids, such as octanoyl-PC (data not shown).

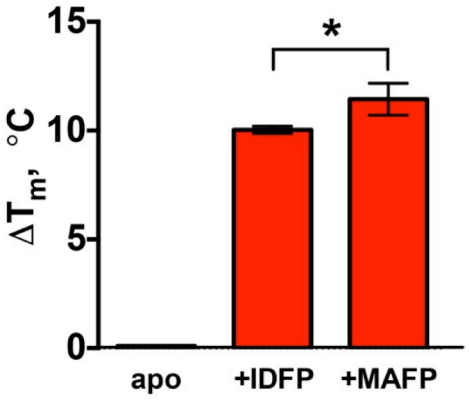

Figure 34. Increase of LPLA2 melting temperature in the presence of covalent inhibitors IDFP and MAFP

For cocrystallization experiments with IDFP and MAFP, LPLA2 was first covalently modified with IDFP or MAFP. For this, 50 μM fluorophosphonate inhibitors (Cayman chemical) in methyl acetate were incubated with 0.4 mg/ml LPLA2 for 1 h at room temperature, and then LPLA2 was concentrated to 10-13 mg/ml. Then we set up commercially available sparse matrix screens (QIAGEN and Hampton) and screened around previously optimized conditions for $LPLA2_{F1}$ crystals. Sparse matrix screening yielded multiple hits that were not observed for apo LPLA2. In particular, a diamond-shaped LPLA2·MAFP crystal form crystallized using 100 mM HEPES pH 7.5, 30% PEG MME 550, 50 mM $MgCl_2$. Due to the high PEG MME concentration, these crystals did not require cryoprotection. The structure was solved in $P\,4_32_12$ space group by molecular replacement (Table 5).

Crystals of LPLA2·IDFP and LPLA2·MAFP were also obtained in conditions similar to apo-$LPLA2_{F1}$ crystals (100 mM HEPES pH 6.5, 3.5% PEG 8000, 28% MPD, and 300 mM ammonium phosphate). In addition, both inhibitors could also be soaked into crystalline LPLA2 using harvesting solution containing 1 mM IDFP or MAFP for 2 d, and then freezing the crystals on nylon loops in liquid N_2. Cocrystallization and soaking with inhibitors resulted in the same LPLA2 conformation with identical ligand orientations. However, datasets from inhibitor soaks diffracted to slightly higher spacings (2.3 Å for *P*1 LPLA2·IDFP and 2.7 for *P*1 LPLA2·MAFP) and, thus, were used for future analysis (Table 5). IDFP and MAFP were modeled into the active site using Coot and refinement was done in REFMAC5 using external restraints generated in JLigand (Lebedev *et al.*, 2012).

We were also able to solve the structures of glycosylated LPLA2 produced in HEK 293 $GnTI^-$ or HEK 293T cells (Tables 4 and 2) by molecular replacement using

$LPLA2_{F1}$ as a search model. For the *P* 6_222 crystals of high-mannose LPLA2, the protein was produced in HEK 293 $GnTI^-$ cells (without endo F1 treatment), conjugated with MAFP and crystallized in 100 mM citric acid pH 3, 0.8 M ammonium sulfate in a condition derived from the JCSG+ screen (Qiagen). Cryoprotection was achieved by harvesting solution containing 30% glycerol, 20 mM HEPES pH7.5, 150 mM NaCl, 100 mM citric acid pH 3 and 0.8 M ammonium sulfate. Comparison and detailed analysis of LPLA2 crystal structures is given in Chapter 4.

Table 5. Data collection and refinement statistics for crystal forms of LPLA2 expressed in HEK 293S $GnTi^-$ cells

	LPLA2·IDFP (+endoF1)	LPLA2·MAFP (+endoF1)	LPLA2 S165A (+endoF1)	LPLA2·MAFP (+endoF1)	LPLA2·MAFP
Data collection					
Beamline	LS-CAT 21 ID-D	LS-CAT 21 ID-D	GM/CA 23 ID-D	GM/CA 23 ID-D	GM/CA 23 ID-D
Space group	*P* 1	*P* 1	*F* 4_1 3 2	*P* 4_3 2_1 2	*P* 6_2 2 2
Cell dimensions					
a, *b*, *c* (Å)	62.8 90.2 99.3	69.1 85.5 90.3	257 257 257	86.8 86.8 366	96.0 96.0 208.0
α, β, γ (°)	100.9 91.1 89.1	88.9 70.9 79.7	90 90 90	90 90 90	90 90 120
Resolution (Å)	30 – 2.30 (2.34 – 2.30)	30 – 2.70 (2.75 – 2.70)	30 – 3.00 (3.05 – 3.00)	30 – 2.85 (2.90 – 2.85)	30 – 2.70 (2.75 – 2.70)*
R_{merge}	0.080 (0.508)	0.088 (0.394)	0.211 (0.911)	0.157 (0.753)	0.132 (0.771)
I/σ_I	10.6 (1.5)	9.3 (1.8)	8.8 (1.9)	22.9 (3.5)	28.6 (3.7)
Completeness (%)	98.2 (97.4)	98.1 (93.7)	98.1 (100)	99.9 (100)	99.9 (98.6)
Redundancy	2.0 (2.0)	2.0 (1.9)	5.3 (5.3)	14.7 (14.8)	12.5 (12.1)
Refinement					
Resolution (Å)	97.53 – 2.28 (2.34 – 2.28)	85.2 – 2.69 (2.76 – 2.69)	29.7 – 3.0 (3.08 – 3.00)	29.8 – 2.84 (2.91 – 2.84)	29.4 – 2.79 (2.86 – 2.79)
No. reflections	90291 (5699)	49231 (3274)	14088 (1012)	32375 (2252)	14002 (970)
R_{work}/ R_{free}	0.178/0.206	0.189/0.222	0.189/0.226	0.197/0.223	0.244/0.308
No. atoms					
Protein	12470	12109	3048	6062	3002
Ligand/ion	538	373	56	84	0
Water	543	193	1	0	0
B-factors					
Protein	26.4	22.9	44.9	61	55.2
Ligand/ion	24.8	54.4	65.4	84.4	
Water	50.6	24.9	2.7	-	
R.m.s deviations					
Bond lengths(Å)	0.011	0.009	0.008	0.01	0.013
Bond angles (°)	1.45	1.22	1.22	1.35	1.71
Ramachandran favored (%)	98	97	94	96	93
Ramachandran outliers (%)	0	0	0.79	0.66	2.4

Each structure was solved using a single crystal.
*Highest resolution shell is shown in parenthesis.

3.4 Determination of the low resolution LCAT structure

We next attempted to determine the structure of LCAT. Unfortunately, we were unable to crystallize $LCAT_{FL}$ or $LCAT_{1-397}$ expressed in HEK 293F cells, but we could generate the crystals for $LCAT_{21-397}$ (Fig. 35 and Table 6 and 7) using 100 mM Na acetate pH 5.0, 13% isopropanol, and 200 mM $CaCl_2$. Cryoprotection was achieved by adding dry glucose to a final concentration of 30% (w/v) in mother liquor, due to the volatility of isopropanol. To determine the $LCAT_{21-397}$ structure, the apo-LPLA2 model was truncated to the last common Cβ and used as a search model in PHASER. An LPLA2-based homology model, built using the UCSF Chimera package (Pettersen *et al.*, 2004), was then superimposed onto the solution and used as the starting point for structure refinement. Four-fold NCS restraints were applied during refinement with restrained and jelly body refinement in REFMAC (Table 6 and Fig. 36). Stunningly, these crystals contained 88% solvent, explaining their diffraction to low resolution (8.7 Å). However, the electron density maps were of excellent quality.

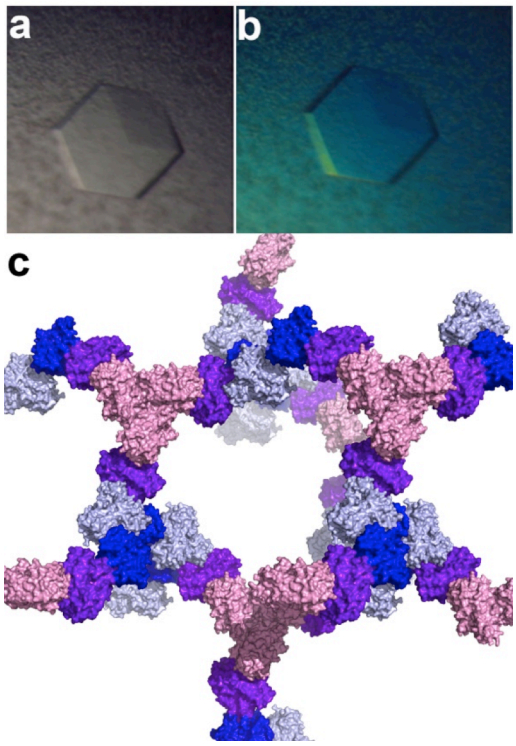

Figure 35. $LCAT_{21-397}$. (a) and (b) show the crystals of $LCAT_{21-397}$ photographed in white and polarized light, respectively. (c) High solvent content of LCAT crystals is due to large solvent channels. Shown are symmetry mates generated by PyMol within a 50 Å radius. Four LCAT monomers are colored separately.

We have also performed extensive crystallization screening for LCAT expressed in the HEK 293S GnTi$^-$ cell line. We have attempted to crystallize it in its apo and IDFP –bound form, with and without detergents (DDM and β-octylglucoside). However, no hits were observed. This could be attributed to the heterogeneity of the sample (Section 2.3.2).

Table 6. Data collection and refinement statistics for $LCAT_{21-397}$

	$LCAT_{21-397}$
Data collection	
Beamline	LS-CAT 21 ID-D
Space group	*H*3
Cell dimensions	
a, *b*, *c* (Å)	367 367 187
α, β, γ (°)	90 90 120
Resolution (Å)	30 – 8.70 (8.85 – 8.70)*
R_{merge}	0.189 (0.529)
$I/\sigma I$	8.2 (1.55)
Completeness (%)	98.8 (94.8)
Redundancy	5.1 (4.8)
Refinement	
Resolution (Å)	29.9-8.69 (8.90-8.69)
No. reflections	6954 (332)
R_{work}/R_{free}	0.152/0.195
No. atoms	
Protein	12224
Ligand/ion	332
Water	0
B-factors	
Protein	298.1
Ligand/ion	338.6
Water	
R.m.s deviations	
Bond lengths (Å)	0.01
Bond angles (°)	1.7
Ramachandran favored (%)	92
Ramachandran outliers (%)	2

Structure was solved using a single crystal.
*Highest resolution shell is shown in parenthesis.

We have tried to reduce heterogeneity by partial protease digest with trypsin and clostripain. Although we were able to obtain a single species of LCAT (data not shown), its low molecular weight, determined by electrospray mass-spectrometry (31122 Da), indicated that a significant portion of the protein was missing. Thus, we decided to not pursue this approach further.

While we have not yet performed extensive screening of LCAT expressed in HEK 293F cells in the presence of swainsonine, we expect this protein form to be the most promising lead in future attempts to obtain LCAT crystals diffracting to a higher resolution.

Table 7. Scaling statistics for $LCAT_{21-397}$ crystals.

Shell limit (Å)		Average I	Average error	Normalized Chi^2	Linear R-factor
Lower	Upper				
30	20.8	91.9	4.9	2.117	0.093
20.8	17.54	55.6	2.9	2.106	0.128
17.54	15.68	39.9	2.5	1.611	0.142
15.68	14.42	31.9	2.4	1.382	0.157
14.42	13.49	31.1	2.5	1.384	0.17
13.49	12.76	29	2.6	1.406	0.186
12.76	12.16	28.6	2.7	1.147	0.175
12.16	11.67	30.2	2.8	1.313	0.187
11.67	11.24	26	2.8	1.078	0.192
11.24	10.87	23	2.9	1.029	0.217
10.87	10.55	19.1	2.9	0.819	0.228
10.55	10.26	15.2	2.8	0.655	0.251
10.26	10	12.6	2.9	0.571	0.274
10	9.76	11.2	3	0.536	0.302
9.76	9.55	10.1	3.1	0.457	0.311
9.55	9.35	8.7	3	0.441	0.37
9.35	9.17	8.6	3.1	0.377	0.345
9.17	9	7.4	3.2	0.367	0.397
9	8.85	5.7	3.1	0.337	0.499
8.85	8.7	5.1	3.3	0.281	0.529
All reflections		24.7	3	0.972	0.189

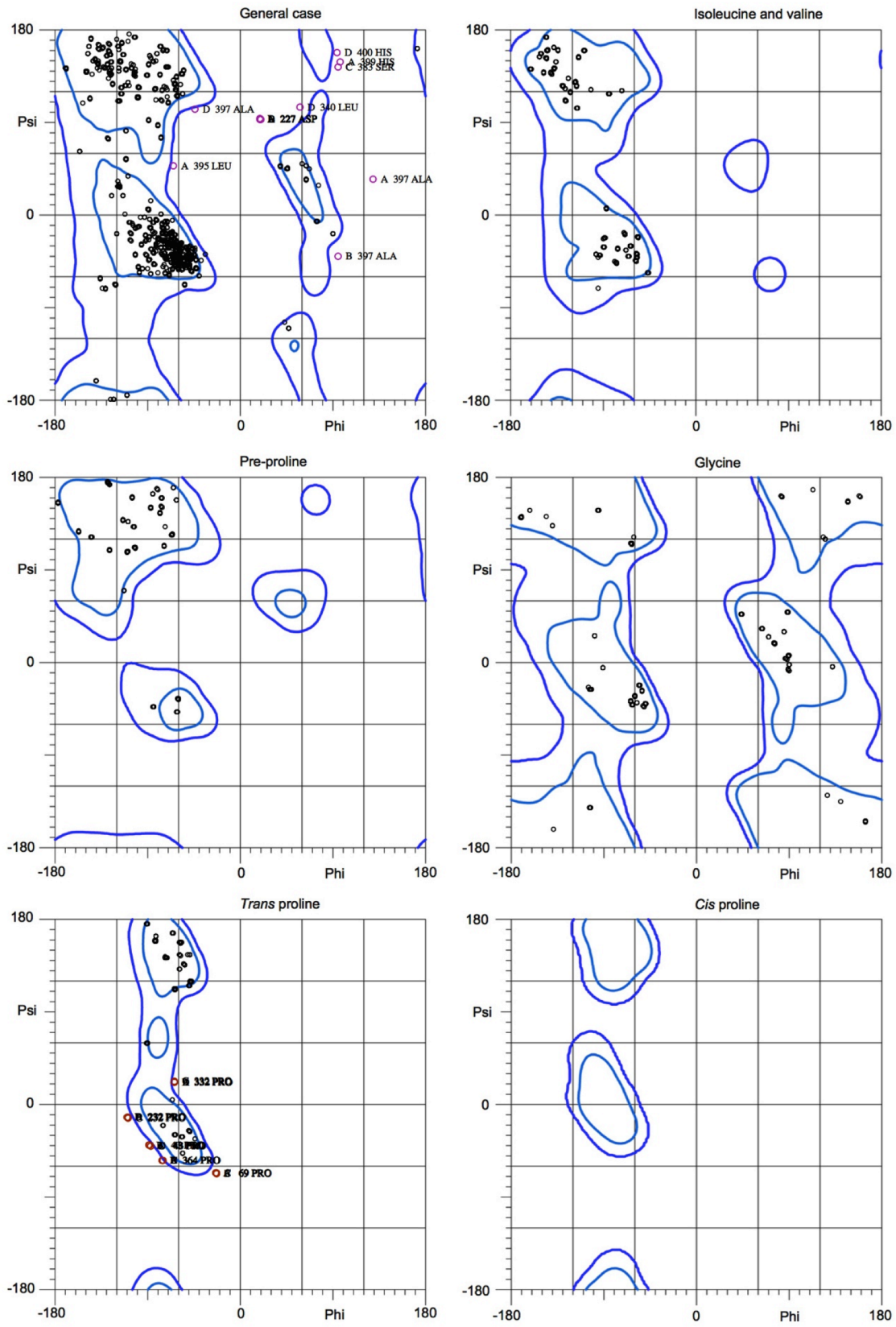

Figure 36. Ramachandran plot for $LCAT_{21-397}$. 92.0% (1391/1512) of all residues were in favored (98%) regions. 98.0% (1482/1512) of all residues were in allowed (>99.8%) regions.

Chapter 4. Structural and functional analysis of LPLA2 and LCAT

4.1 Atomic Structure of LPLA2.

The crystal structure of human LPLA2 (Fig. 37) was determined to 1.83 Å spacings using protein secreted from HEK293S GnTI$^-$ cells and deglycosylated with endoF1 ($LPLA2_{F1}$) (Fig. 18a-d, Table 3). Experimental phases for the structure were obtained via single wavelength anomalous diffraction from crystals containing SeMet labeled protein (Table 3). LPLA2 bears several structural and functional similarities to Family I bacterial triacylglycerol lipases (Arpigny & Jaeger, 1999). First, it contains a 6-stranded α/β hydrolase domain, lacking the first two strands of the canonical fold (Ollis *et al.*, 1992). The catalytic triad of the domain is found at conserved topological positions in the fold, with Ser^{165} in a nucleophile elbow between β5 and αC, Asp^{327} in a loop before αE, and His^{359} in a loop following β8 (Fig. 37b). Second, the enzyme has a "cap" domain formed by the β6-β7 and β7-αE loops of the α/β hydrolase domain. In the bacterial lipases, the cap domain contributes to the ligand binding site and typically features a flexible lid element that shields the hydrophobic active site from solvent in the soluble form of the enzyme (Nardini & Dijkstra, 1999; Schrag *et al.*, 1997). The LPLA2 cap domain is unrelated in fold, but contains two helices (a3 and a5) that are structurally analogous to two key helices found in bacterial lipase cap domains (α4 and α6), which help to form the binding site for the scissile acyl chain of the triacylglycerol substrate (Fig. 38).

Unique to LPLA2, however, is a domain inserted in the loop between β3 and αA´ that contains the sole disulfide bond of the protein and a rare non-proline cis-peptide bond between Trp43 and Leu44 that allows both of their hydrophobic side chains to project into the active site. Relative to Family I bacterial lipases, the domain occupies a similar topological position as the lid element (α5) in its open configuration (Fig. 38b-c).

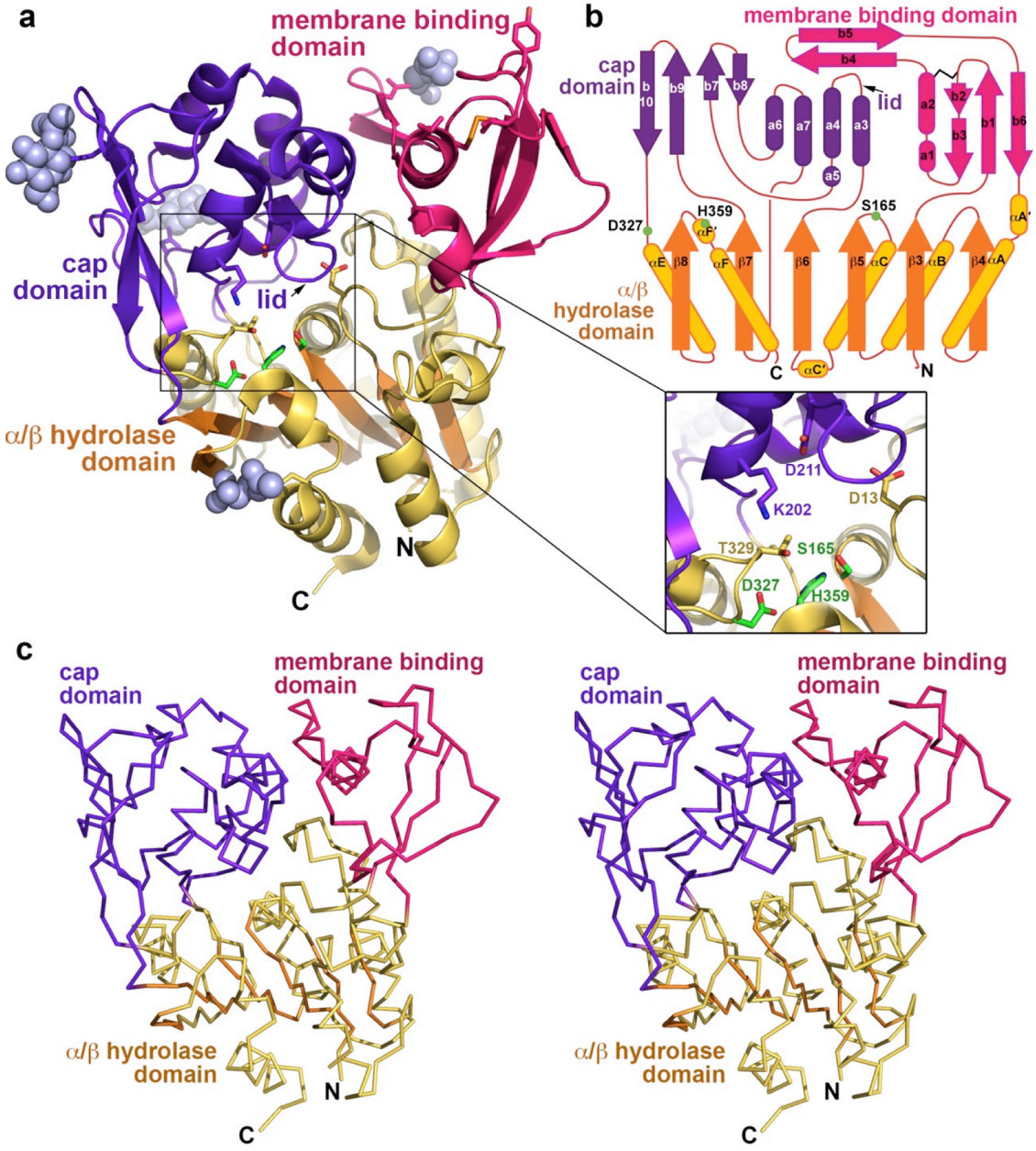

Figure 37. Architecture of LPLA2. **(a)** The α/β hydrolase (gold with orange strands), membrane binding (magenta), and cap (purple) domains associate to form a large concave active site cleft. Catalytic triad residues are drawn with green carbons. *N*-acetylglucosamine sugars (grey spheres) are observed at Asn66, Asn240, Asn256, and Asn365. The sole disulfide bond between Cys32 and Cys56 is drawn with yellow sulfur atoms. Side chains shown to play a role in membrane binding are shown as magenta sticks. Inset displays a close up view of the catalytic triad region. **(b)** LPLA2 topology. Because LPLA2 lacks the first two β strands of the canonical fold, the first strand of the α/β hydrolase domain is denoted as β3 (Schrag et al., 1997). **(c)** Cross-eyed stereo image of the LPLA2 Cα trace. Domain coloring is the same as in (a), and the observed amino and carboxyl terminal residues are labeled N and C, respectively.

The domain forms extensive interactions with the cap domain, in particular via its extended b4-b5 hairpin loop (residues 61-75), which buries 1055 Å^2 (calculated using PISA software (Krissinel & Henrick, 2007)) of accessible surface area. Because this domain features a conserved hydrophobic surface that faces away from the active site (Fig. 37a) and, as shown later, mediates LPLA2 interactions with membranes, it is henceforth referred to as the membrane binding domain.

The three domains of LPLA2 assemble to form a large concave surface containing the catalytic triad at the bottom, with all three domains providing many surface exposed hydrophobic residues that would favor the binding of lipid reactants. Compared to other lipases, which are known to have both active (open) and inactive

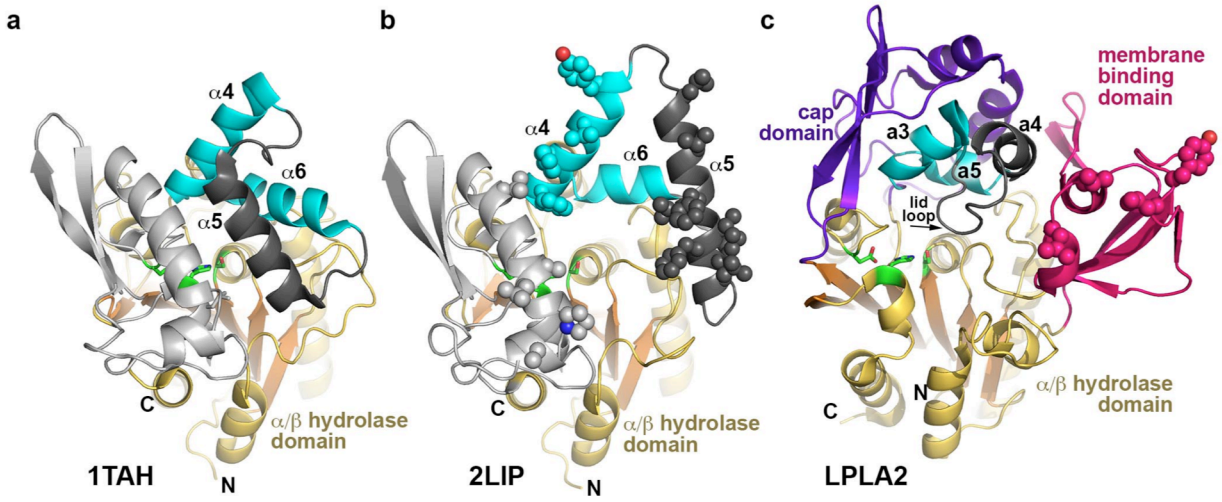

Figure 38. Structural comparison of Family I triacylglycerol lipases with LPLA2. These enzymes have a similar α/β hydrolase core and have cap domains containing a topologically and structurally similar motif of two helices (colored cyan) separated by a loop with an intervening helix (dark grey). In the bacterial lipases, this helix (α5) functions both as an active site lid in the closed state and membrane binding element in the open state. **(a)** Closed conformation of triacylglycerol lipase from *Pseudomonas glumae* (PDB entry 1TAH). **(b)** *Pseudomonas cepacia* lipase (PDB entry 2LIP) in an open conformation. Potential membrane binding residues are shown as spheres. **(c)** In comparison, LPLA2 seems to exhibit an open conformation, and its membrane binding domain occupies a similar topological location with respect to the active site as the α5 helix in panel B. Hydrophobic residues shown to be involved in membrane binding are shown as spheres. The lid loop and subsequent a4 helix of the cap domain (dark gray) is topologically equivalent to α5 in panels A and B.

(closed) conformations (Nardini & Dijkstra, 1999; van Tilbeurgh *et al.*, 1993), access to the LPLA2 active site seems unimpeded except for a flexible ten residue loop between the a3 and a4 helices of the cap domain, topologically equivalent to the larger lid elements found in Family I bacterial lipases (Fig. 38). Because this element (the "lid loop") is not highly conserved in sequence between LPLA2 and LCAT enzymes, it could play a role in determining their selectivity for NAS and cholesterol, respectively (see below), as acyl acceptor substrates.

4.2 Phospholipid Substrate Binding Site of LPLA2.

Phospholipids or phospholipid analogs have not yet been co-crystallized with either wild-type or catalytically inactive LPLA2-S165A. However, structures of LPLA2 bound to fluorophosphonate inhibitors are expected to mimic the tetrahedral acyl intermediate transition state of the reaction (Abe *et al.*, 2010) (Table 5). The structures of LPLA2 bound to IDFP (2.3Å spacings) and MAFP (2.7 Å spacings) have a root-mean-square deviation (RMSD) of 0.17 for 376 equivalent Cα atoms compared to apo LPLA2, and thus induce no major structural rearrangements despite increasing the melting point (T_m) by 10-12 ˚C (Fig. 34). Omit map density reveals strong electron density for the MAFP and IDFP head groups, wherein the phosphonate group is covalently bound to Ser^{165} and occupies the oxyanion hole formed by the backbone amides of Asp^{13} and Met^{166} (Fig. 39 and 40). The density becomes progressively weaker after the C3 carbon of their alkyl chains. Heterogeneity in the position of the aliphatic tail of IDFP suggests that there are two distinct hydrophobic tracks (A and B) leading away from the catalytic triad (Fig. 39a and c) that likely correspond to the binding sites for the *sn*-1 and *sn*-2 acyl tails of the phospholipid substrate. Track A, which modeling indicates could readily accommodate at least 18 carbons, is curved and follows a hydrophobic band of residues on helices a3 and a5 in the cap domain, ending in a hydrophobic cleft formed by the side chains of Trp43, Trp57, Ile61, and Trp130 (Fig. 39a and b). An unusual feature of this track is the side chain of Asp^{13}, which in bacterial lipases is conserved as leucine or methionine. The acyl chain occupying track A would therefore need to skirt around this residue to avoid unfavorable contacts, although in the

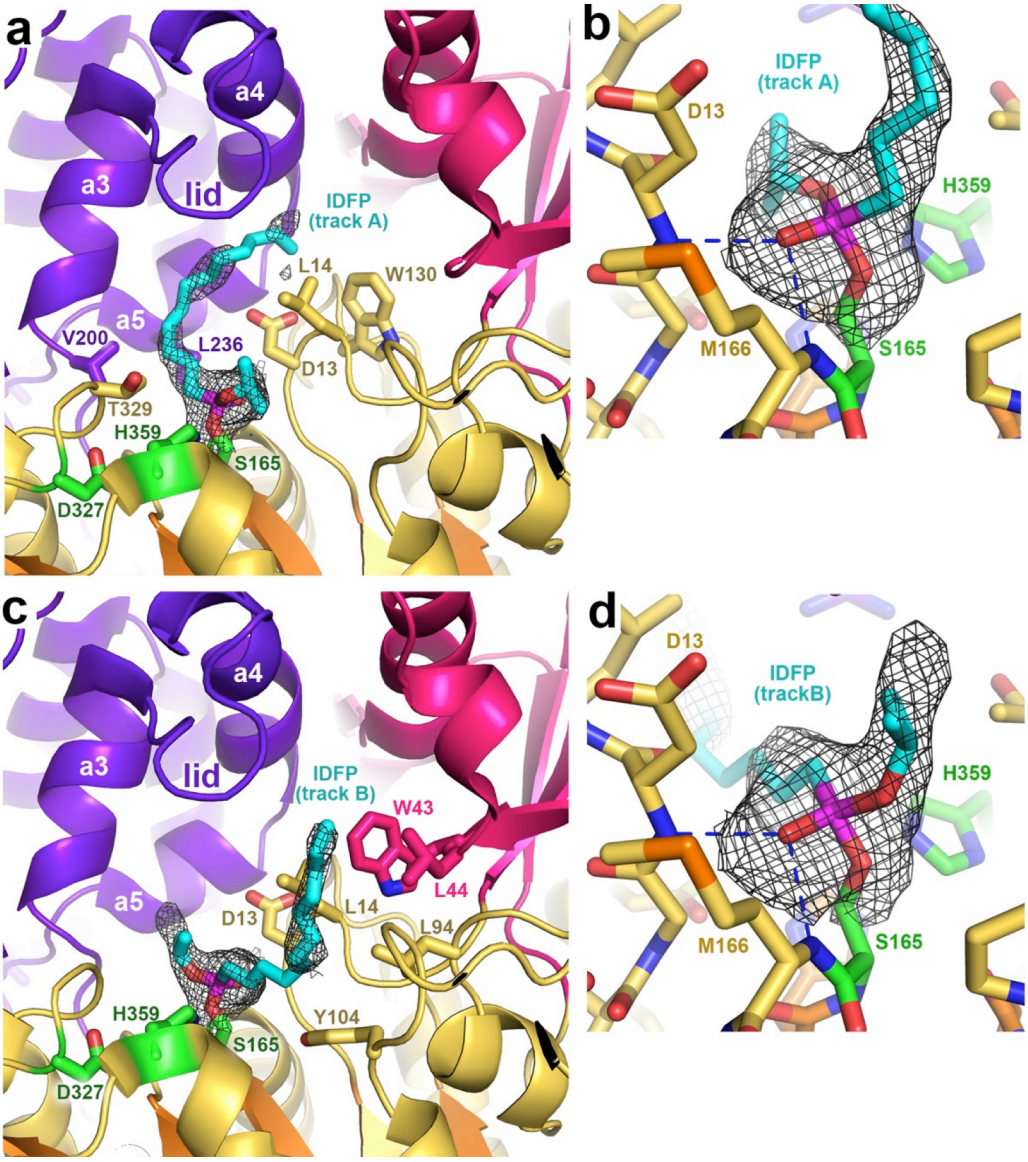

Figure 39. Complexes with fluorophosphonate inhibitors help define the catalytic cycle of LPLA2. **(a)** IDFP (cyan sticks) occupying track A. Wire cages in panels a-d correspond to 2.5 σ $|F_o|$-$|F_c|$ omit maps. **(b)** Backbone amides of Asp13 and Met166 form the oxyanion hole of LPLA2 and coordinate the phosphonate group. **(c)** IDFP in chains A, B and D of the LPLA2·IDFP structure occupies track B. **(d)** Regardless of the track, the phosphonate of the IDFP head group forms hydrogen bonds (dashed blue lines) with the backbone amides of Asp13 and Met166 comprising the oxyanion hole. Residues defining tracks A and B are shown as sticks with carbons colored according to their domain assignment as in Figure 37.

low pH of the lysosome this residue should be at least partially protonated. Notably, Asp13 is conserved as Cys31 in LCAT, a position well established as being important for cholesterol binding and modulation of LCAT catalytic activity (Boone *et al.*, 2012;

Francone & Fielding, 1991a; Jauhiainen *et al.*, 1988). Interestingly, the pK_a of cysteine is such that Cys^{31} will likewise be partially deprotonated in its native environment in human plasma at pH 7.4.

Track B is much more solvent accessible and linear than track A, starting adjacent to the oxyanion hole between the side chains of Leu14 (which contributes to both tracks) and Tyr104 in the catalytic domain, then extending along the surface of the membrane binding domain, including residues Trp43 and Leu44, within a channel formed between the lid loop of the cap domain, the αA´-αA loop of the catalytic domain, and the a1 helix of the membrane binding domain (Fig. 39c and d). Consistently, MAFP, which has a long arachidonyl group (20 carbon atoms), is only found occupying track B (Fig. 40)

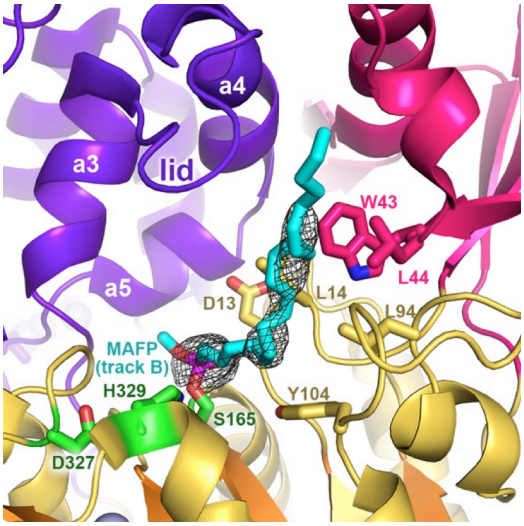

Figure 40. MAFP occupies track B of LPLA2. Residues defining track B are shown as sticks with carbons colored according to their domain assignment as in Figure 37.

4.3 Catalytic Cycle.

Although LPLA2 exhibits some structural homology with bacterial lipases, their substrates are fundamentally different in that LPLA2 and LCAT hydrolyze glycerophospholipids, which contain polar, charged head groups. Accordingly, there are modifications in conserved elements of the catalytic and cap domains of LPLA2 that can accommodate this difference. Lys202 in the a3 helix and Thr329 in the catalytic domain are invariant in LPLA2 and LCAT, but are conserved as hydrophobic residues in bacterial triacylglycerol lipases. Modeling indicates that they could form specific hydrogen bonds with the phosphate in the phospholipid head group (Fig. 41). The guanidinium of Arg214 in the lid loop is also in close proximity, although this residue is substituted with glycine in LCAT. The K202A, N213Q/R214A, and T329A mutations all retained full ability to hydrolyze the soluble substrate *p*-nitrophenylbutyrate (pNPB), indicating proper fold (Fig. 42a), but only K202A and T329A were deficient in catalyzing acyl transfer to NAS (Fig. 42b), indicating that Lys202 and Thr329, but not Arg214, are important for phospholipid binding. These results allowed creation of a docking model for a typical preferred phosphatidylcholine (PC) substrate with a saturated acyl group in the *sn*-1 position (palmitate), and an unsaturated, longer fatty acid (oleic acid) in the *sn*-

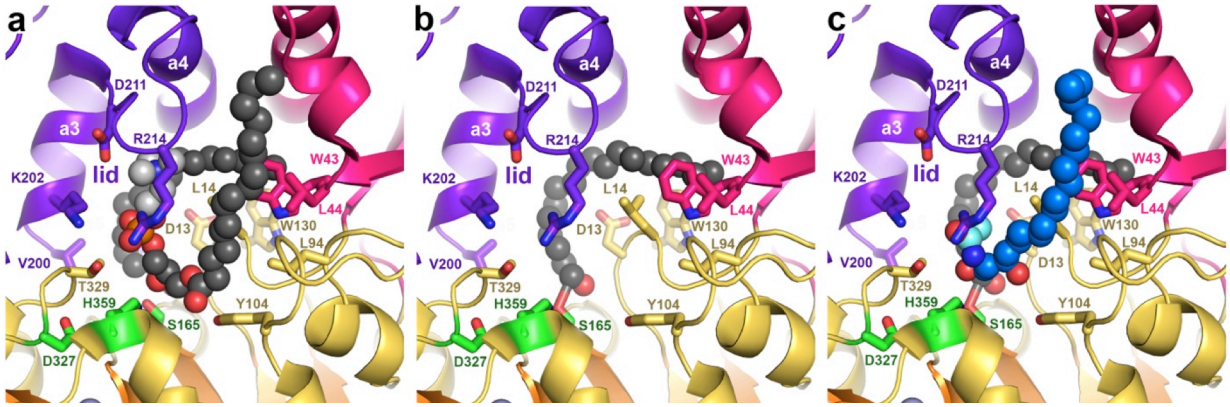

Figure 41. Models of the LPLA2 catalytic cycle. **(a)** Model of POPC (spheres) bound in the active site such that its *sn*-2 chain occupies track A, and *sn*-1 track B. The head group (light grey spheres) is coordinated by Lys202, Asp211, and Thr329. **(b)** After dissociation of the lysophosphatidylcholine product, the acyl intermediate remains in track A, which would allow His359 to deprotonate the incoming alcohol nucleophile. **(c)** Model of NAS (blue spheres, cyan acetyl group) bound in track B.

2 position (Fig. 41a) (Abe *et al.*, 2006). In support of the model, the A and B tracks extending from the catalytic triad adopt trajectories that loosely match the physicochemical propensities of each acyl chain (i.e. kinked vs. linear), which may help explain the preference of LPLA2 for unsaturated lipids in the *sn*-2 position. Based on constraints of the phosphate interacting with Lys202 and Thr329, the positively charged amine of the choline head group would be close enough to form favorable electrostatic interactions with the side chain of Asp211 in the lid loop, an invariant residue in both LPLA2 and LCAT. Although LPLA2 has relatively broad head group selectivity (Abe & Shayman, 2009), LCAT is fairly specific for PC (Pownall *et al.*, 1985) and the analogous residue (Asp227) may be important for this property.

The side chain of Asp13 is also expected to be involved in substrate binding, perhaps by helping to dictate the course of acyl chains in track A. Accordingly, the D13A mutation decreased both soluble substrate pNPB hydrolysis and acyl transfer (Fig. 42a, b), suggesting that truncation of the side chain at this position disrupts the formation of favorable van der Waals contacts with the butyric group of the substrate.

The above data suggest the following steps for phospholipid binding, acyl intermediate formation, lysophospholipid release, and transfer to acyl acceptor. The phospholipid acyl chain that binds in track A corresponds to the scissile chain given the homology of this site to those of bacterial lipases and the fact that the catalytic triad histidine is situated such that it can only protonate the lysophospholipid leaving group if it resides in track B (Fig. 41a). However, because LPLA2 has both phospholipase A2 and A1 activity, whether the *sn*-1 or *sn*-2 chain binds in track A also depends on its physicochemical properties (size and curvature). Indeed, LPLA2 prefers to transfer oleic (C18:1) and linoleic (C18:2) fatty acids (Abe *et al.*, 2006) perhaps because their length and unsaturation enables them to pack more efficiently in track A. After dissociation of the lysophospholipid product (Fig. 41b) the more accessible track B is left open for binding water (leading to lipase activity) or lipophilic alcohols (leading to acyl transferase activity) (Fig. 41c). A model of NAS docked into track B of the LPLA2 active site potentially explains the preference of the enzyme for lipophilic alcohols with a short side chain, such as C2 ceramide (Abe, Hiraoka, & Shayman, 2007b), because longer chains could collide with the acyl-intermediate bound in track A (Fig. 41c). The residues that

coordinate the phosphate of the PC head group may also form specific hydrogen bonds with the *N*-acetyl group of NAS.

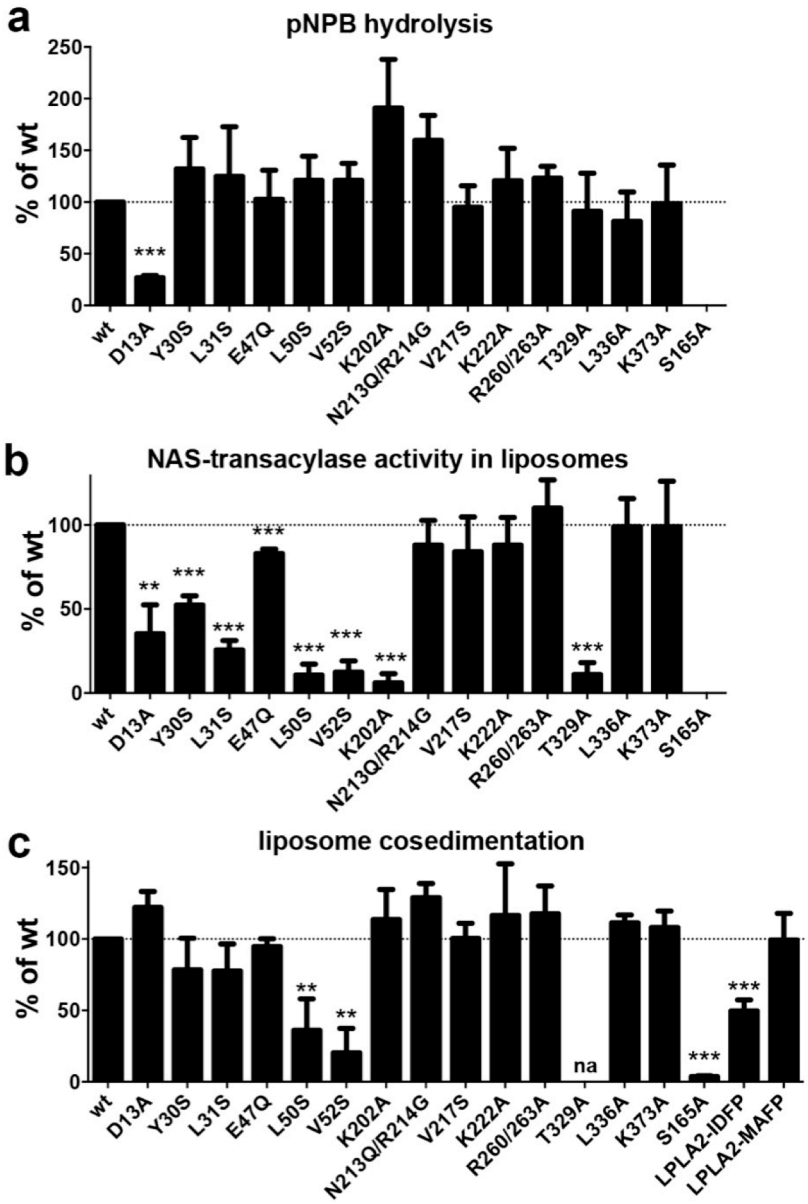

Figure 42. Enzymatic activity and membrane binding of LPLA2. **(a)** Hydrolysis of the soluble substrate pNPB at pH 7.5. All mutations except D13A were not significantly different from wild-type (wt). **(b)** Transacylase assay using NAS-DOPC-sulfatide liposomes. Transacylase assays were performed by V. Hinkovska-Galcheva. **(c)** LPLA2 co-sedimentation with DOPC-sulfatide liposomes. Error bars represent the standard deviation of three independent experiments. ** $0.001<p<0.01$, ***$p<0.001$. na, not assayed due to poor protein expression.

4.4 Conformational Flexibility of LPLA2.

Conformational flexibility is often an important structural property of lipases, as interaction with a lipid bilayer is often thought to induce a conformational change that opens the active site (Verger, 1997). Among the eight unique crystal forms for apo- and inhibitor-bound LPLA2 reported here (Tables 2-4), the most conformationally variable element is the lid loop (residues 210-220) (Fig. 43a). The αA´-αA loop (residues 96-102) and the a1 helix of the membrane binding domain are also among the most flexible elements, consistent with their temperature factors in the free enzyme structure (Fig. 43b). Interestingly, all three of these elements contribute residues to track B, suggesting that their structural plasticity allows for the binding of distinct ligands in this track, as is required by the catalytic cycle. Sequence alignment of these regions in LPLA2 and LCAT reveals high conservation within each enzyme family, but less so between LPLA2 and LCAT (Fig. 43c), and thus these loops could play a role in dictating acyl acceptor selectivity. However, despite similarities to Family I bacterial lipases (Fig. 38), there is as of yet no evidence of a large conformational change that would transition LPLA2 from a closed to an open state upon membrane binding.